EARTH SCIENCES HONOURS THESIS

BASEFLOW CONTRIBUTION OF THE UNCONFINED AQUIFER SUPPLYING THE LOWER REACHES OF THE CLYBURN BROOK, CAPE BRETON ISLAND, NOVA SCOTIA

Author: Beverley Smith

Advisor: Dr. David Hansen

Submitted as an Honours Thesis in partial fulfillment of the Bachelor of Science Degree
at Dalhousie University
April 17, 2002

Distribution License

DalSpace requires agreement to this non-exclusive distribution license before your item can appear on DalSpace.

NON-EXCLUSIVE DISTRIBUTION LICENSE

You (the author(s) or copyright owner) grant to Dalhousie University the non-exclusive right to reproduce and distribute your submission worldwide in any medium.

You agree that Dalhousie University may, without changing the content, reformat the submission for the purpose of preservation.

You also agree that Dalhousie University may keep more than one copy of this submission for purposes of security, back-up and preservation.

You agree that the submission is your original work, and that you have the right to grant the rights contained in this license. You also agree that your submission does not, to the best of your knowledge, infringe upon anyone's copyright.

If the submission contains material for which you do not hold copyright, you agree that you have obtained the unrestricted permission of the copyright owner to grant Dalhousie University the rights required by this license, and that such third-party owned material is clearly identified and acknowledged within the text or content of the submission.

If the submission is based upon work that has been sponsored or supported by an agency or organization other than Dalhousie University, you assert that you have fulfilled any right of review or other obligations required by such contract or agreement.

Dalhousie University will clearly identify your name(s) as the author(s) or owner(s) of the submission, and will not make any alteration to the content of the files that you have submitted.

If you have questions regarding this license please contact the repository manager at dalspace@dal.ca.

Grant the distribution license by signing and dating below.

_____ _____

Name of signatory Date

ABSTRACT

The Clyburn Brook, in the Cape Breton Highlands National Park, is an important source of freshwater. The brook overlies an unconfined aquifer that supplies potable and irrigation water for the Ingonish area. The Clyburn Brook is partially fed by baseflow and is affected by withdrawal from the aquifer. This thesis examines the physical characteristics of the lower reaches of the Clyburn Brook using seismic techniques and finite difference numerical modelling.

In the area of study, the bedrock is the Ingonish River tonalite (555 ± Ma), which is overlain by glaciofluvial sand and gravel of Quaternary age and modern fluvial deposits. Refraction seismic data indicates a depth to bedrock of 7 to 9 m in the 'bottleneck' area of the Clyburn Brook. Reflection seismic data indicates depths to bedrock ranging from 15 to 47 m. Some of this data is used to generate lateral and trough-like profiles of the canyon.

Finite difference numerical modelling of the canyon aids in the examination of aquifer flow characteristics in different water level settings. Survey data prepared by Dr. David Hansen, topographical and seismic data assist in the construction of two models, one in plan view and the other in a cross-sectional view. The models are connected to data tables that allow water level settings to be altered with ease. The models are examined in relation to six scenarios, representing water table elevation differences of 0, 0.05, 0.5, 1.0, 2.5 and 3.0 m between the stream and the canyon walls. Based on topography, it is determined that 3 m represents the maximum water level elevation difference. Using Darcy's Law, the hydraulic head values obtained are used to determine flow rates, which are subsequently examined in relation to baseflow contribution to the stream. That is, the contribution to stream discharge from groundwater seeping into the base of the stream. This study utilizes data from previous baseflow recession work by Dr. Hansen, in which the declining rate of discharge of the stream, when fed by baseflow only, was examined.

Using discharge and baseflow recession data, two volume calculations are made: (1) a hydrograph recession-based volume calculation to determine the volume of water lost from storage for each scenario, and (2) a geometric volume calculation for the plan-view model, change in water table elevation of 2.5 m (scenario #5). The first volume is then examined, using Darcy's Law and baseflow recession formulae, to determine the hydraulic conductivity value sufficient to produce a volume comparable to the geometric volume calculation for scenario #5. A hydraulic conductivity value of 0.6 to 0.7 m/d is produced, which is much lower than the 213.3 m/d value from a previous pump test. Finally, baseflow recession analyses are compared to acceptable low flow rates for different species of fish. A figure of depth versus recession time is generated and the impact on fish habitat and water quality is assessed. It is determined that, after 90 to 96 days of recession, fish habitat preferences are negatively impacted. When flow rates decline to 1.0 to 0.1 m^3/s, pumping could have a detrimental impact on the quantity of water in the brook and the quality of salmonid habitat.

TABLE OF CONTENTS

LIST OF FIGURES

LIST OF TABLES

NOMENCLATURE

For the analytical equations presented in this thesis, the following nomenclature was used:

F	force
L	length
M	mass
T	time

For the empirical equations presented in this thesis, the appropriate units of measurement were indicated below each equation.

ACKNOWLEDGMENTS

First, I would like to acknowledge and thank my thesis advisor Dr. David Hansen for allowing me to assist with certain aspects of his ongoing project on the Clyburn Brook. Dr. Hansen contributed survey data, baseflow recession components, and fish habitat preferences for the Clyburn Brook. Second, I would like to acknowledge and thank Dr. Patrick Ryall and Charlie Walls for assisting me with the reflection seismic study and for providing data relating to the previous refraction seismic study. Dr. Ryall also provided guidance throughout the project and helped tremendously with the seismic interpretation and background theory.

I would like to thank Brian Fisher of the Department of Natural Resources, who assisted in preparing the GIS maps for this project. The time he spent on the bedrock geology and seismic location maps was greatly appreciated.

I would also like to acknowledge and thank Heather Cross for taking the time to answer my questions and for looking over my geology and previous work chapter.

Thank you to Fred Baechler of ADI – Nolan Davis (NS) Limited for giving me a guided tour of the Clyburn Brook in June 2001 and some ideas for the project in its beginning stages.

Thank you to James Bridgeland of Canadian Heritage Parks Canada for allowing us to perform the seismic study, giving us access to the Clyburn Brook, and a place to stay at the Park campground.

Thank you also to Dawn Allen of Canadian Heritage Parks Canada for providing some background data on the Clyburn Brook, especially the 3-D rendering of the brook.

I also want to thank my husband Darren, who supported me throughout the project.

1 INTRODUCTION

1.1 Thesis Statement and Scope

The purpose of this study is to examine the physical characteristics of the Clyburn Brook canyon in relation to the unconfined aquifer in the lower reaches of the Clyburn Brook, Cape Breton Highlands National Park, Nova Scotia. In particular, an examination of the depth to bedrock in certain areas of the canyon was undertaken and the contribution by baseflow to the unconfined aquifer supplying the lower reaches of the Clyburn Brook was ascertained.

The study area is within federal parklands, which currently operate under a policy of minimal interference with natural processes. Therefore, certain limitations were imposed on the study. As a result, the only intrusive method used was the drilling of auger holes during the seismic study.

1.2 Importance of Study

The Clyburn Brook watershed is an important source of freshwater (Figures 1 and 2). Initially, the watershed was used to service only the Cape Breton Highlands National Park (CBHNP) with potable water and water for irrigation purposes. However, as a result of increased demand, the watershed began servicing other areas in the vicinity of the CBHNP. At the present time, the Clyburn Brook watershed supplies water for irrigation of the Highland Links golf course and potable water for the Park administration buildings and campground, the Keltic Lodge and several houses in the nearby community of Ingonish.

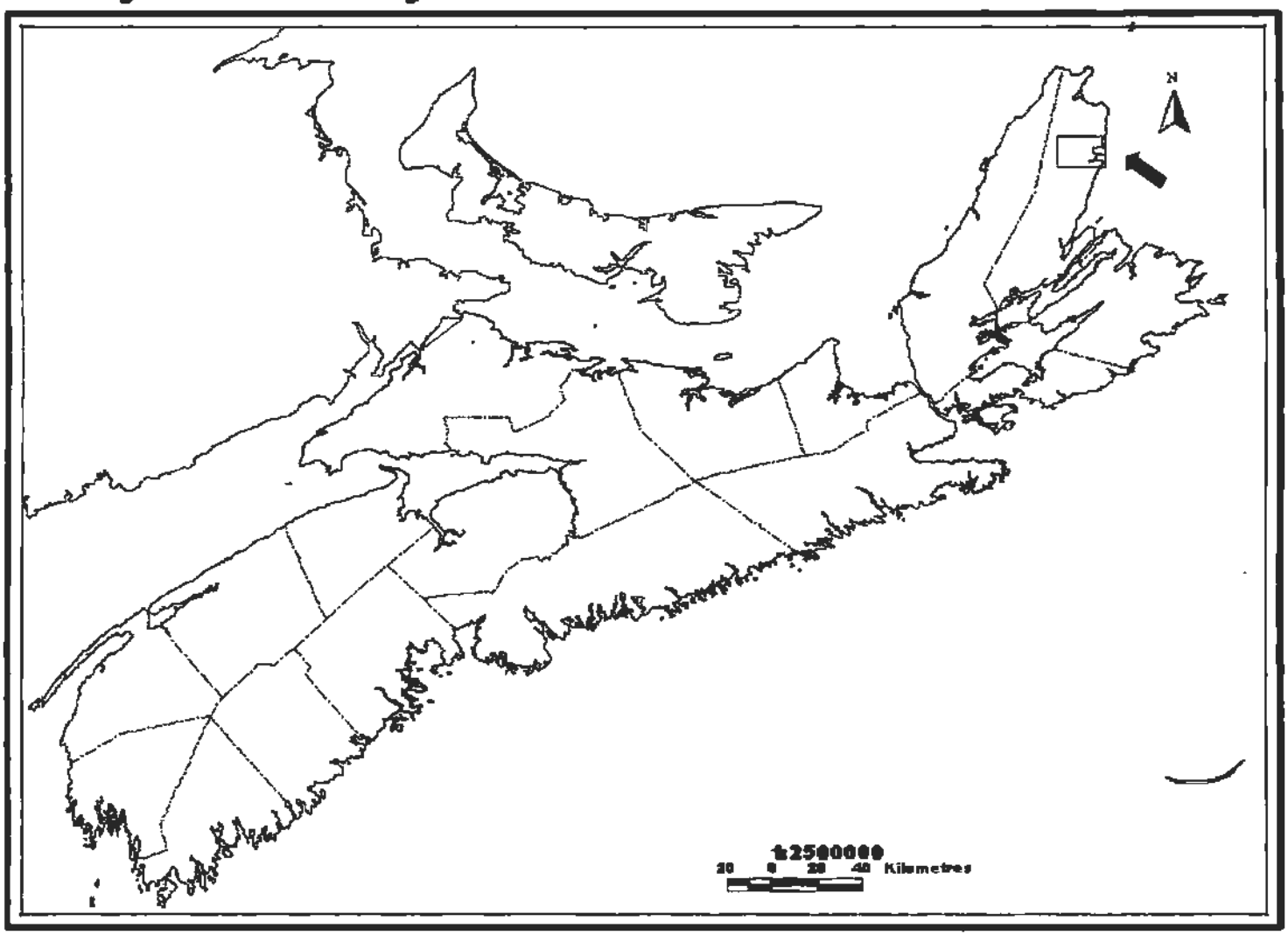

Figure 1. Site location map.

Clyburn River Watershed and Sub-Watershed Metrics

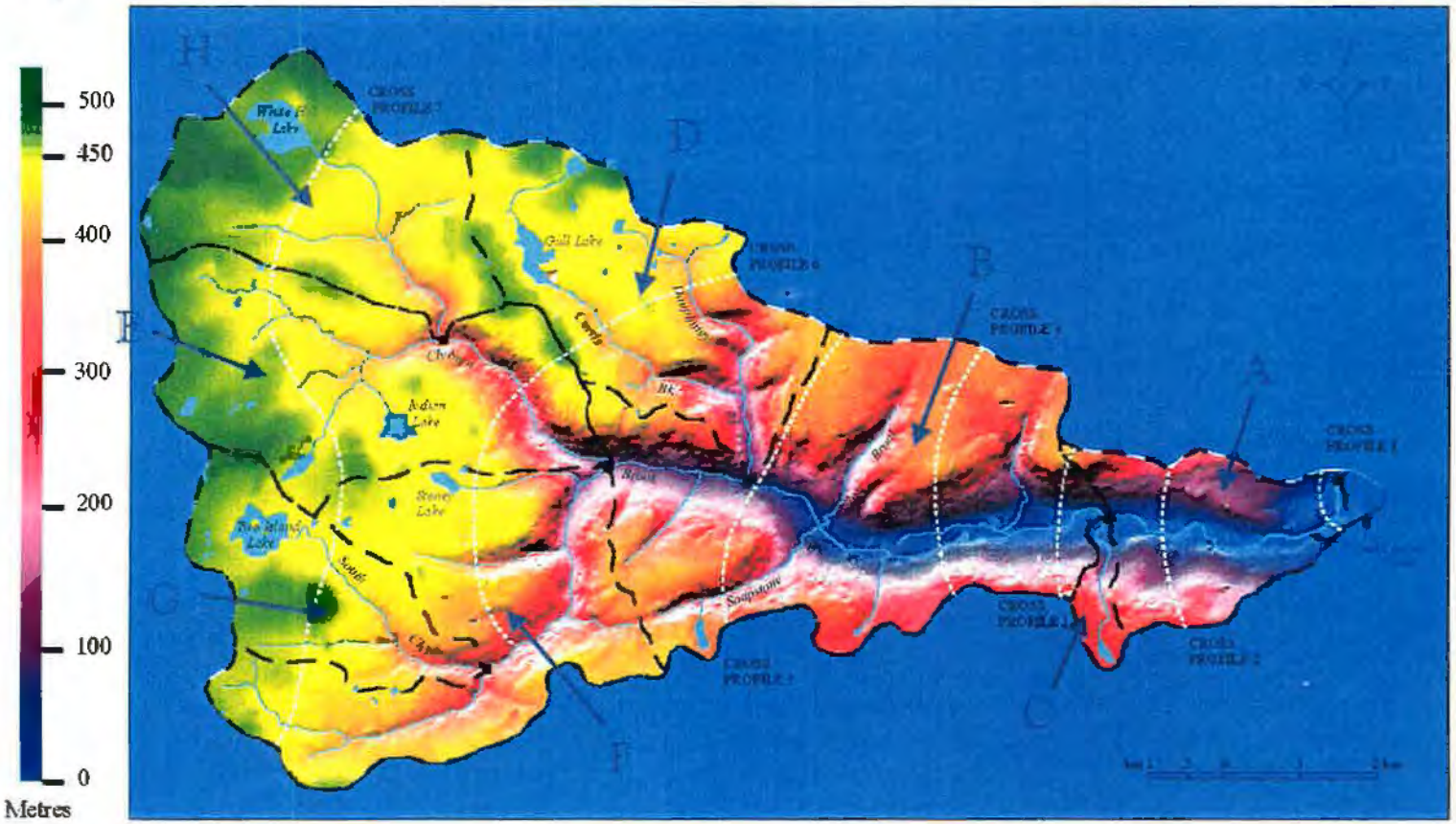

Figure 2. Clyburn Brook watershed and sub-watersheds (A to H) (Allen, 1999).

The impact of increased pumping rates on the watershed is an important concern. The Clyburn Brook flows within the CBHNP boundaries and the level of standing water within the brook has impacts on the animals and fish species located there. For example, the Clyburn Brook supports an annual salmon migration and is used by various other fauna, such as moose, deer, black bears, foxes, coyotes, and birds. Pumping rates are a concern since demand could increase in the future. It is, therefore, crucial to discern the physical parameters of the brook, such as the actual physical size of the aquifer (depth to bedrock) that underlies it and the amount of baseflow that the unconfined aquifer supplies to the brook.

1.3 Organization of Thesis

Chapter 2 of this thesis contains information on the study area, such as the bedrock and surficial hydrogeology of the surrounding area, its geological history, and previous work performed by private firms and governmental agencies. The data obtained and methods used for this thesis are outlined in Chapter 3. Chapter 4 contains a discussion of the data and the implications drawn from the methods that were applied. Finally, the conclusions drawn based on the entire study and the recommendations for further work are outlined in Chapter 5.

1.4 Terminology

The geological and hydrogeological terms used in the presentation of this thesis are outlined in Appendix A (after Fetter, 1988 unless otherwise stated).

2 STUDY AREA

The study area of this thesis is the Clyburn Brook, which is located within the Cape Breton Highlands National Park (CBHNP), near Ingonish, Cape Breton Island, Nova Scotia (Figure 1). The CBHNP was established in 1936. The Highland Links golf course was built in the 1930's. The natural topography and materials of the area were used in the construction of the golf course as much as possible. An infiltration gallery was installed to supply water for CBHNP facilities sometime during 1966-1968.

The Clyburn Brook originates in the highlands and drains into North Bay Ingonish. Therefore, drainage in the study area is to the southeast. The Nova Scotia Department of Environment delineates the Clyburn Brook watershed as drainage area 1FD-12A-G. The Clyburn Brook is presently used to irrigate the Highland Links golf course and as a potable water source for the CBHNP administration buildings and campground, the Keltic Lodge, and several homes in Ingonish.

2.1 Topographic and Physiologic Setting

The Cape Breton Highlands form an uplifted peneplain, with a maximum elevation of 531 m (Raeside and Barr, 1992). This area has been physiographically divided into two upland areas, the eastern highlands and the North Mountain (Figure 3). The Clyburn Brook is located within a portion of the eastern highlands that forms a gently, eastward-dipping peneplain. Elevations range from 530 m to near sea level between Ingonish and White Point. The upland areas, which overlie impermeable crystalline basement rocks, tend to be very boggy.

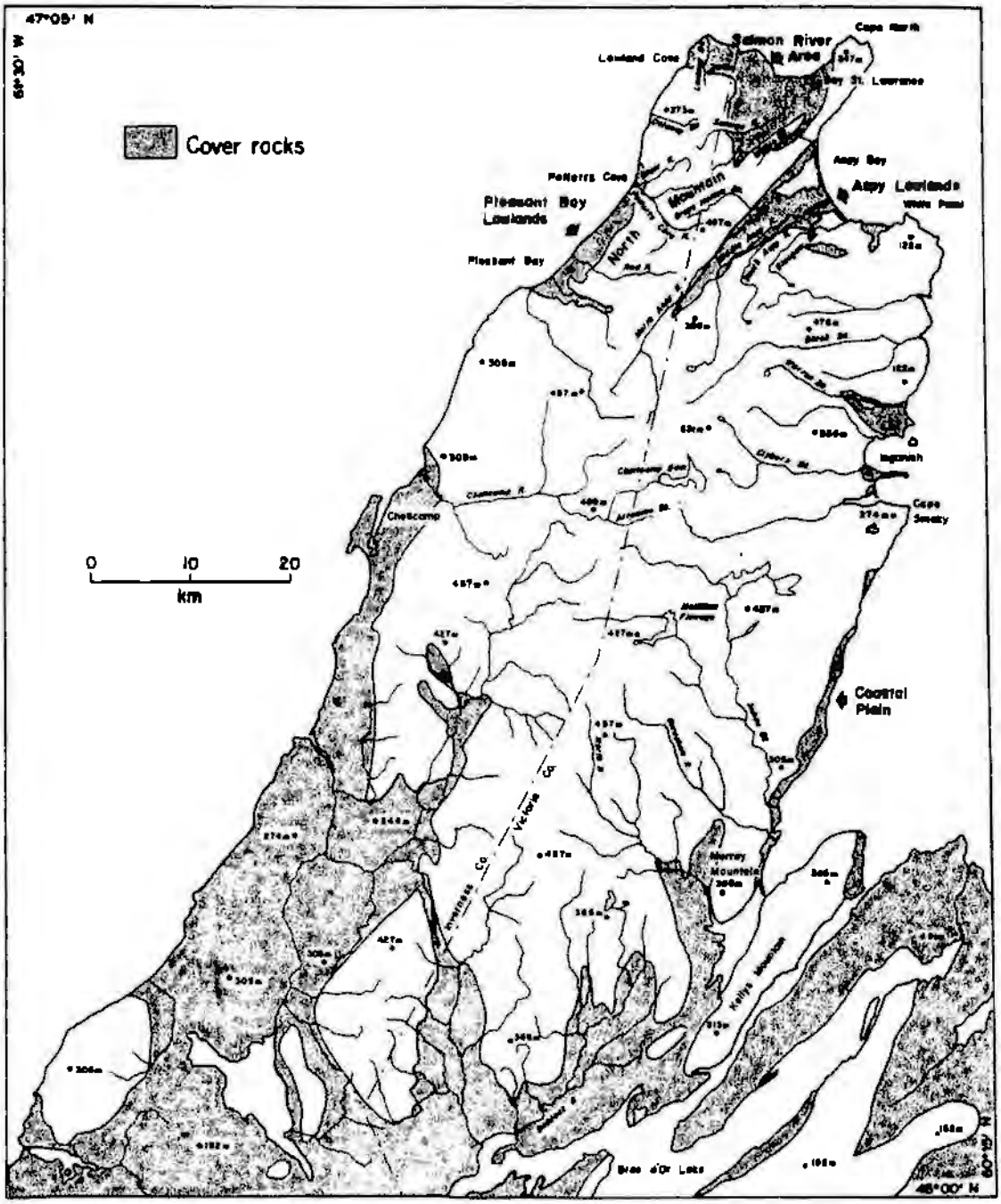

Figure 3. Physiography of the Cape Breton Highlands. Shaded areas are underlain by Carboniferous sedimentary rocks, areas without shading are underlain by metamorphic and igneous rocks (Raeside and Barr, 1992).

The Clyburn Brook is surrounded by steep canyon walls (see Figure 2). Maximum elevations range from 426 m on the north canyon wall to 338 m on the south canyon wall. The valley lowlands range in elevation from 45 m to 15 m. The canyon walls slope into the valley lowland at a gradient of 0.35 to 0.45 (ADI, 1993).

2.2 Hydrogeologic Setting

2.2.1 Bedrock hydrogeology

The bedrock geology in the area of the Clyburn Brook is highly variable, see Figure 4 and summary legend. At its origin in the eastern highlands, the Clyburn Brook is within the Black Brook Suite of Devonian-age granite and granodiorite. At the mouth of the canyon, the Black Brook Suite comes into contact with the Middle clastic member of the McMillan Flowage Formation. This formation is composed of Hadrynian-age semipelitic, pelitic and mafic schists, amphibolites, and quartzites. The Clyburn Brook passes through a 600 m section of Roper Brook amphibolite, also a member of the Hadrynian-age McMillan Flowage Formation, then the bedrock is once again the Middle clastic member of the McMillan Flowage Formation. The Clyburn Brook is intersected by the Eastern Highlands shear zone, which runs NNE-SSW. This shear zone is intersected by the Clyburn Brook Fault, which runs NE-SW and, at its eastern end, branches into a Y-shape. In between the northern and southern branches, the geology is undivided Hadrynian-age gneissic rocks.

The Clyburn Brook follows the southern branch of the Clyburn Brook Fault. On the southern side of the brook is Ingonish River tonalite, Hadrynian to Cambrian-age rock. At the eastern end of the fault, the Clyburn Brook is within Cameron Brook granodiorite, Devonian-age rock. The brook then winds back and forth through

Ingonish River tonalite and Cameron Brook granodiorite. East of the Cabot Trail Highway, the southern side of the brook is within undivided Carboniferous, unmetamorphosed sedimentary rocks. The Clyburn Brook then terminates at North Bay Ingonish.

In relation to the study area, the lower reaches of the Clyburn Brook overlie the Ingonish River tonalite and Cameron Brook granodiorite. The Nova Scotia Department of Environment monitoring station is located on the Cameron Brook granodiorite. The area of interest in the finite difference modelling study is located on the Ingonish River tonalite (Sections 3.2 and 3.3).

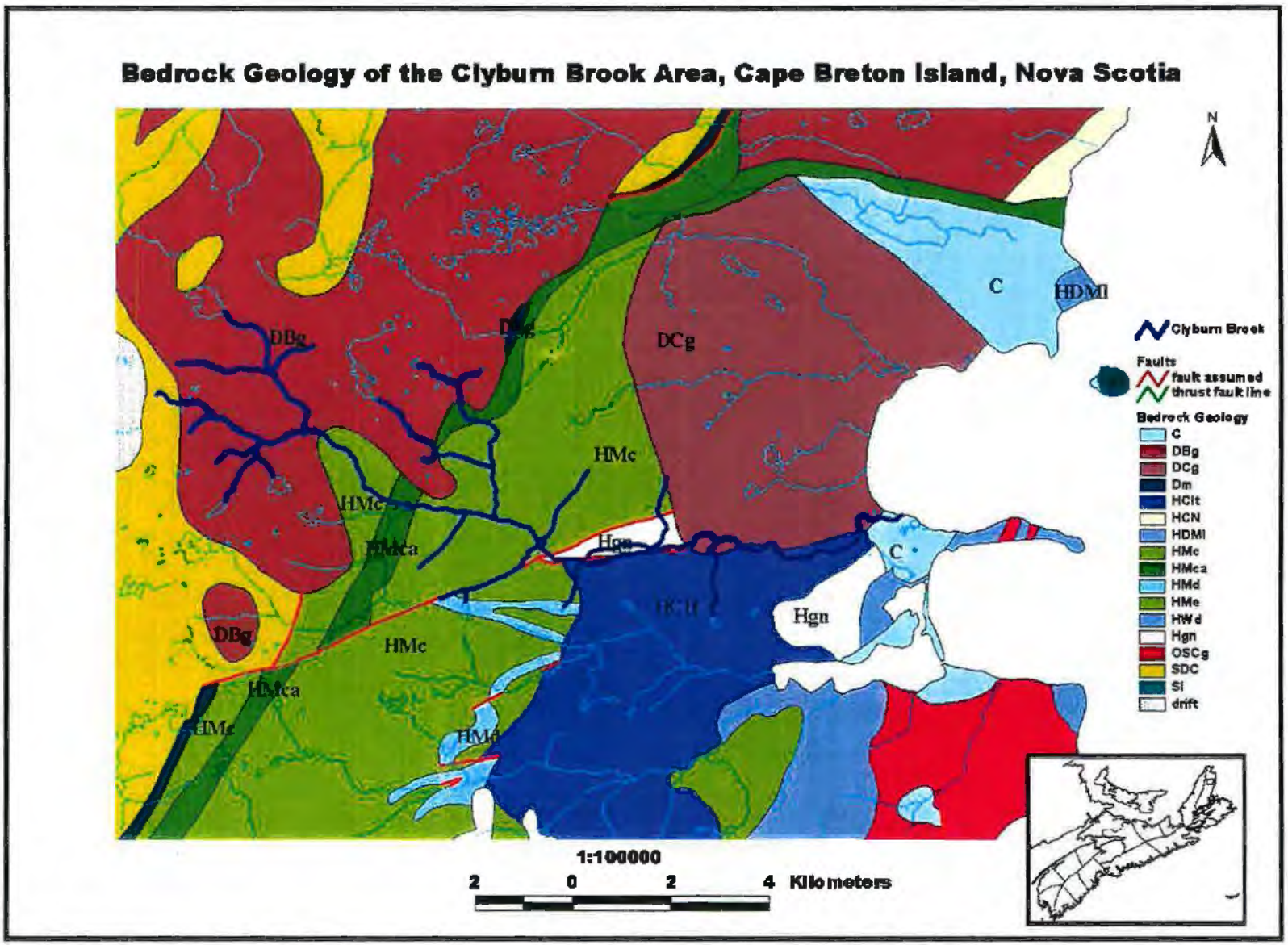

Figure4. Bedrock Geology and summary legend (following page).

Summary Legend - Bedrock Geology
[taken from GSC Map 1752A (Barr, *et al.*, 1992)]

Hadrynian

HGn	undivided Hadrynian gneissic rocks
HMca	McMillan Flowage Formation, Roper Brook amphibolite
HMc	McMillan Flowage Formation, Middle clastic member; semipelitic, pelitic and mafic schists, amphibolite, quartzite

Hadrynian to Cambrian

HClt	Ingonish River tonalite (555 ± Ma, U-Pb [zircon], Dunning *et al.*, in press)

Devonian

DBg	Black Brook Suite (granite and granodiorite), including White Point, Black Brook, Warren Brook, and Clyburn Brook plutons of Wiebe, 1972, 1975 (373 ± 2 Ma, U-Pb [monzanite], Dunning *et al.*, in press)
DCg	Cameron Brook megacrystic granodiorite (402 ± 3 Ma, U-Pb [zircon], Dunning *et al.*, in press)

Carboniferous

C	undivided unmetamorphosed Carboniferous sedimentary rocks

2.2.1.1 Structural history

There are four recognizable tectonostratigraphic zones within the Appalachian system of Cape Breton Island (Raeside and Barr, 1992) (Figure 5). The Clyburn Brook is located within the Aspy Terrane and the Bras d'Or Terrane. In between the two terranes is the Eastern Highlands shear zone, in which deformation took place mainly in the Late Silurian (Lin, 1995). The Silurian orogeny caused intense and widespread deformation, metamorphism and magmatism in Cape Breton Island and Newfoundland, and has been related to the final phase of collision between Laurentia and Avalon (Lin, 1995).

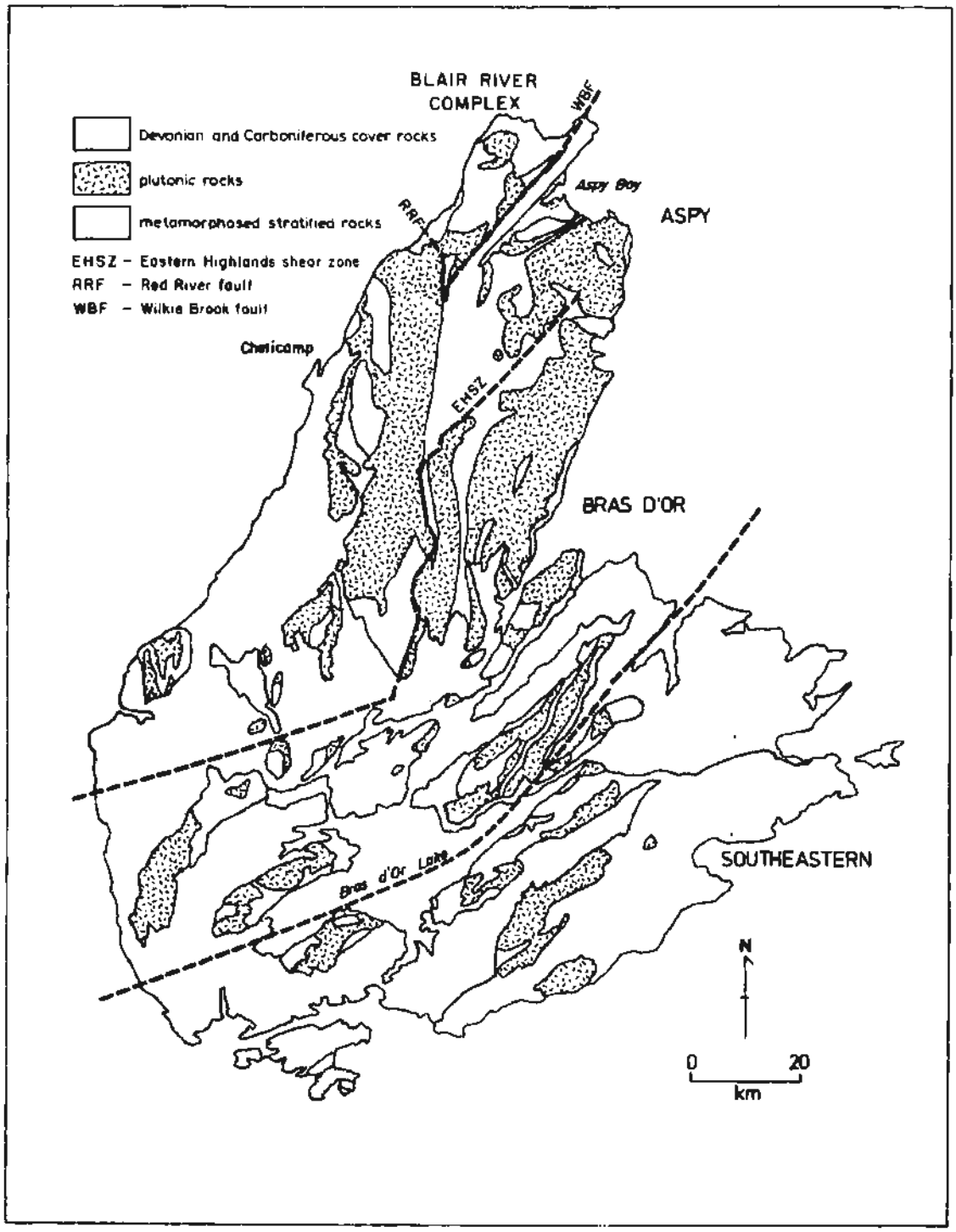

Figure 5. Tectonostratigraphic terranes of northern Cape Breton Island (Raeside and Barr, 1992).

The Black Brook Granitic Suite is part of the Aspy Terrane. The Clyburn Brook Pluton, a muscovite-biotite granite, forms part of this large granodioritic to granitic intrusion. The main difference between the Aspy Terrane and the Bras d'Or Terrane is the lack of dykes, sheets, and plutons of similar composition. Also, the Devonian plutons of the Aspy Terrane are widely emplaced.

The Bras d'Or Terrane includes the McMillan Flowage Formation (including the Roper Brook amphibolite), undifferentiated gneissic rocks, the Ingonish River tonalite, and the Cameron Brook granodiorite. The McMillan Flowage Formation is a large, compositionally variable, continuous, stratified unit of Precambrian age. This formation was regionally folded and then cut by the Ingonish River tonalite (Raeside and Barr, 1992). Generally, the McMillan Flowage Formation "is composed of three sections, a lower pelitic and semipelitic part with thin amphibolites and calc-silicate lithologies, a middle section containing abundant interstratified quartzites and amphibolites with fewer pelitic units, and an upper section of semipelitic schists and less abundant quartzite and amphibolite layers" (Raeside and Barr, 1992).

Within the middle clastic division, a kilometre-scale syncline has been recognized in the Clyburn Brook area (Raeside and Barr, 1992). The middle clastic division can be up to 2000 m thick and, in the area of the Clyburn Brook, contains five metamorphic zones (Figure 6). The lowest grade is the chlorite zone, which is located near the Clyburn Brook and Slate Brooks. Up the Clyburn Brook, grade rapidly increases through the biotite zone, the garnet zone to the staurolite zone.

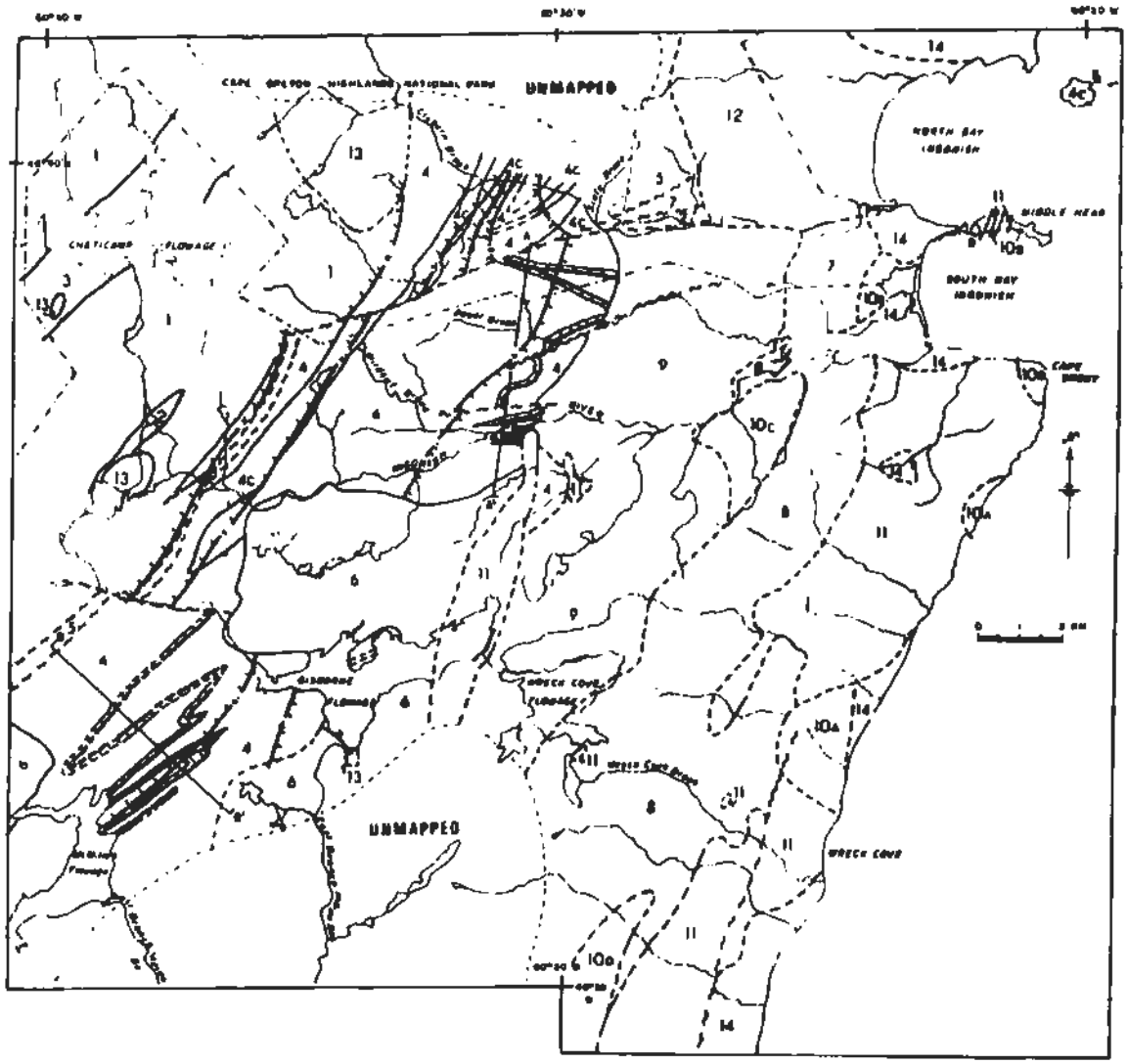

METAMORPHIC BOUNDARIES AND OTHER SYMBOLS

Appearance of biotite .....-bi-
Appearance of garnet .....-gt-
Actinolite + albite + chlorite = hornblende + plagioclase .....-hb-
Staurolite + muscovite + quartz = sillimanite + garnet + biotite ..-si-
Quartz + muscovite = K-feldspar + sillimanite .....-K-

Geological boundary (approximate, assumed) .....
Metamorphic boundary (ticks on high grade side) .....
Fault (approximate, assumed) .....

Figure 6. Geological map of the Ingonish River-Wreck Cove area, showing faults and metamorphic zones near Clyburn Brook, and legend (Raeside *et al.*, 1984).

The Roper Brook amphibolite is categorized within the upper part of the middle clastic division. It is a prominent amphibolite horizon, up to 800 m thick (Raeside *et al.*, 1984). In the Clyburn Brook area, the amphibolite appears at lower metamorphic grades as volcanic breccias, tuffs, and aphanitic flows (Raeside *et al.*, 1984).

The undifferentiated gneissic rocks, exposed north of the Clyburn Brook, are primarily tonalitic in composition, with some granitic bands (Raeside *et al.*, 1984). These gneissic rocks have a more varied lithology than the Ingonish River tonalite described below. South of the Clyburn Brook Fault, the undifferentiated gneissic rocks have been severely cataclased by the fault and intruded by the Cameron Brook granodiorite (Raeside and Barr, 1992).

The Ingonish River tonalite is the youngest dioritic intrusion. Foliation is variable and near the Clyburn Brook it is gneissic in appearance. It is differentiated from the gneissic rocks previously discussed by the presence of abrupt contacts between the two rock types (Raeside and Barr, 1992).

The Cameron Brook granodiorite forms a pluton that intruded the McMillan Flowage Formation on the west. The intrusion created a contact metamorphic aureole adjacent to the pluton and metamorphic grades formed in the McMillan Flowage Formation as a result. On the south side of the pluton, the Ingonish River tonalite has been intruded. The Cameron Brook granodiorite does not appear to be affected by the extensive mylonitic shearing in the Clyburn Brook, however, the northern margin of the pluton is sheared by the branch of the Eastern Highlands shear zone (Raeside and Barr, 1992). Movement along the Eastern Highlands shear zone and associated

faults occurred during Mid-Devonian to Early Mississippian (ADI, 1993). Some parts of this system had more than one phase of movement. The Clyburn Brook Fault is cut off by the Cameron Brook granodiorite. These two terranes compose the uplifted peneplain mentioned in Section 2.1. Carboniferous sedimentary rocks are found at the base of the Clyburn Brook. This bedrock is the youngest type in the area and does not exhibit any metamorphic deformation.

Most of the bedrock in the study area is igneous and metamorphic crystalline rocks, which have very little, if any, primary porosity. Therefore, some form of secondary porosity must be established in order for groundwater to occur in these rock types. Secondary porosity can be created through weathering, fracturing or faulting. In the study area, brittle fracturing bas occurred, however, the greatest source of groundwater is found in the surficial deposits (see Section 2.2.2).

2.2.2 Surficial hydrogeology

The surficial geology in the area of the Clyburn Brook has been mapped by Grant (1988) (Figure 7). A legend of unconsolidated materials is provided with Figure 7. Age connotations and stratigraphic terminology of the deposits are set out in Figure 8 (Grant, 1994).

In the highlands region of the Clyburn Brook, steep valley walls contain thin, blocky rubble that overlies till in some areas (7a). Further downstream, the Clyburn Brook flows over glaciofluvial deposits from the last glacial period. Laid down as a glacial outwash plain or fan, this deposit is composed of a sandy, coarse gravel layer up to 30 m thick (3b). The Clyburn Brook then passes through a thick blanket of non-fluvial valley fill, with older till and fluvial deposits buried at depth (7b). Again, the

Clyburn Brook flows over a region of glaciofluvial deposits (3b). At the lower end of the Clyburn Brook, in the area of the Highland Links golf course, the deposits are mainly fluvial in origin. Older sediments were laid down as paraglacial and postglacial alluvial terraces and fans (5a). This water-laid sediment varies from muddy angular debris to clean rounded gravel. Modern fluvial sediment occurs as floodplains of sandy pebble alluvium that is usually less than 3 m thick (5b). This younger sediment is commonly underlain by the coarser glaciofluvial sediment. On the southern side of the lower reach of the Clyburn Brook (about 600 m from the Cabot Trail Highway), sandy glacial tills 2 to 4 m thick are found (2b).

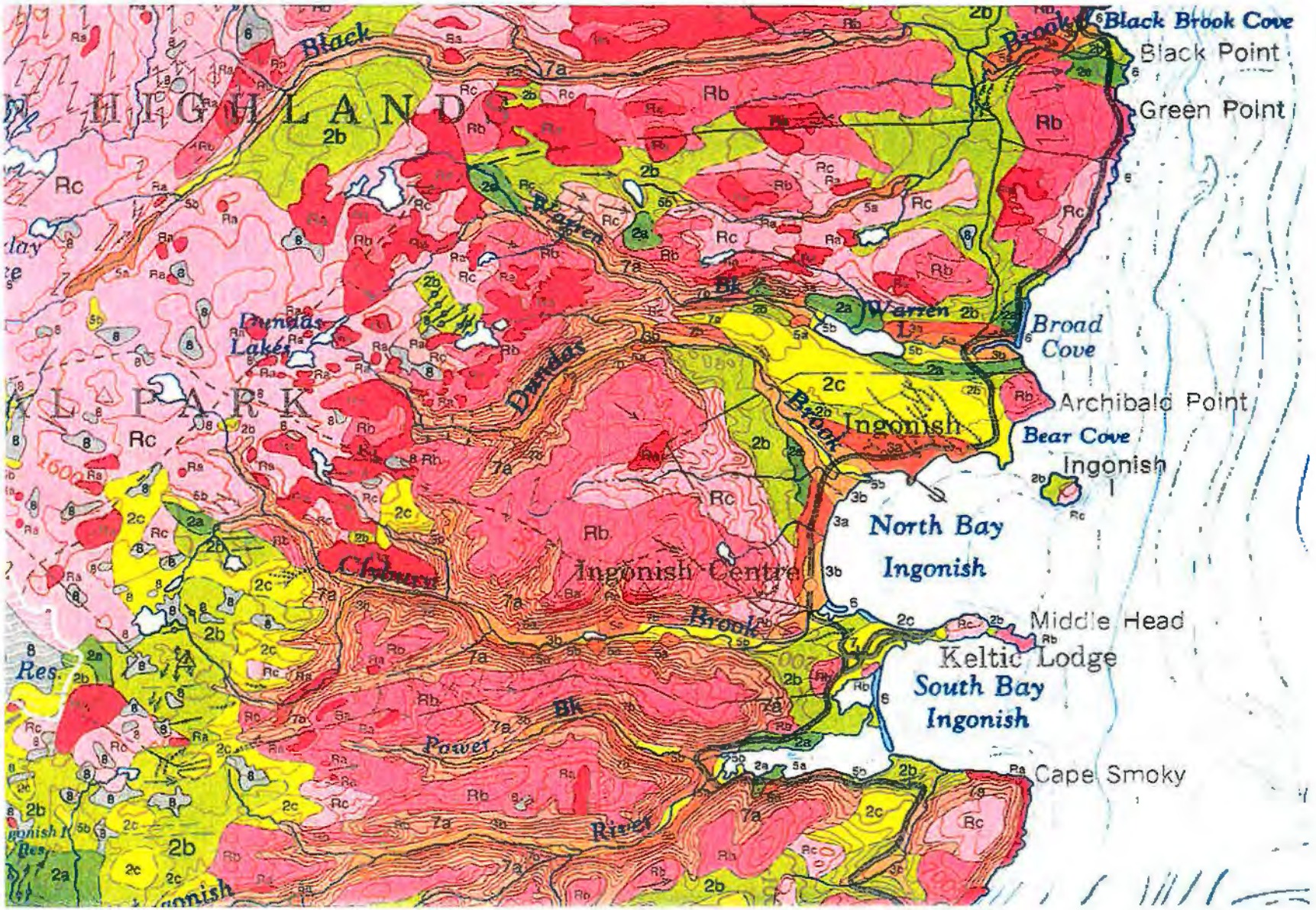

Figure 7. Surficial Geology map (1:125 000) with partial legend (following page) (Grant, 1988).

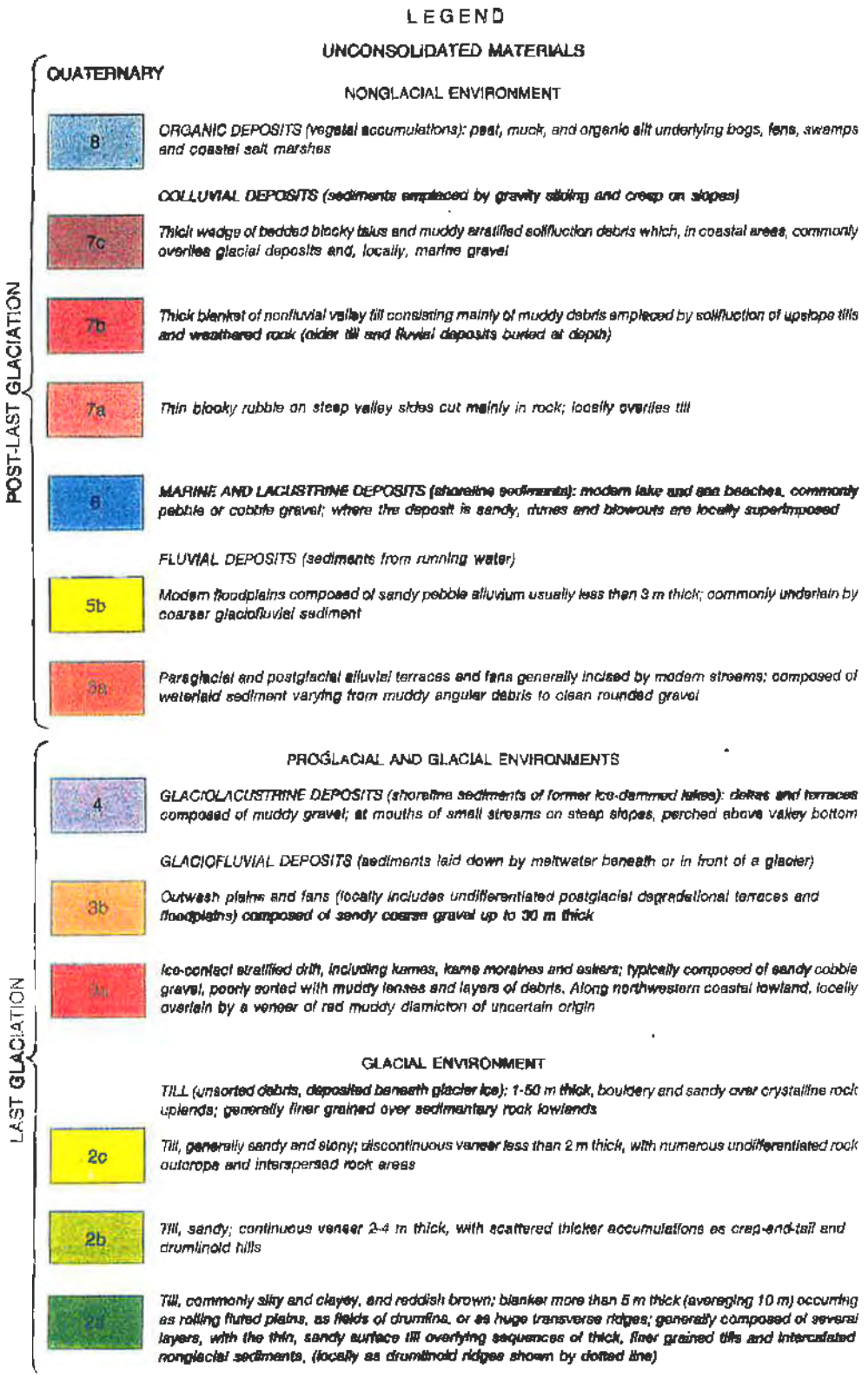
LEGEND
UNCONSOLIDATED MATERIALS
QUATERNARY
NONGLACIAL ENVIRONMENT
POST-LAST GLACIATION
8
ORGANIC DEPOSITS (vegetal accumulations): peat, muck, and organic silt underlying bogs, fens, swamps and coastal salt marshes
COLLUVIAL DEPOSITS (sediments emplaced by gravity sliding and creep on slopes)
7c
Thick wedge of bedded blocky talus and muddy stratified solifluction debris which, in coastal areas, commonly overlies glacial deposits and, locally, marine gravel
7b
Thick blanket of nonfluvial valley till consisting mainly of muddy debris emplaced by solifluction of upslope tills and weathered rock (older till and fluvial deposits buried at depth)
7a
Thin blocky rubble on steep valley sides cut mainly in rock; locally overlies till
6
MARINE AND LACUSTRINE DEPOSITS (shoreline sediments): modern lake and sea beaches, commonly pebble or cobble gravel; where the deposit is sandy, dunes and blowouts are locally superimposed
FLUVIAL DEPOSITS (sediments from running water)
5b
Modern floodplains composed of sandy pebble alluvium usually less than 3 m thick; commonly underlain by coarser glaciofluvial sediment
5a
Paraglacial and postglacial alluvial terraces and fans generally incised by modern streams; composed of waterlaid sediment varying from muddy angular debris to clean rounded gravel
PROGLACIAL AND GLACIAL ENVIRONMENTS
LAST GLACIATION
4
GLACIOLACUSTRINE DEPOSITS (shoreline sediments of former ice-dammed lakes): deltas and terraces composed of muddy gravel; at mouths of small streams on steep slopes, perched above valley bottom
GLACIOFLUVIAL DEPOSITS (sediments laid down by meltwater beneath or in front of a glacier)
3b
Outwash plains and fans (locally includes undifferentiated postglacial degradational terraces and floodplains) composed of sandy coarse gravel up to 30 m thick
3a
Ice-contact stratified drift, including kames, kame moraines and eskers; typically composed of sandy cobble gravel, poorly sorted with muddy lenses and layers of debris. Along northwestern coastal lowland, locally overlain by a veneer of red muddy diamicton of uncertain origin
GLACIAL ENVIRONMENT
TILL (unsorted debris, deposited beneath glacier ice): 1-50 m thick, bouldery and sandy over crystalline rock uplands; generally finer grained over sedimentary rock lowlands
2c
Till, generally sandy and stony; discontinuous veneer less than 2 m thick, with numerous undifferentiated rock outcrops and interspersed rock areas
2b
Till, sandy; continuous veneer 2-4 m thick, with scattered thicker accumulations as crag-and-tail and drumlinoid hills
2a
Till, commonly silty and clayey, and reddish brown; blanket more than 5 m thick (averaging 10 m) occurring as rolling fluted plains, as fields of drumlins, or as huge transverse ridges; generally composed of several layers, with the thin, sandy surface till overlying sequences of thick, finer grained tills and intercalated nonglacial sediments, (locally as drumlinoid ridges shown by dotted line)

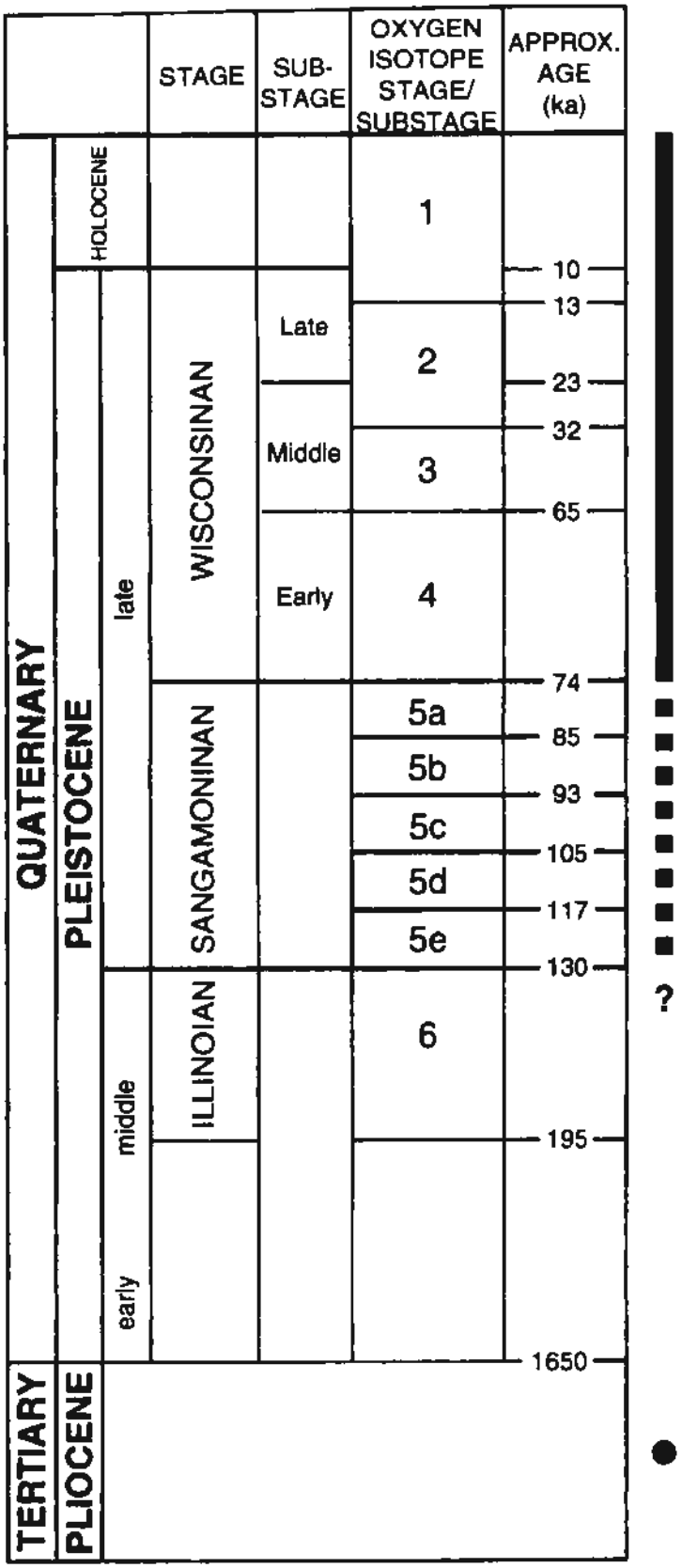

Figure 8. Age connotations and stratigraphic terminology (the solid, broken and dotted line indicates the degree to which the time interval is represented by sedimentary sequences) (Grant, 1994).

2.2.2.1 Glacial history

This discussion of the last glacial period, in relation to Cape Breton Island, has been summarized from Grant (1994). The first map of Cape Breton Island, showing the great variety of ice-flow directions, was presented by Prest and Grant (1969). They postulated a series of local ice caps variously affected by downward movements, with some outlet glaciers reaching marine bays and being affected by calving.

Grant realized that ice flow sequences may not be complete and each may not be a separate event. Therefore, in his discussion, patterns of ice flow ("phases") were lettered A-H (Figure 9). The area of the Clyburn Brook watershed was affected by Phases A, C and H.

Phase A: At the end of the last inter-glaciation, the climate gradually cooled and glacial ice formed on the northern plateau of the Cape Breton Highlands. This early ice cap is hypothesized to have spread downslope onto the fringing lowlands. The first movement (Phase A) is considered to be a northeastward flow. Grant has assumed that cold-based conditions prevailed under the central portions of this early ice cap because no glacial erosional or depositional features were formed in the central highlands area.

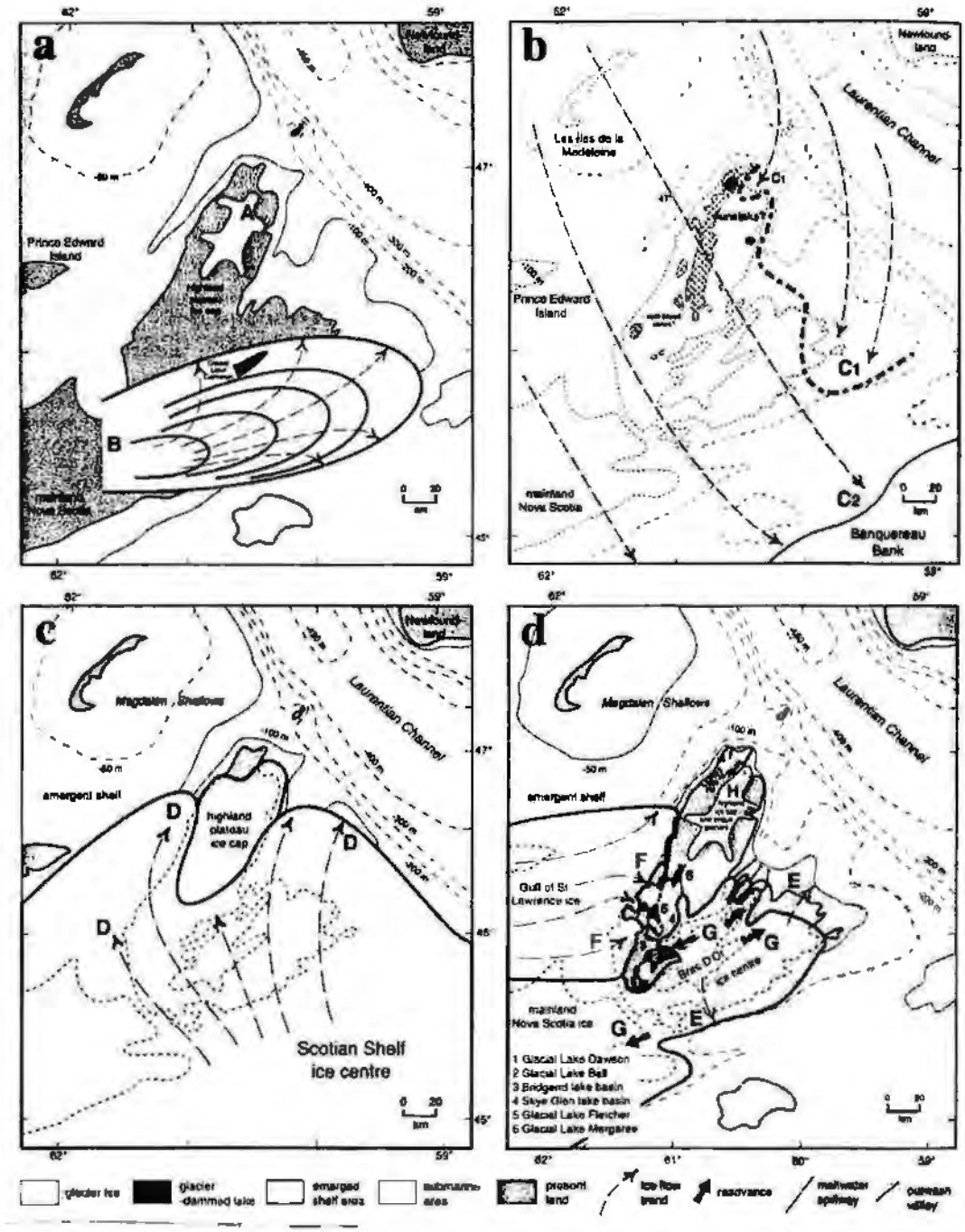

Figure 9. Paleogeographic reconstruction of the main glacial configurations and their constituent ice-flow patterns (Grant, 1994)

a. Glacial flow phases A and B. Flow phase A: formation of ice cap on northern highlands plateau; Flow phase B: eastward advance of ice from mainland Nova Scotia over southern lowlands.

b. Glacial flow phase C: ice from Laurentian Channel lobing onto Sydney Shelf (C1), thickening to regional ice sheet over Gulf of St. Lawrence which overrode highlands (C2), except possibly for small nunataks.

c. Glacial flow phase D: ice from Scotia Shelf advanced northward over the southern part of the island.
d. Glacial flow phases E-H: establishment of a Bras d'Or ice dispersal centre (E, G), while Gulf of St. Lawrence ice abuts on the west coast (F), impounding proglacial lakes (Dawson, Bell, Fletcher and Margaree) in western intermontane valleys, while a plateau ice cap persisted (H).

Phase C: A regional ice sheet moved southeastward over the whole island, including the highlands (Phase C2). The lack of evidence for this flow phase in the central parts of the northern highlands plateau most likely indicates that the ice was cold-based and frozen to its bed over this area. Cold-based conditions may have existed because the ice slid over the top of the pre-existing ice cap, which was assumed to have been cold-based.

Phase H: The independent ice cap, which occupied the highlands plateau and was in contact with lowland ice for a time (Phase C2), continued to flow actively, sending glaciers down the major valleys, one of which was the Clyburn Valley. After a time, the ice cap retreated to the highest part of the plateau until it was about 10 km in diameter. Retreat of highland ice is marked by a period of radial flow (Phase H). End moraines were constructed at the lower reaches of some valleys by retreating outlet glaciers and are perpendicular to the final eastward flow of the plateau glacier. It is noted that kames and small kame moraines "choke" some northern valleys, such as that of the Clyburn Brook. Meltwater channels cut in the residuum show that the ice cap shrank to a small carapace of about 5 km in diameter. Figure 10 depicts some of the features commonly found in a glaciated terrane.

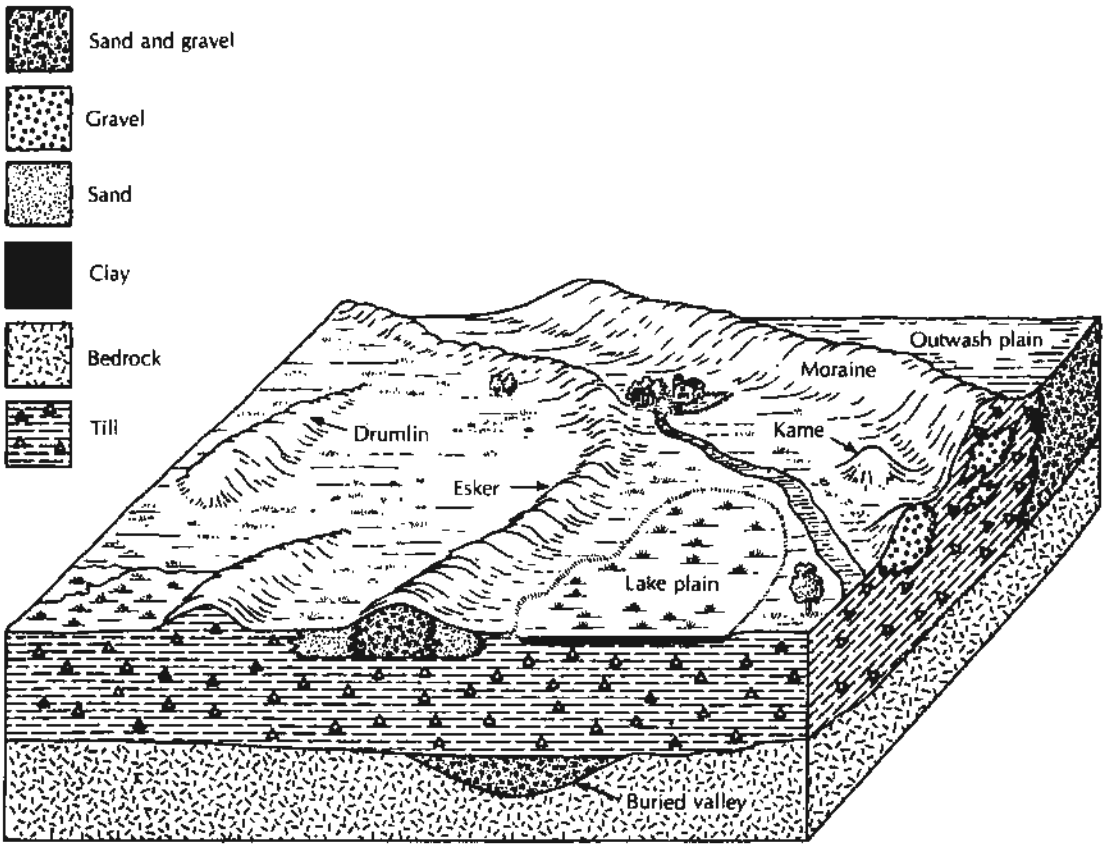

Figure 10. Depositional features in a glaciated terrane (Fetter, 1994).

There was generally a minimal effect of Quaternary erosion and deposition upon the resistant crystalline rocks forming the peneplain. These rocks remained largely intact with few or no glacial basins having been excavated. The southern Gulf of St. Lawrence region, including Cape Breton Island, has been subsiding at a rate of 20-40 cm/100 years during the last several millennia. Ongoing subsidence shows that isostatic crustal recovery is still underway to return the crust to its previous position relative to sea level. It is of general belief that subsidence is occurring because of the collapse of a northward-migrating glacial crustal forebulge. Southern areas of paleoshore

have been subsiding longer and, therefore, northern areas of paleoshore have yet to be lowered as much as its southern end.

Unconsolidated sands and gravels, and glacial drift form potential sources of groundwater. Deposits of material that are well-sorted and free of clays form the best aquifers. Some of the highest hydraulic conductivities can be found in deposits of unconsolidated sands and gravels. Therefore, in relation to the study area, a glacial deposit could form a good aquifer if it has been reworked, i.e. sorted and clay-size sediments removed; most sources of groundwater are found within the glaciofluvial sand and gravel.

2.3 Previous Work and Results

2.3.1 ADI-Nolan Davis (NS) Limited

In 1993 a study of coastal and fluvial processes of the Clyburn River was prepared for the CBHNP by ADI – Nolan Davis (NS) Limited. One of the objectives of the study was to "undertake an analysis of littoral and fluvial sedimentation processes around the mouth and over the lower 5 km reach of river" (Figure 11).

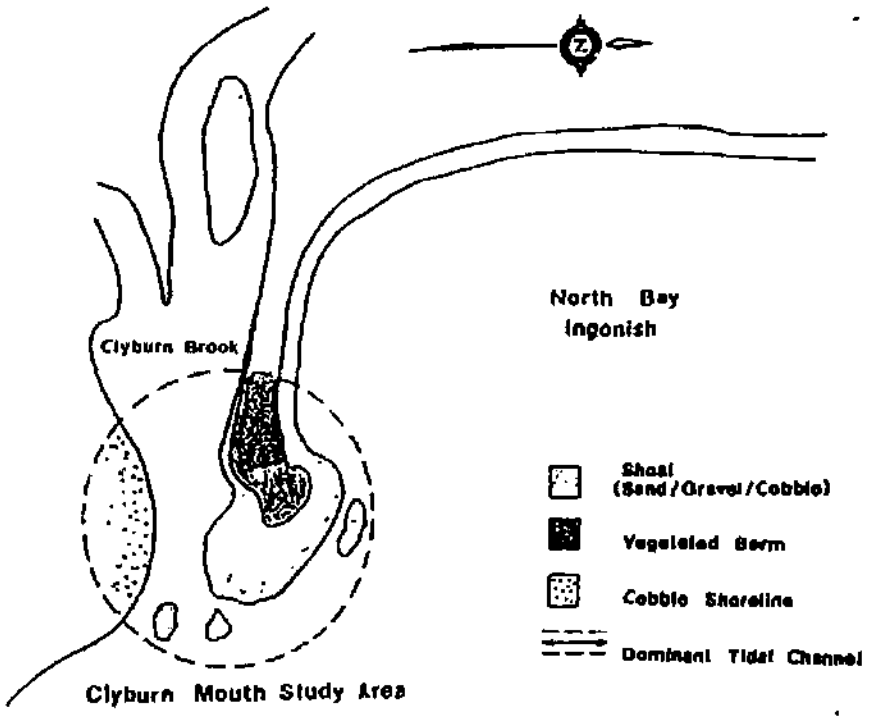

Figure 11. Littoral and fluvial sedimentation study area (ADI, 1993).

ADI-Nolan Davis determined that:

(1) at the mouth of the river the northern shoal had migrated across the mouth toward the south shoreline and narrowed the main channel (Figure 12, a and b), and

(2) channel flow velocities at the mouth have been reduced through a combination of rising sea level and "damming of the mouth" (ADI, 1993).

A shoal is also known as a barachois, which is a spit of unconsolidated sediments that forms a barrier between the mouth of the river and the sea. The river eventually bypasses the barrier and connects to the sea, but it does so at some lateral distance from the original connection to the sea.

The recent shoal migration possibly reduced the hydraulic efficiency at the mouth. This lower efficiency of water removal at the mouth could increase the potential for flooding and/or ice jams.

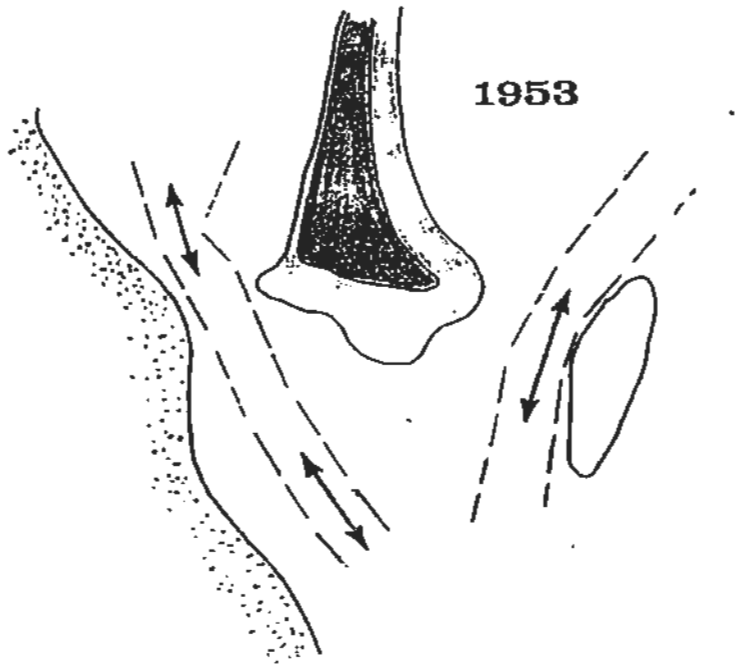

Figure 12. (a) Shoal location: 1953 (ADI, 1993).

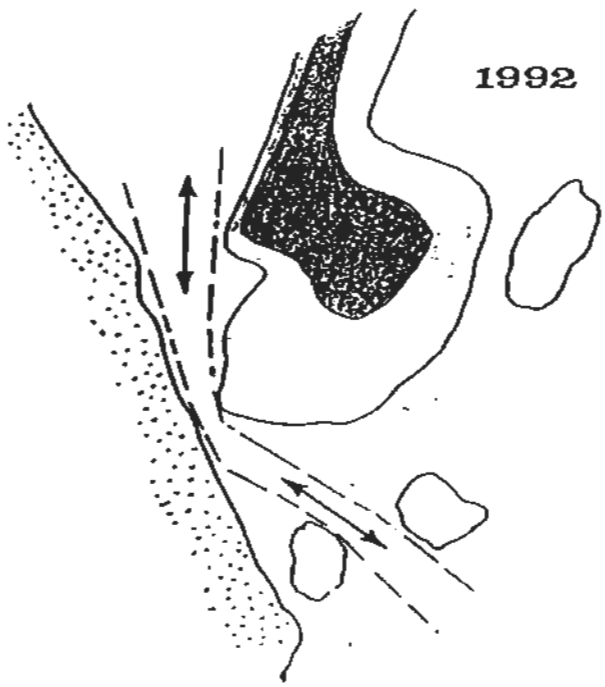

Figure 12. (b) Shoal location and migration: 1992 (ADI, 1993).

Suggestions made as a result of the ADI-Nolan Davis study were as follows:

(1) install a hydrometric station in the brook. This would take continuous readings of stage water height (and implies the necessity of developing a stage-discharge rating curve for the station);

(2) implement surface and groundwater chemistry sampling throughout the year;

(3) survey channel cross-sections; and

(4) establish a long-term climate monitoring station.

2.3.2 CBCL Limited

In 1995 CBCL Limited, Consulting Engineers, undertook an aquifer assessment of the Clyburn Brook. CBCL examined the impact of increased demand on groundwater resources. The assessment focused on the existing infiltration gallery constructed in the 1960's, near hole number 12 of the Highland Links golf course. The results of a pump test are outlined in Table 1 below.

Table 1 – Comparison of CBCL three-day pump test data and unconfined aquifer values

	Transmissivity (T)	Effective radius of influence	Storativity (S)	K_r	K_z	$K_r : K_z$
				Hydraulic conductivity in radial direction (r)	Hydraulic conductivity in vertical direction (z)	Ratio
Three-day pump test	1115 m^2/d to 1208 m^2/d (90,000-100,000 USgpd/ft) Distance drawdown: 909 m^3/d/m (73,000 USgpd/ft)	91.4 m (300 ft)	0.2	213.3 m/d (700 ft/d)	21.3 m/d (70 ft/d)	10-20/1
Unconfined aquifer values (typical)		Up to 305 m (1,000 ft)	0.01-0.3			10/1 common for this type of setting

Conversions: 1 USgal = 0.134 ft^3 1 ft^3 = 0.02832 m^3 1 ft^2 = 0.0929 m^2

After three days of pumping at a constant rate of 2087 L/min (550 USgpm) with a 6 hour recovery, a drawdown of only 3.8 m (12.6 ft) was observed in the pumping well. This suggested that the well was performing at 60% efficiency. Well efficiency is determined by comparing the actual drawdown (measured) to the theoretical drawdown using the Theis equation. This value was noted as being relatively high. The calculated long-term (20 year) safe yield was 1328 L/min (350 USgpm); short-term (2 year) was 1518 L/min (400 USgpm). It was stated that three wells would, therefore, be required to meet the demand of 3605 L/min (950 USgpm). An analysis of low flow conditions suggested that the brook could not yield the required base flow of 25% of the mean annual flow. Consequently, during low-flow conditions, it was

suggested that the brook be monitored closely and used for irrigation purposes only with proper authorization from the CBHNP.

Based on this study, the following recommendations were made:

(1) During low flow conditions, irrigation should be monitored and reduced. If flow in the brook becomes less than 826 m^3/s (13,060 USgpm), irrigation should cease;

(2) All wells should be located along the length of the brook. Wells for potable water should be spaced at least 30.5 m (100 ft) apart. Three new irrigation wells should be constructed using a vertical screened well design and separated by at least 152 m (500 ft);

(3) Future production wells should undergo a seven-day pump test analysis and at least one additional observation well should be constructed. Before additional pump tests, the natural water level trend should be established over a period of 3 to 7 days prior to the test. That is, if the water level is naturally fluctuating downward or upward, it can affect the observed drawdown, making it appear to be more or less than it actually is;

(4) Environmental impacts should be considered prior to well installation, pipeline or electrical conduit construction; and

(5) Water sampling should be performed on a regular basis and implemented into a reporting database (random water samples taken during 1973-1991 formed part of the CBCL study).

As a result of the CBCL study, two potable wells and three irrigation wells were constructed in the area (Figure 13).

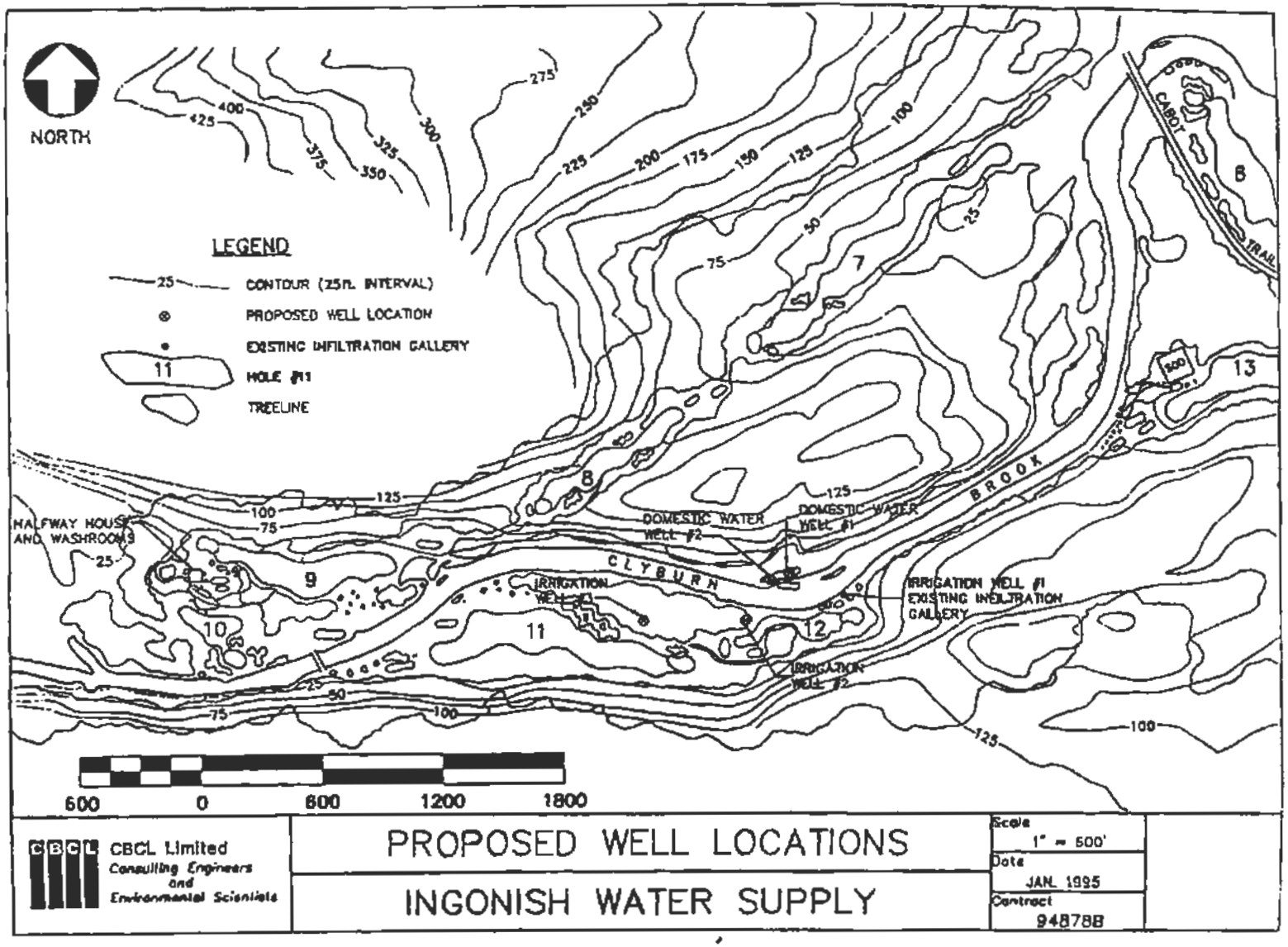

Figure 13. CBCL proposed well location map (CBCL, 1995).

2.3.3 Canadian Heritage Parks Canada

Canadian Heritage Parks Canada (CHPC) has implemented a study of the Clyburn Brook watershed and sub-watersheds. In 1999, Dawn Allen of CHPC created a graphical summary of the Clyburn Brook watershed and sub-watersheds. This summary contains a location map and some of the delineated features of the watershed, such as hypsometry, topography, slope, vegetation, soil texture, aspect, and drainage data. This data is presented in the form of digital watershed maps, with pie charts showing distribution among the sub-watersheds. The topographic data is a 3-D digital elevation model, generated using the SPANS program (see Figure 2). The 3-D model shows the locations of sub-watersheds A to H. Elevation cross-sections through various parts of the watershed have also been generated.

2.3.3.1 Dalhousie University

Dr. David Hansen of Dalhousie University is currently doing research for CHPC. He has measured streamflow velocities, water levels (W/L) and discharge, and has studied areas of fish habitat within the brook. During the course of the year 2000, D. Hansen and others surveyed the Clyburn Brook, cross-sections for the 'Upstream Reach' and 'Downstream Reach' portions of the brook were the result (Figures 14 and 15). In Figures 14 and 15, the contour interval is 5 m. The first bold contour line to the right or left of the brook in Figure 14 is 25 m. At the bottom of Figure 15, the first bold contour line to the right or left of the brook is also 25 m. Each cross-section (XS) contained elevation data referenced to Canadian Geodetic Datum (CGD) and

ran from the ground surface of the south bank to the north bank of the brook, and included water surface elevations in metres (CGD). Figure 16 contains survey cross-sections 3 and 7. In particular, the 'Upstream Reach' began at the golf cart bridge as XS 8 and ended to the southeast at XS 1; the 'Downstream Reach' began at XS 6 and ended to the southeast at XS 1 [note: not the same location as Upstream Reach XS 1], near the Cabot Trail Highway bridge.

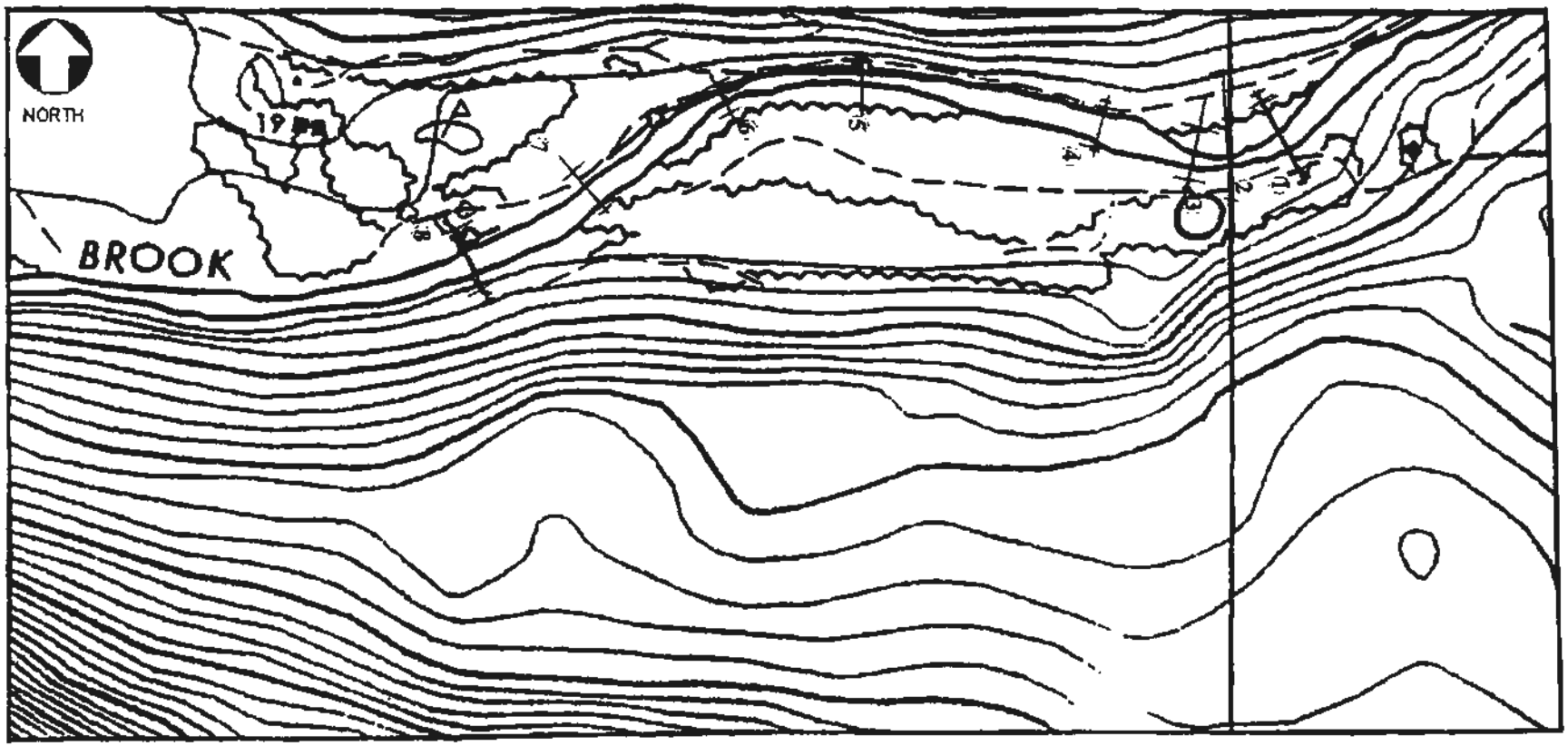

Figure 14. Upstream Reach of Clyburn Brook showing locations of surveyed cross-sections 8 to 1 from west to east (scale 1 cm = 56 m) (contour interval = 5 m) (coordinates: bottom left corner = N5162800 E4582000, top left corner = N5169000 E4582000).

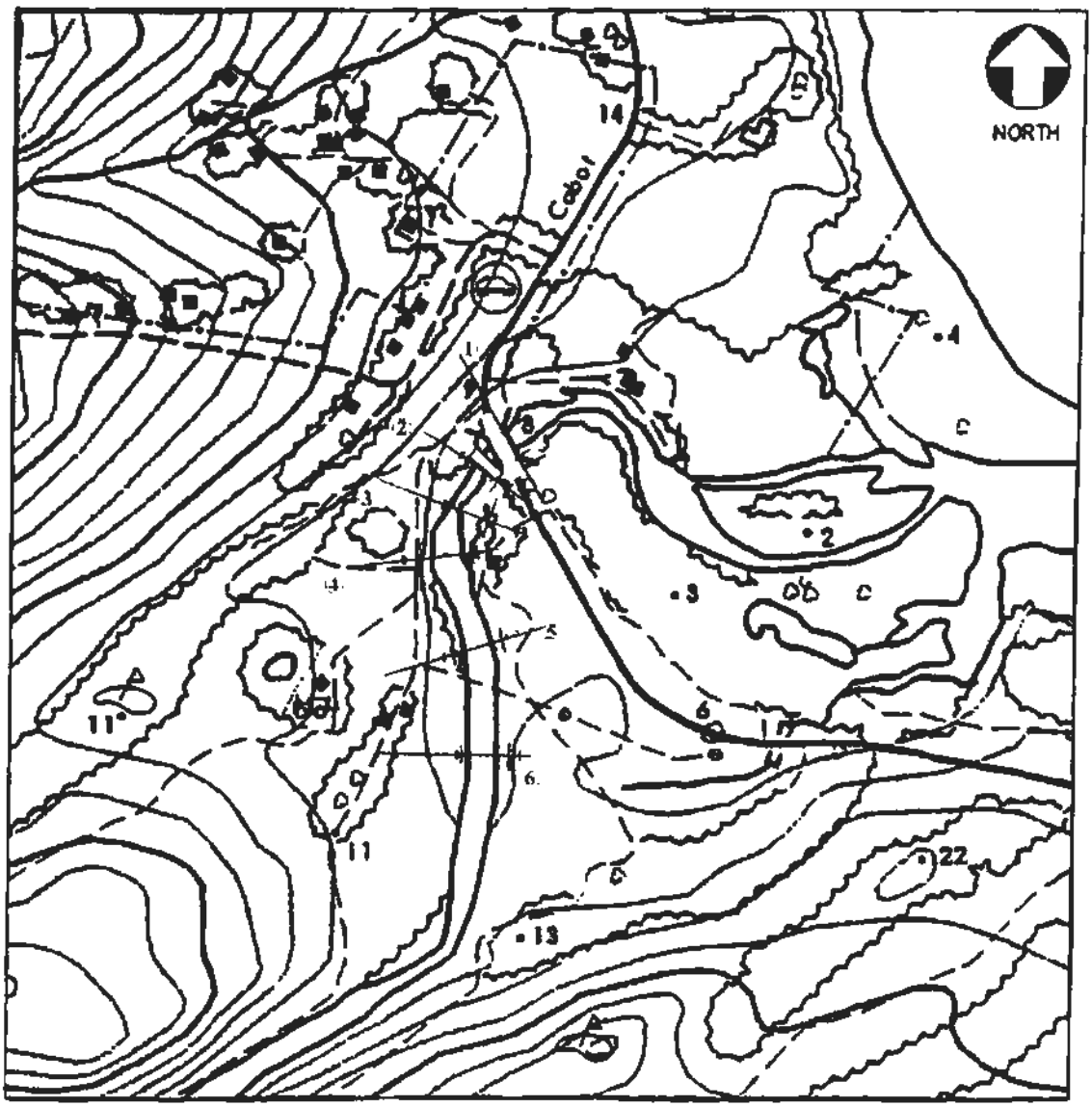

Figure 15. Downstream Reach of Clyburn Brook showing locations of surveyed cross-sections 1 to 6 from east to west (scale 1 cm = 48 m) (contour interval = 5 m) (coordinates: bottom left corner = N5169000 E4583000, top left corner = N5170000 E4583000).

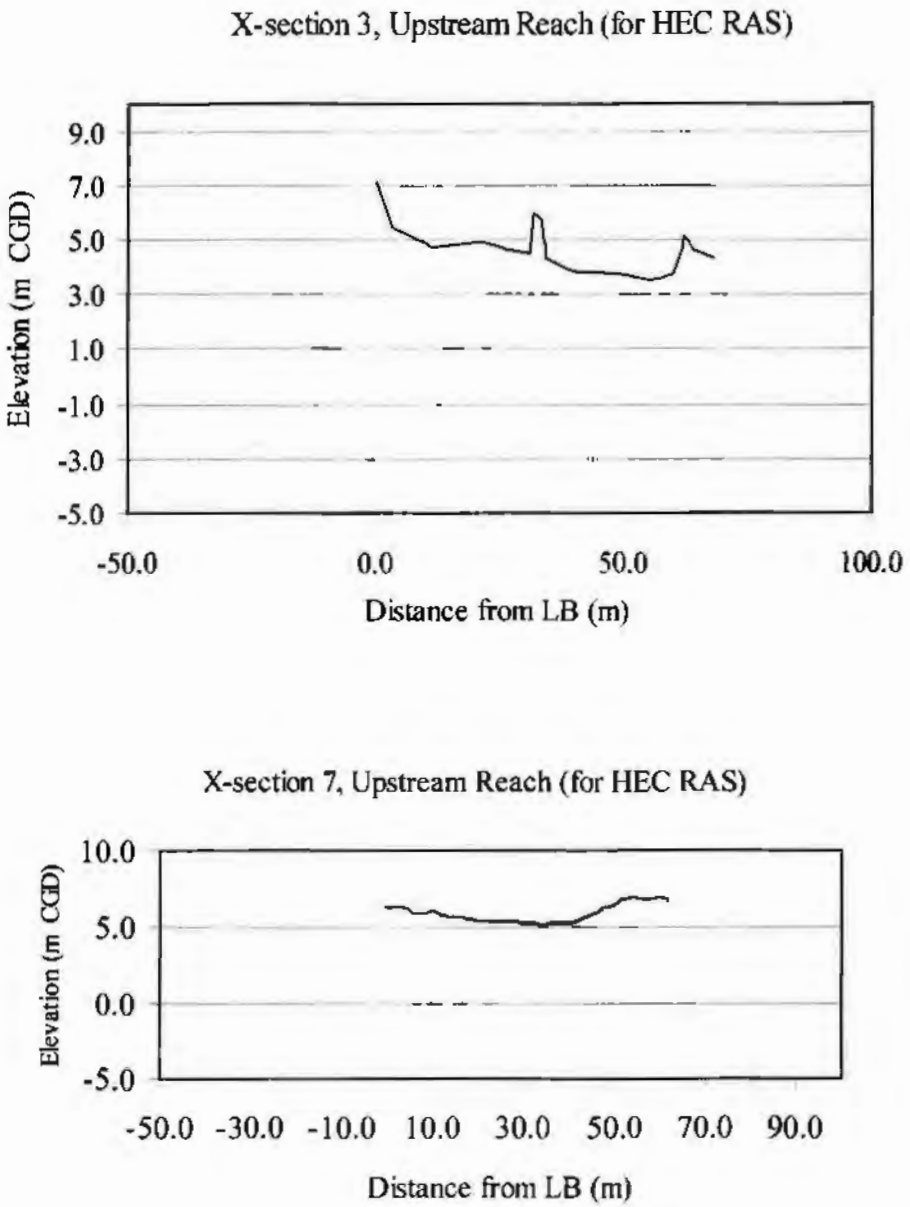

Figure 16. Survey cross-sections 3 and 7 (LB = left bank (south), whereas right bank is to the north) (Hansen *et al.*, unpublished).

A summary of the data collected is set out below:

Upstream portion				
		Elevation (m CGD)		
Cross-section	Length (m)	South Bank	North Bank	W/L (m CGD)
8	81.0	7.63	7.26	5.46
7	61.6	6.35	6.93	5.20
6	38.7	5.19	5.27	3.88
5	47.7	7.41	5.65	4.12
4	49.3	5.85	5.17	4.13
3	68.1	5.94	5.16	3.89
2	139.1	4.72	4.23	3.67
1	83.1	4.99	5.38	3.54

Downstream portion				
		Elevation (m CGD)		
Cross-section	Length (m)	South Bank	North Bank	W/L (m CGD)
6	59.6	2.41	2.39	0.87
5	66.2	1.46	2.67	1.20
4	66.3	3.78	2.04	0.50
3	49.8	2.56	2.82	0.55
2	57.5	6.39	4.42	0.30
1	116.9	5.37	4.60	0.15

In 2001, a baseflow recession analysis was undertaken by Hansen *et al.* of Dalhousie University (unpublished). Solinst® units were placed in the brook, which recorded pressure and temperature every 15 minutes. The data collected was used to calculate water surface elevations and to compile stage records for the Clyburn Brook. The stage records were converted to hydrographs using a rating curve that was based on five actual flow measurements. Flow measurements were made using a current meter and the velocity-area method (Herschy, 1998) by Environment Canada personnel. The hydrographs, shown in Figures 17, 18 and 19, were then analyzed with respect to baseflow recession.

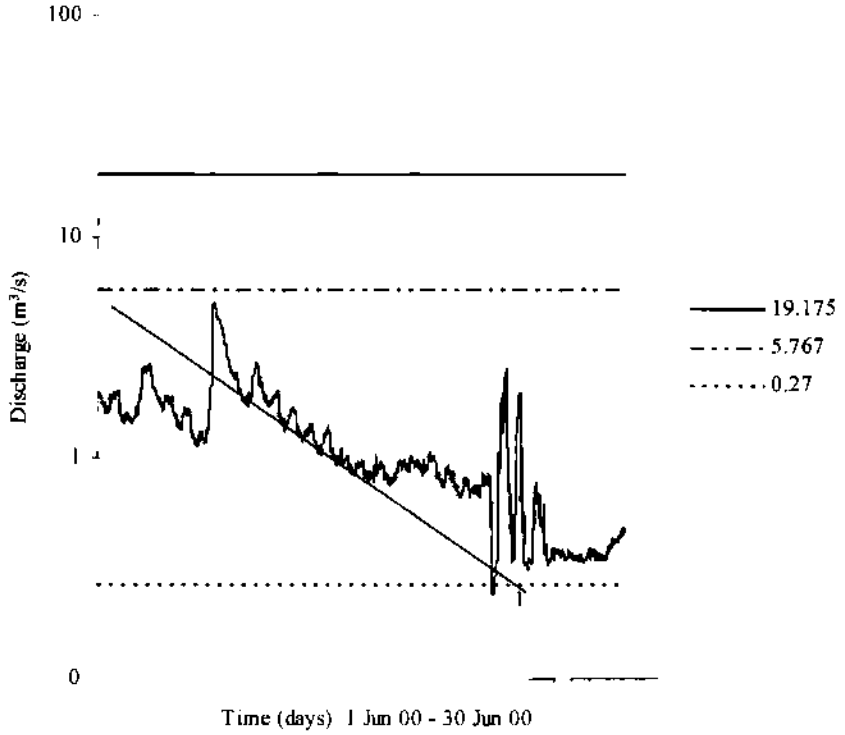

Figure 17. Clyburn Brook hydrograph for June 2000 showing recession line 1 (Hansen *et al.*, unpublished).

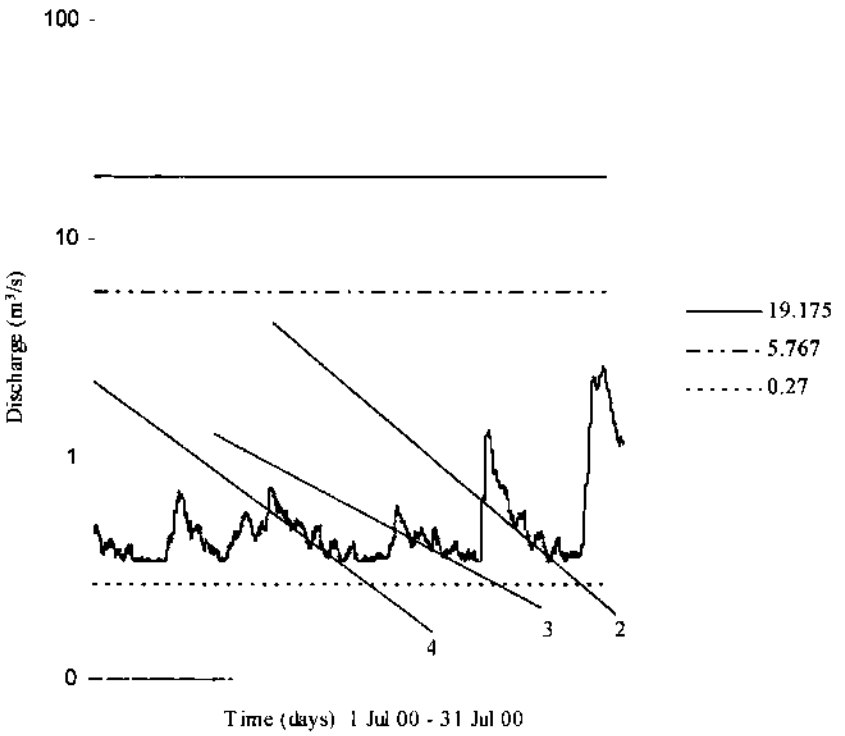

Figure 18. Clyburn Brook hydrograph for July 2000 showing recession lines 2, 3 and 4 (Hansen *et al.*, unpublished).

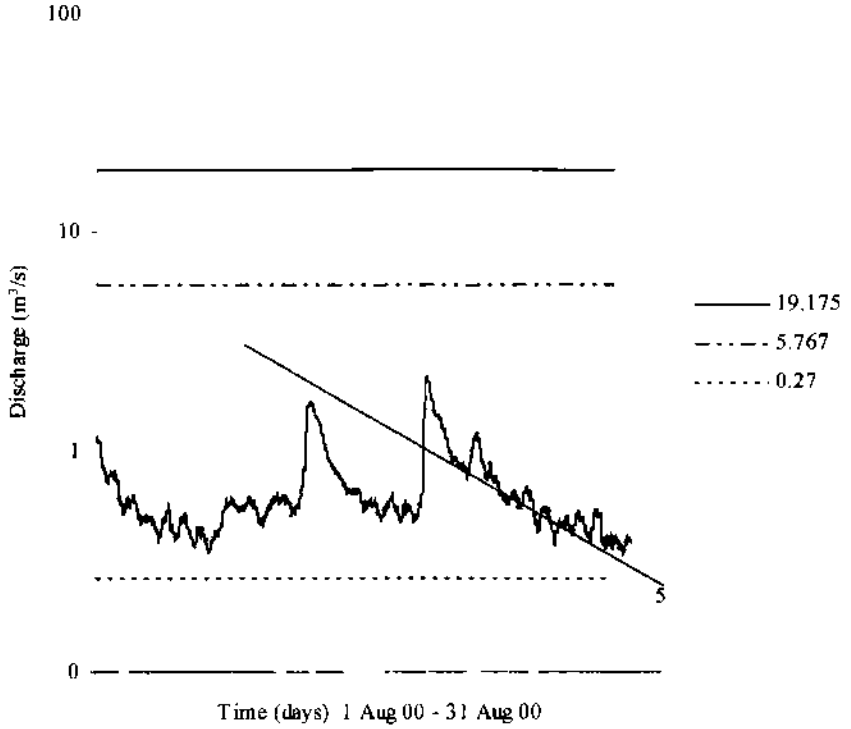

Figure 19. Clyburn Brook hydrograph showing recession line 5 (Hansen *et al.*, unpublished).

The data used for the baseflow recession analysis is summarized in Table 2 (Hansen *et al.*, unpublished).

Table 2 – Baseflow recession calculations for Clyburn Brook

Recession Line #	Q (m^3/s)	Q_o (m^3/s)	Δt (days)	K_{rec}
1	0.80	4.80	15	0.887
2	0.22	3.80	19	0.861
3	0.22	1.00	16	0.910
4	0.18	2.00	18	0.875
5	0.30	2.85	22	0.903
			K_{rec} (mean)	0.887
			t_s	8.35 days

where Q_o = initial flow
Q_1 = flow at $t + \Delta t$
Δt = time increment
K_{rec} = recession constant
t_s = time of storage [see Section 3.3.1]

The information gathered by Hansen *et al.* (unpublished) was used in the studies outlined herein. The survey data, time of storage (t_s) of the Clyburn Brook watershed, and fish habitat analysis were of particular interest.

The hydraulic assessment also examined fish habitat preferences and fish habitat quality during rates of low flow in the Clyburn Brook using criteria such as those found in Tenant (1976). The results are summarized in a plot of depth versus flow, with some fish habitat preferences indicated thereon (Figure 20).

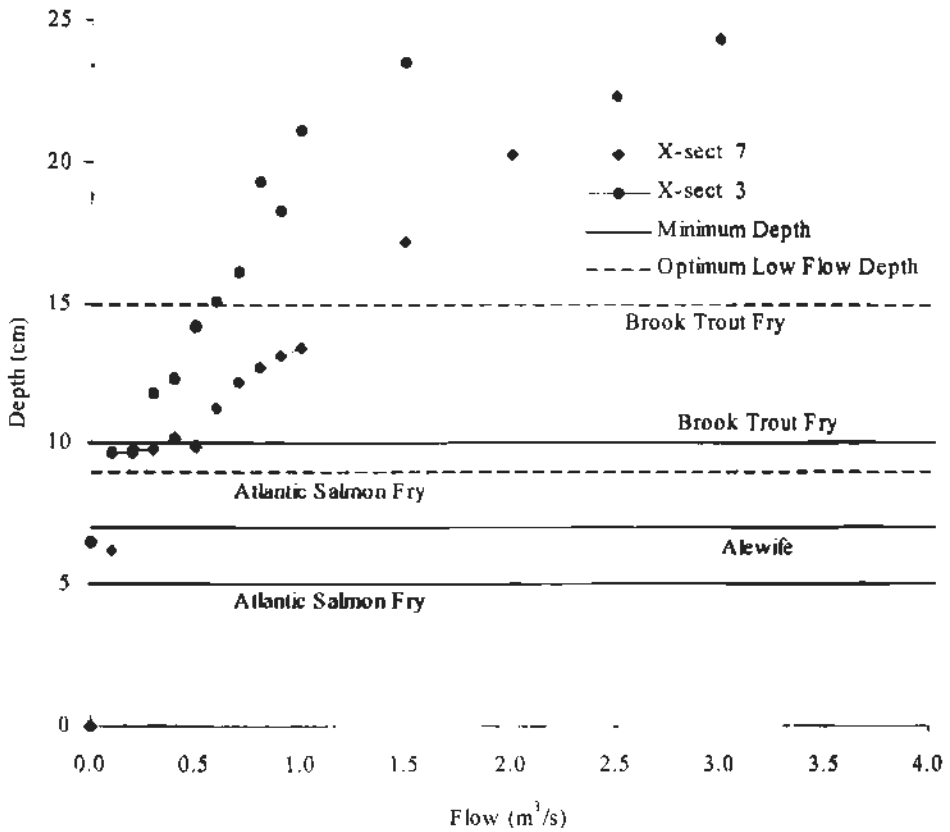

Figure 20. Depth versus flow for two riffle sections and some fish habitat preferences. Cross-sections 3 and 7 were located in the Upstream Reach of the Clyburn Brook (Hansen *et al.*, unpublished).

The baseflow recession behavior presented by Hansen *et al.* (unpublished) was compared to the results obtained in this research; in particular, the numerical modelling and baseflow contribution studies. These comparisons form part of the discussion in Chapter 4.

3 DATA AND METHODOLOGY

3.1 Seismic Study

A seismic study is an important tool for gaining information on the physical characteristics of rock materials underground. The equipment required is several geophones (e.g. 12), a spread cable of a pre-determined length (e.g. 12, 36 or 120 m), a shot source, and a seismograph (the data recording unit).

A geophone commonly records more than one arrival of seismic energy. This occurs because the energy may radiate from the source in a variety of forms (body or surface waves) and body waves are refracted and reflected along different paths when they encounter boundaries (Lillie, 1999). The travel times and known horizontal distances can be used to determine the velocity of the seismic wave, the material it is passing through, and its depth of penetration.

3.1.1 Refraction Theory

Seismic energy travels from the source along raypaths. When a ray crosses the interface between two layers, the ray is refracted toward the interface if the velocity of the upper layer (V_1) is less than the velocity of the lower layer (V_2) (Figure 21).

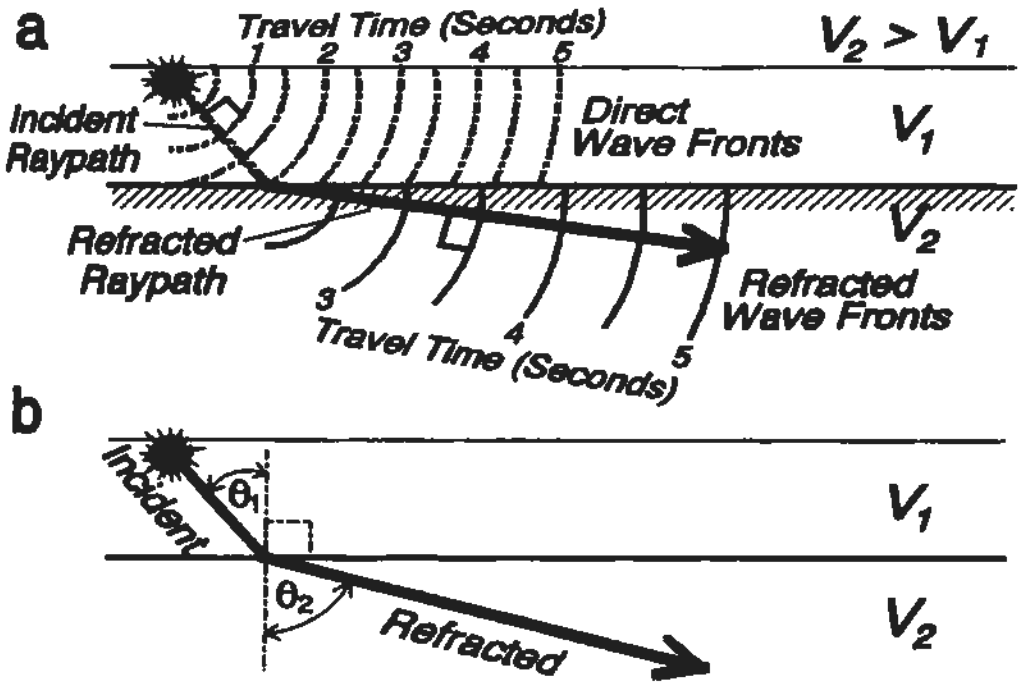

Figure 21. Refraction from layer 1 to layer 2. a) Wave fronts are distorted from perfect spheres as energy is transmitted into a material of different velocity. Raypaths, therefore, bend ("refract") across an interface where velocity changes. b) The incident (Θ_1) and refracted (Θ_2) angles are measured from a line drawn perpendicular to the interface between the two layers. (Lillie, 1999)

Raypaths refract according to Snell's Law:

$$\frac{\sin\Theta_1}{V_1} = \frac{\sin\Theta_2}{V_2} \qquad [1]$$

where Θ_1 = angle of incidence (degrees)
Θ_2 = angle of refraction (degrees)
V_1 = seismic velocity of incident medium (m/s)
V_2 = seismic velocity of refracting medium (m/s)

A special situation occurs when the angle of refraction reaches 90°. This only occurs when $V_2 > V_1$ and is known as critical refraction. The angle of incidence necessary

for critical refraction is known as the critical angle (Θ_c). At the critical angle, Snell's Law becomes:

$$\Theta_c = \sin^{-1}\left(\frac{V_1}{V_2}\right) \quad [2]$$

where V_1 = seismic velocity of the upper layer (m/s)
V_2 = seismic velocity of the lower layer (m/s)

A critically refracted wave travels along the boundary and a direct wave travels in the upper, lower velocity layer (Figure 22). Therefore, at distance, the refracted signal may arrive at the geophone before the direct signal (Lillie, 1999). The travel time (t) for a critically refracted arrival from a single horizontal interface is:

$$t = t_1 + \frac{x}{V_2} \quad [3]$$

with

$$t_1 = \frac{2h_1 \cos\Theta_c}{V_1} \quad [4]$$

where t_1 = travel intercept time (s), at x = 0
x = horizontal distance (m)
h_1 = thickness or depth of layer 1 (m)

The time it takes for the sound to reach each geophone is its travel time. The travel time depends on the seismic velocity of the Earth material it is encountering and the presence and shape of boundaries between various types of material (Lillie, 1999).

Seismic arrivals are plotted on a graph of distance vs. time (Figure 22). The direct arrivals are observed first. The refracted arrivals only appear after the critical

distance (X_c). At the critical distance, the reflected waves and the critically refracted waves arrive at the same time.

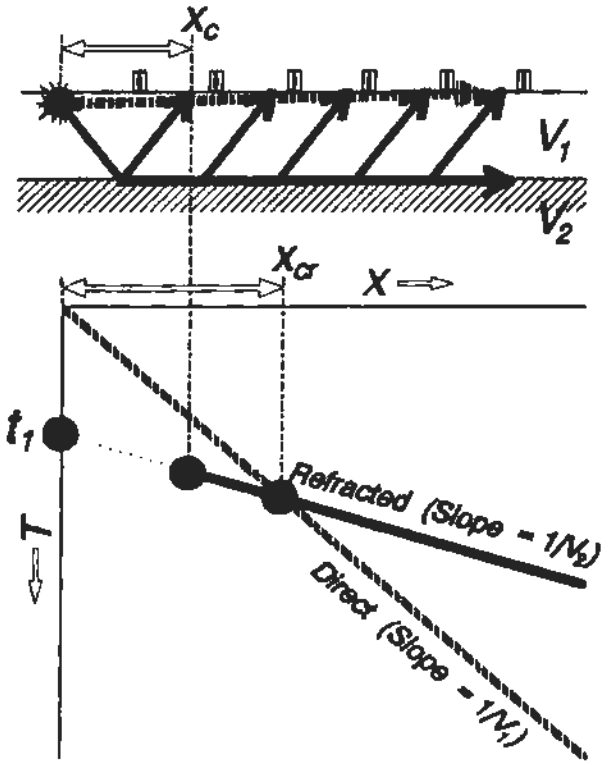

Figure 22. Raypaths and travel-time graph for direct and critically refracted arrivals. X_c = critical distance; X_{cr} = crossover distance. (Lillie, 1999)

Best-fit lines are compared to the data points to obtain the slope of each line (direct and refracted). The slope of the line (s/m) is equal to the inverse velocity (1/V). For the refracted arrival, the t-intercept is the travel intercept time (t_I). The critical distance is determined by

$$X_c = 2h \tan \Theta_c \qquad [5]$$

Near the source, the direct wave appears before the critically refracted wave. At the crossover distance (X_{cr}), the direct and critically refracted waves appear at the same

time. With increasing distance, the critically refracted arrival appears first because proportionally more of the refracted travel path is through the higher velocity layer (V_2) (Lillie, 1999). The crossover distance is determined by

$$X_{cr} = 2h\sqrt{\frac{V_2 + V_1}{V_2 - V_1}} \qquad [6]$$

True velocity refers to the actual speed at which seismic energy travels through a material along a straight line. A seismic wave emerging at Earth's surface, however, appears to travel with a certain velocity across a horizontal array of receivers (Lillie, 1999). This apparent velocity is defined as

$$V = \frac{\Delta x}{\Delta t} \qquad [7]$$

For a single dipping interface, the apparent velocities observed at the surface are not equal (Lillie, 1999). In the field, this means that for a forward shot and a reverse shot along the same line, two different velocities would be measured. When the source shoots downdip toward the geophones, the apparent velocity is lower than the true velocity. The opposite occurs when shooting updip. By shooting reversed refraction profiles, the dip of the interface can be determined. Seismic travel times are then plotted on the same travel-time graph using the same scale and analyzed. The intercept times for the updip and downdip shots are not equal, however, the travel times from end to end should be equal because the same raypath is followed.

The apparent velocities for the refracted arrival when shooting in the downdip and updip directions are defined as

$$V_{2d} = \frac{V_1}{\sin(\Theta_c + \alpha)} \qquad V_{2u} = \frac{V_1}{\sin(\Theta_c - \alpha)} \qquad \textbf{[8, 9]}$$

where V_{2d} = apparent velocity shooting downdip (m/s), measured from graph
V_{2u} = apparent velocity shooting updip (m/s), measured from graph
V_1 = velocity of the overlying layer (m/s) (direct ray)
Θ_c = critical angle (degrees)
α = dip of the interface (degrees)

The dip of the interface and the critical angle can be determined by substituting V_{2d} and V_{2u} in the following equations:

$$\alpha = \frac{\sin^{-1}\left(\frac{V_1}{V_{2d}}\right) - \sin^{-1}\left(\frac{V_1}{V_{2u}}\right)}{2} \qquad \textbf{[10]}$$

$$\Theta_c = \frac{\sin^{-1}\left(\frac{V_1}{V_{2d}}\right) + \sin^{-1}\left(\frac{V_1}{V_{2u}}\right)}{2} \qquad \textbf{[11]}$$

The true value of V_2 can be determined from the travel-time graph by obtaining the velocity of the overlying layer (V_1) from the travel-time graph and then solving for the velocity of the refracting layer (V_2) using Snell's Law. The vertical depths to the interface are (Telford, *et al.*, 1976):

$$z_d = \frac{V_1 t_{2d}}{2\cos\Theta_c} \qquad \textbf{[12]}$$

$$z_u = \frac{V_1 t_{2u}}{2\cos\Theta c} \qquad \textbf{[13]}$$

where z_d = vertical distance to interface shooting downdip (m)
z_u = vertical distance to interface shooting updip (m)

t_{2d} = V_{2d} travel intercept time (s), at x = 0
t_{2u} = V_{2u} travel intercept time (s), at x = 0

These mathematical relationships are used to determine the physical characteristics of materials under the Earth's surface.

3.1.2 Reflection Theory

When seismic energy reaches a boundary between two layers, some of the energy is reflected back into the first layer. According to Snell's law, the angle of incidence (Θ_1) and the angle of reflection (Θ_2) must be equal because both rays travel at the same velocity (Lillie, 1999). Consequently, reflected raypaths are v-shaped (Figure 23).

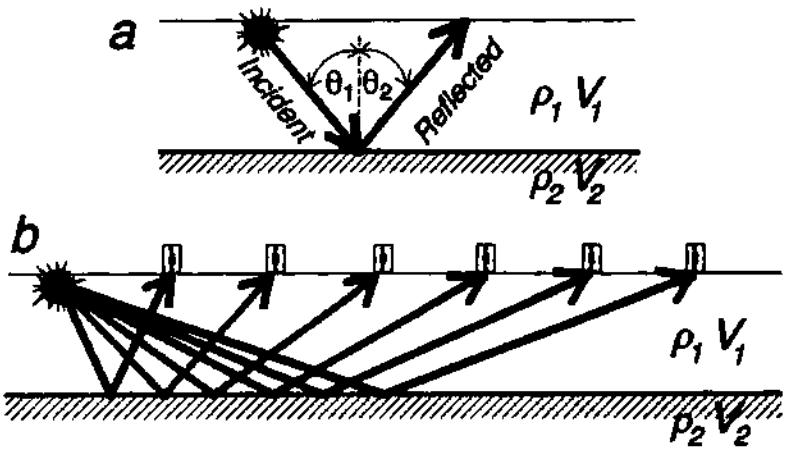

Figure 23. Reflection from horizontal interface. a) Geometry of reflected raypath. b) Raypath from source to receivers. (Lillie, 1999)

The travel time for a reflected wave, from source to receiver at horizontal distance (x), can be calculated by determining the total time spent in the constant velocity

layer (V_1). The time (t_o) to go vertically down to the boundary and straight back up to the shot location is, a constant, defined as

$$t_o = \frac{2h}{V_1} \qquad \textbf{[14]}$$

The travel-time equation for a reflected wave from a horizontal interface overlain by a constant velocity medium is defined as

$$t = \sqrt{t_0^2 + \frac{x^2}{V_1^2}} \qquad \textbf{[15]}$$

This is the equation of a hyperbola on a travel-time graph (Figure 24), where t_o = t-axis intercept time (s).

The value of t_o can be ascertained using the $X^2 - T^2$ method (eqn. 15 squared), in which the square of the travel time values (t^2) are plotted against the square of the distance values (x^2). This plots as a straight line, with a slope of $1/V_1^2$ and y-intercept of t_o^2. The square root of these values can be inserted into eqn. 14 to solve for depth.

A relationship occurs between the direct, critically refracted, and reflected arrivals. For instance, at long distances from the source, the travel-time curve for reflected arrivals is approximately the same as the travel-time curve for the direct wave through the upper layer (Lillie, 1999). At the critical distance, the reflected wave and the critically refracted wave have equal arrival times.

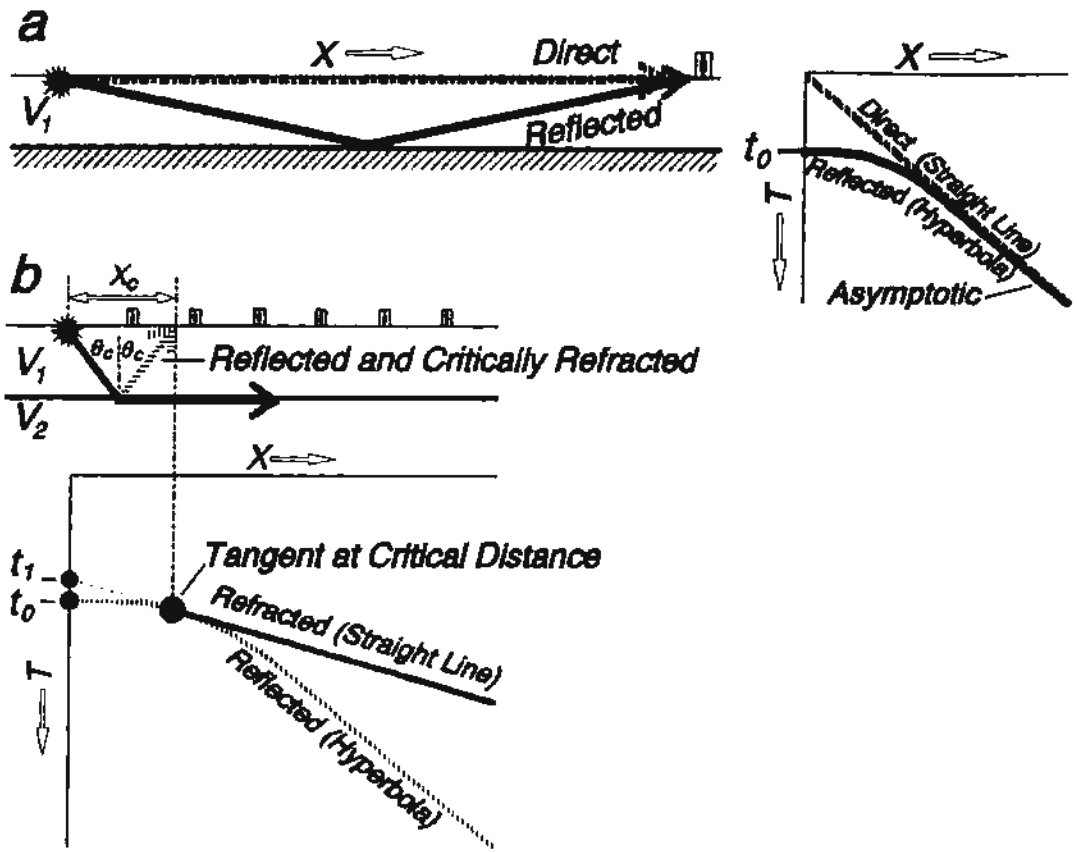

Figure 24. Relationships between reflected and other arrivals. a) Direct and reflected arrival curves are asymptotic at large distance from the source. b) Critically refracted arrival curve is tangent to that of the direct arrival at the critical distance (X_c) (Lillie, 1999).

There are several techniques for analyzing shot information. For example, some methods include the shot gather, the common mid-point (CMP) gather, and the normal moveout correction and stack (Lillie, 1999) (Figure 25).

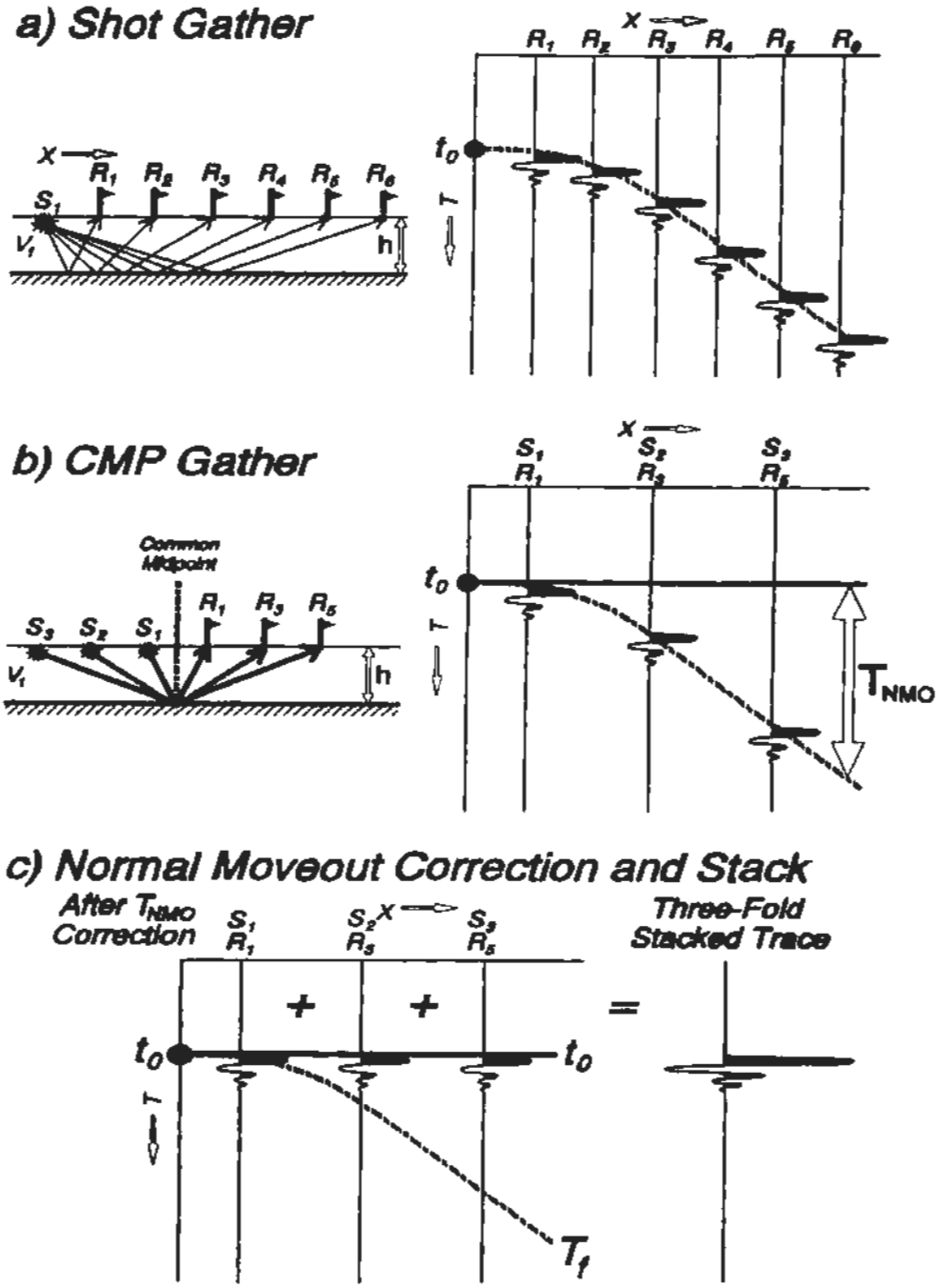

Figure 25. Raypath diagrams and travel-time graphs for shot and CMP gathers. a) Left: Raypaths for one shot with six receiver positions. Right: A shot gather is a travel-time graph of the resulting seismic traces, plotted according to horizontal distance (X) from the source. b) Left: Raypaths centered around a common midpoint, selected from shots 1, 2 and 3. Right: A common midpoint (CMP) gather is the travel-time graph, plotted according to horizontal distance (X) from the respective sources. c) Left: CMP gather after normal moveout (T_{NMO}) correction. The events are from the horizontal interface are in phase; peaks and troughs align so that they

constructively interfere when the traces are added together. Right: The reflected event on the resulting (3-fold) seismic trace shows enhanced amplitude (Lillie, 1999).

If a seismic shot is recorded with a simple array of 6 or 12 geophones along a straight line away from the shot point, the data can be analyzed using the shot gather method (Figure 25a). A seismic line can be analyzed by comparing travel times and their respective distances from the shot point. Provided that $\Delta x < h$, the apparent velocity of the seismic arrival can then be calculated using:

$$V = \frac{\Delta x}{\sqrt{2t_o \Delta T_{NMO}}} \qquad [16]$$

where t_o = t-axis intercept time (s)
ΔT_{NMO} = change in travel time (s)
Δx = change in distance (s)

If data from various shots are analyzed together, the common midpoint method can be used (Figure 25b). This method utilizes a common point on the surface that is halfway between the source and receiver pairs. Both the shot gather and the CMP gather plot as a hyperbola on a travel-time graph.

In addition to manipulating eqn. 14, the depth of the reflecting layer can also be interpreted using the following equation, which incorporates a correction for horizontal distance based on the geometry of the reflector (v-shaped).

$$h = \sqrt{\left(\frac{t^2 V^2}{4}\right) - (Op)^2} \qquad [17]$$

where Op = the optimum offset (m)

The means of determining the optimum offset is set out below.

According to Pullan and Hunter (1990), the optimum offset technique is a method that has proven beneficial in shallow reflection studies. It is well suited to mapping the overburden-bedrock interface and produces a large-amplitude reflection. Using this method, the output of a single geophone is examined, which is separated from the source by a pre-determined offset. The source and recording geophone are moved progressively down the line in equal increments, and the final seismic section is produced trace-by-trace using the reflected arrival of the geophone of interest. The optimum offset is chosen beforehand based on a few test reflection records. The first step is to record a number of test reflection shots in the survey area so as to determine the best recording parameters (including filter settings) and to choose the optimum offset. The seismic records should show a prominent bedrock reflection, characterized by the hyperbolic shape of the reflected arrivals. The first arrivals on the seismic record are formed by energy that has been refracted from the top of the WT, with the reflected arrivals appearing later in a characteristic hyperbolic shape. The optimum offset is chosen from within the optimum window. The optimum window is considered to be within the range of offsets that allows the reflection from the target horizon to be observed with a minimal amount of interference. The optimum offset is, therefore, chosen on a case-by-case basis (see Section 3.1.4.2).

As with the refraction method, the mathematical relationships of reflected arrivals can be used to ascertain the physical character of Earth materials underground.

3.1.3 Method

The seismic study was implemented using a controlled source at the shot point and 12 geophones laid out in a straight line (Figure 26). The geophones were equally spaced (e.g. 3 m) and connected to a cable, which was attached to the recording station.

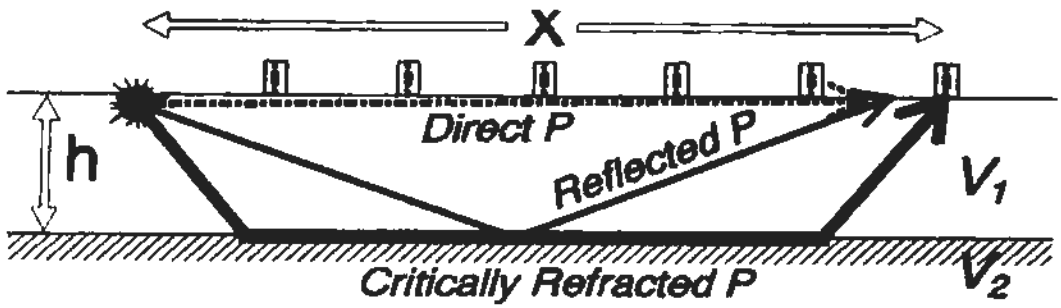

Figure 26. Seismic arrival raypaths (direct, critically refracted, and reflected) (Lillie, 1999)

The seismic energy was generated using a 'buffalo gun' and 12-gauge shotgun shells. The 'buffalo gun' is a long metal tube, about 1 m in length, with a screw-on barrel that holds a shotgun shell. A trigger switch on the gun was attached to the seismic recording unit. A hole was dug about 30 to 60 cm into the ground using a hand-held auger. Then, the gun was held upright and placed into the hole, barrel end down. When a rod was dropped through the 'buffalo gun', it hit the top of the shotgun shell, firing it. The firing of the shell into the ground generated a seismic impulse. This was heard only as a light thumping sound from aboveground. The energy traveled radially outward. Upon reaching each of the 12 geophones, an electrical voltage was generated and recorded by the seismograph. The seismograph

recorded an arrival at each of the 12 geophones and stored the information in one record file. The record file was usually maintained through several shots, with the arrivals at each geophone accumulating as primary reflectors. This improved the amplitude of reflections generated by stratigraphic changes, while lowering the amount of background noise (Lillie, 1999). After at least three shots, the signal-to-noise ratio was enhanced.

The seismic study was initially run in refraction mode using twelve 30 Hz geophones and spread cables of 1 m, 3 m, and 10 m spacing. The longest spread cable available, therefore, was 120 m.

3.1.4 Data

3.1.4.1 Refraction

The first seismic study at the Clyburn Brook was conducted in June 2000. Dr. Patrick Ryall and Charlie Walls of Dalhousie University operated the seismic equipment in refraction mode. The locations of the refraction seismic lines are shown in Figure 27, as a) eastern end and b) western end. The data was processed as part of this thesis study. The methods used to interpret the data are outlined in Section 3.1.1 above and the equations used referenced by number.

The purpose of the refraction study was to ascertain the depth to bedrock in certain areas within the Clyburn Brook canyon. All seismic lines were shot as reversed refraction profiles. Only the most representative seismic lines are outlined in this study. These lines were all located within the eastern end (Figure 27b). Calculated apparent velocities ranged from 350 to 6500 m/s. The lower range was

interpreted as dry till and the higher range as approaching typical bedrock velocities. An average depth of penetration was 8 m. As noted in Section 2.2.1, the bedrock in this vicinity is the Ingonish River tonalite. According to Telford *et al.* (1976), seismic velocities for granite and metamorphic rocks range from 3000 to 7000 m/s and alluvium lies in the lower range, from 0 to 2300 m/s. Lillie (1999) states velocities for seismic waves through igneous and metamorphic rocks as ranging from 3900 to 6200 m/s and unconsolidated sediments from 0 to 1900 m/s. Dry, unconsolidated sediments have low velocities, 300 to 500 m/s, whereas a velocity of approximately 1500 m/s is typical for water-saturated unconsolidated sediments (Pullan and Hunter, 1990).

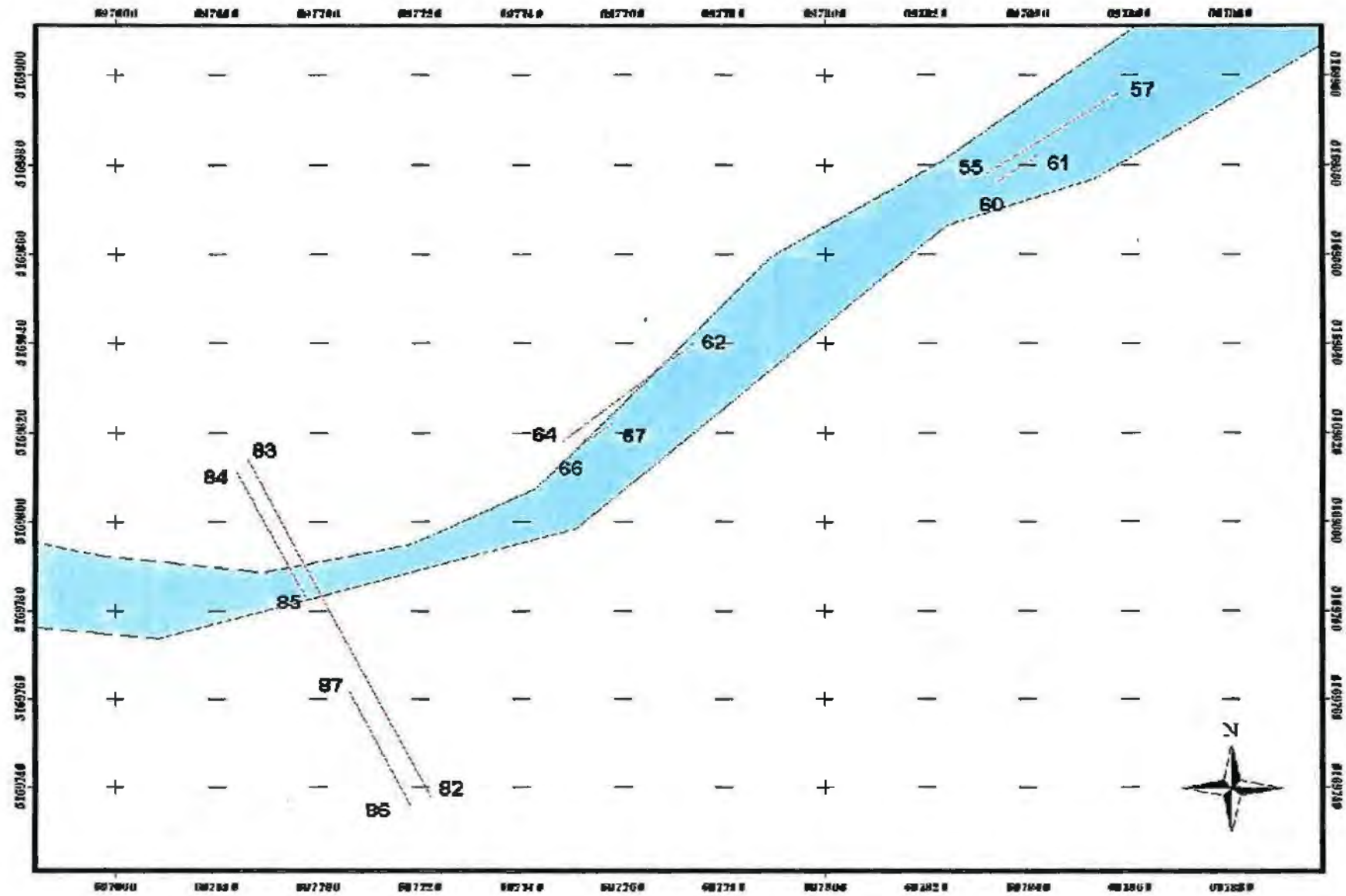

Figure 27. Refraction seismic study location maps (with location of the Clyburn Brook shown): **a)** eastern end.

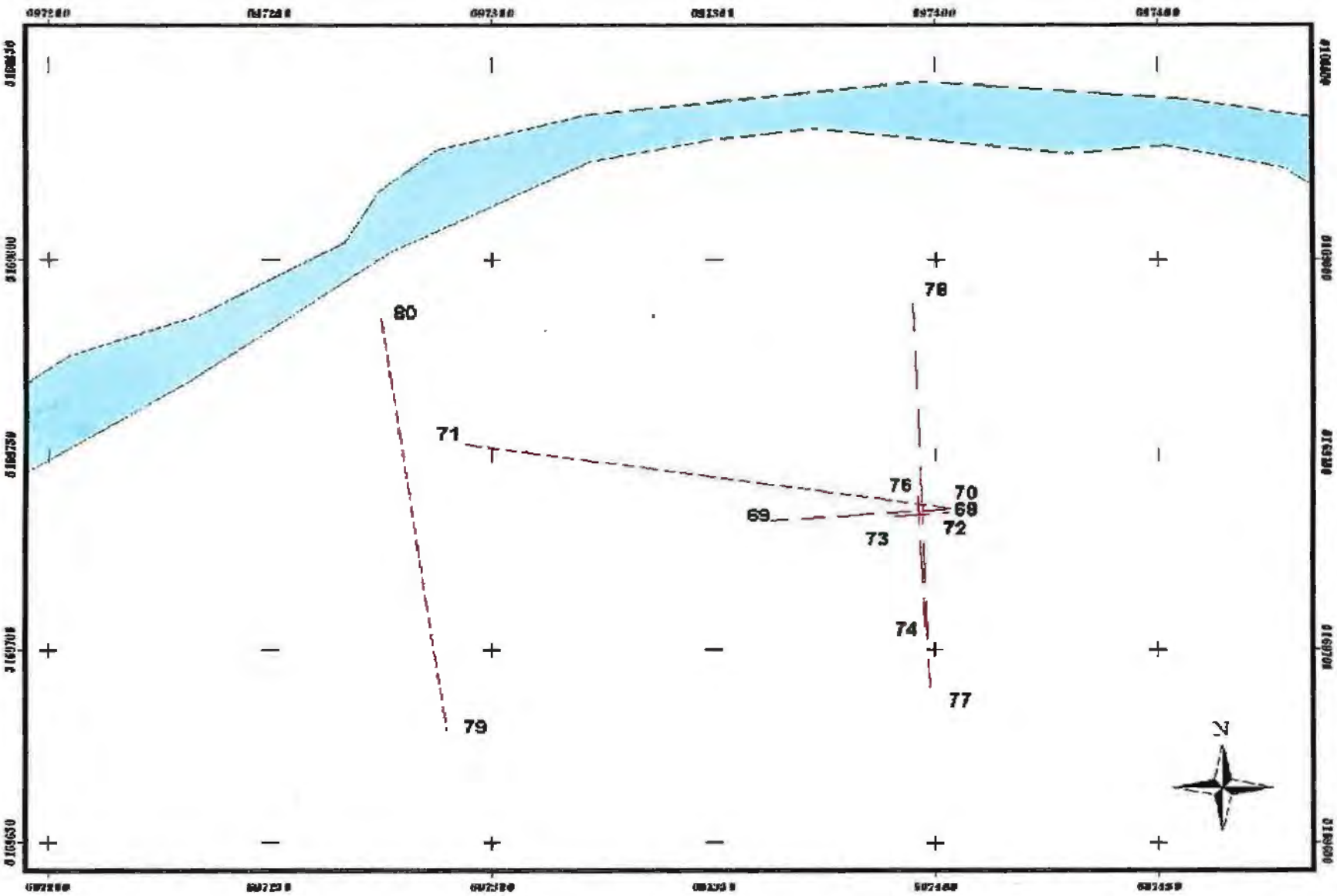

Figure 27. Refraction seismic study location maps (with location of Clyburn Brook shown): **b)** western end.

Refraction lines were shot as shown in Figure 27, a and b. Seismic lines 55 (forward) and 57 (reverse) were shot in the Clyburn Brook, in an area known as the bottleneck, at 3 m spacing. The 'bottleneck' is a portion of the Clyburn Brook that is constricted by and in closest proximity to the canyon walls. Each geophone was spaced 3 m apart and the shot point was 3 m away from the first geophone. The raw seismic data for these lines is shown in Figures 28 and 29.

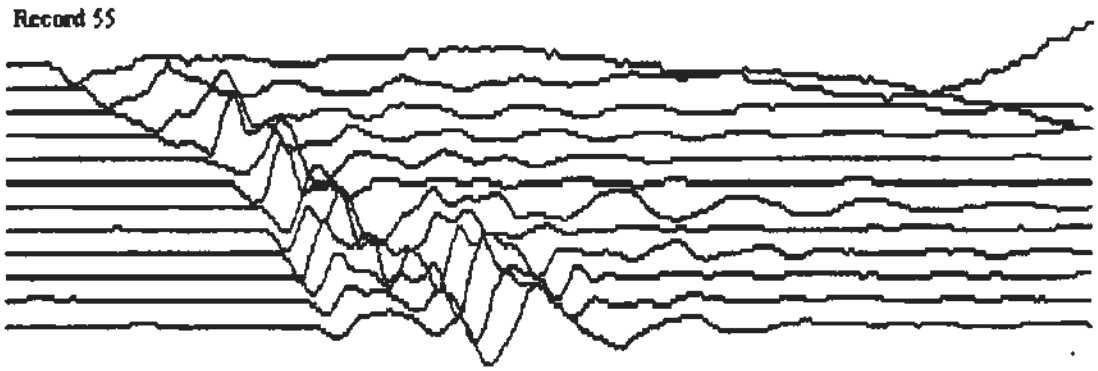

Figure 28. Raw seismic refraction data for forward shot, 55 (horizontal time scale = 50 ms).

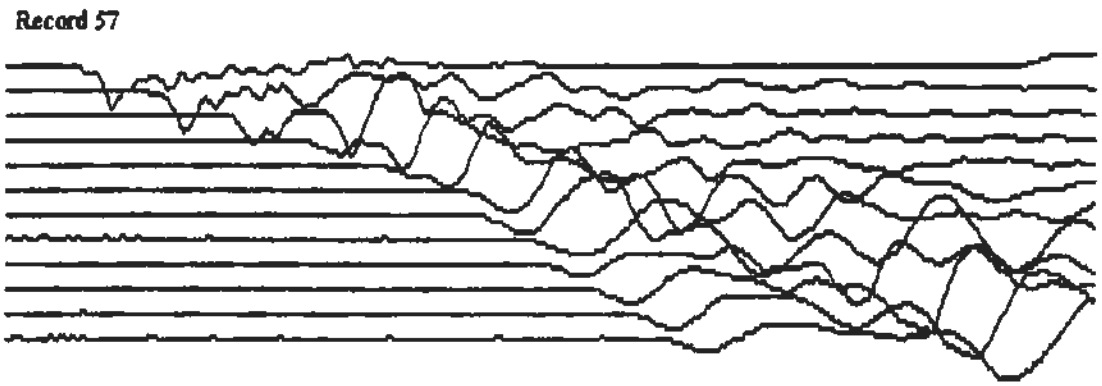

Figure 29. Raw seismic refraction data for reverse shot, 57 (horizontal time scale = 25 ms).

It was easy to observe two distinct travel-time velocities on each of the above figures. A slower velocity and then a faster velocity were recorded. The following travel times were measured from the raw seismic data:

Seismic Line 55 forward, 3m spacing		**Seismic Line 57** reverse, 3m spacing	
Distance (m)	55 Time (ms)	Distance (m)	57 Time (ms)
0	0.000	0	0.000
3	1.920	3	14.040
6	3.168	6	13.368
9	4.896	9	12.864
12	5.952	12	11.928
15	8.496	15	10.872
18	9.600	18	10.104
21	10.896	21	9.744
24	11.184	24	8.160
27	11.856	27	6.144
30	12.864	30	4.728
33	13.440	33	3.024
36	13.824	36	1.632

These travel times were then plotted on a distance vs. time graph (Figure 30).

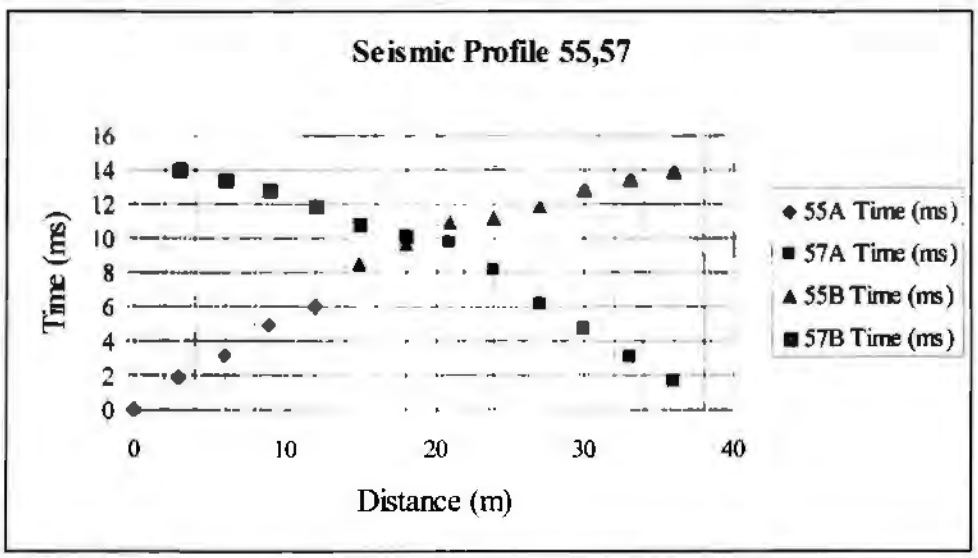

Figure 30. Travel-time graph, refraction seismic lines 55 and 57.

Apparent velocities were derived from the slopes on the travel-time graph. The slope (m) was determined using the equation of a best-fit trendline (y = mx + b). Since velocity is the inverse of slope, an average V_1 was derived from a plot of 55, 57A (Figure 31), V_{2d} from the 57B trendline and V_{2u} from the 55B trendline (Figure 32).

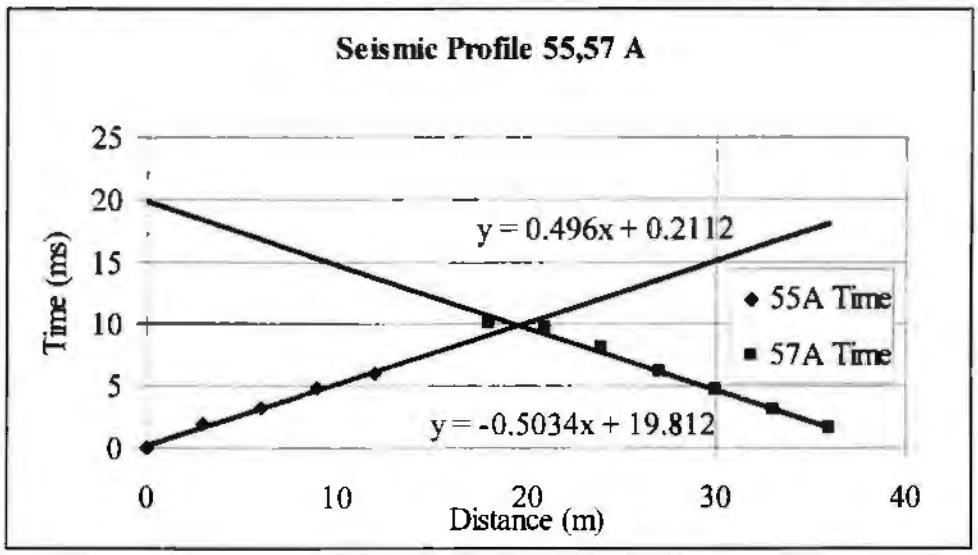

Figure 31. Determination of V_1 from refraction data

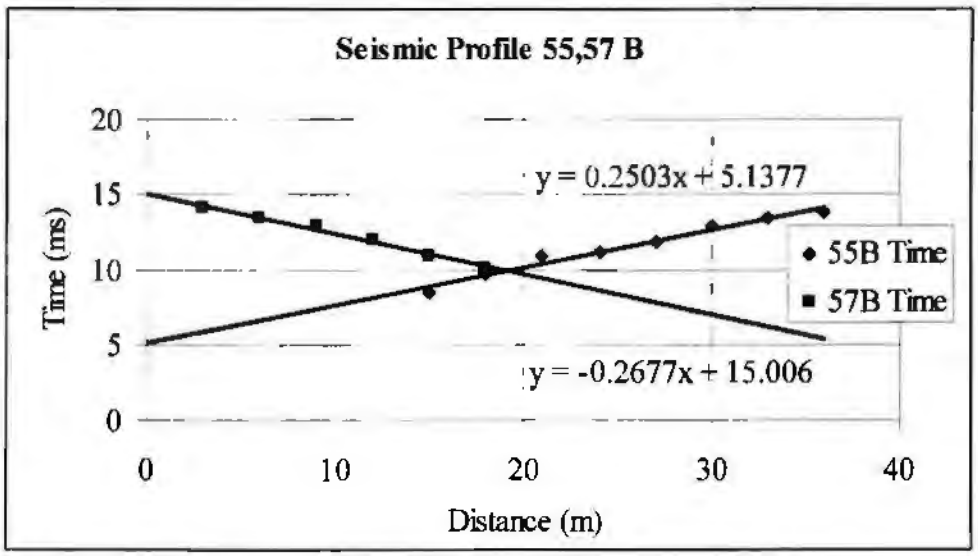

Figure 32. Determination of V_{2u} and V_{2d} from refraction data

As noted in Figures 31 and 32, the following slopes were calculated:

Line	Slope	Avg. Slope
V_1	0.4960 (Line 55) 0.5034 (Line 57)	0.4997
V_{2d}	0.2677	
V_{2u}	0.2503	

The dip angle and critical angles were calculated with eqns. 10 and 11 and used in eqns. 12 and 13 to determine the depths of penetration. A calculated V_2 (true velocity) was found using eqn. 2. The interpretation of these refraction seismic lines produced the results shown in Table 3.

Table 3 – Refraction seismic lines 55 and 57 interpretation and results

Seismic Lines 55 and 57		
V_1	2000 m/s	
V_{2d}	3735 m/s	Line 57
V_{2u}	3995 m/s	Line 55
α	1.2°	
Θ_c	31.2°	
V_2	**3860 m/s**	
t_{2d}	5.65×10^{-3} s	
t_{2u}	**8.10×10^{-3} s**	
downdip depth	**6.61 m**	
updip depth	**9.48 m**	

I interpret V_1 as representing the sediments in the brook (glaciofluvial sand and gravel) and V_2 as representing the bedrock under these sediments.

Refraction seismic lines 62 (reverse) and 64 (forward) were shot at 3 m spacing. These lines were shot in the same orientation as lines 55 and 57 but were located to the west of lines 55 and 57 (see Figure 27a). The following travel times were recorded:

Seismic Line 62 reverse, 3m spacing		**Seismic Line 64** forward, 3m spacing	
Distance (m)	62 Time (ms)	Distance (m)	64 Time (ms)
0	0.000	0	0.000
3	12.960	3	1.224
6	12.480	6	2.544
9	12.072	9	4.272
12	11.688	12	5.760
15	11.064	15	6.936
18	-	18	8.376
21	8.664	21	-
24	7.272	24	10.056
27	5.808	27	10.632
30	4.488	30	11.064
33	3.000	33	11.736
36	1.176	36	12.456

Interpretation of the seismic data was performed in the same manner as above and produced the slopes set out below and the results shown in Table 4.

Line	Slope		Avg. Slope
V_1	0.4912	Line 62	0.4823
	0.4734	Line 64	
V_{2d}	0.1960		
V_{2u}	0.1528		

V_{2d} corresponds to line 64 and V_{2u} corresponds to line 62.

Table 4 – Refraction seismic lines 62 and 64 interpretation and results

Seismic Lines 62 and 64		
V_1	2075 m/s	
V_{2d}	5102 m/s	Line 64
V_{2u}	6544 m/s	Line 62
α	2.75^o	
Θ_c	21.2^o	
V_2	**5727 m/s**	
t_{2d}	6.10×10^{-3} s	
t_{2u}	7.90×10^{-3} s	
downdip depth	**6.79 m**	
updip depth	**8.79 m**	

I interpret V_1 as representing till which is below the water table and V_2 as representing the bedrock.

Refraction seismic lines 82 (reverse) and 83 (forward) were shot at 10 m spacing (see Figure 27a), along the fairway of hole #11. Each geophone was spaced 10 m apart, however, the shot point was 4 m away from the first geophone for line 82 and 7 m away for line 83. The following travel times were recorded:

Seismic Line 82 reverse, 10m spacing 4m gap between SP and GP1		**Seismic Line 83** forward, 10m spacing 7m gap	
Distance (m)	82 Time (ms)	Distance (m)	83 Time (ms)
0	0.0	0	0.0
10	-	10	-
20	**44.7**	20	7.5
30	38.2	30	5.7
40	38.2	40	12.8
50	35.0	50	16.6
60	32.6	60	18.9
70	28.3	70	20.5
80	28.6	80	27.0
90	22.8	90	29.0
100	17.2	100	32.6
110	11.1	110	35.7
120	7.1	120	38.9

Refraction lines 82 and 83 were interpreted in a similar manner and produced the slopes set out below and the results shown in Table 5.

Line	Slope	Avg. Slope
V_1	0.4689 (Line 82) 0.3097 (Line 83)	0.3893
V_{2d}	0.3050	
V_{2u}	0.2740	

V_{2d} corresponds to line 83 and V_{2u} corresponds to line 82.

Table 5 – Refraction seismic lines 82 and 83 interpretation and results

Seismic Lines 82 and 83		
V_1	2680 m/s	
V_{2d}	3278 m/s	Line 83
V_{2u}	3650 m/s	Line 82
α	3.8 °	
Θ_c	51.1 °	
V_2	**3447 m/s**	
t_{2d}	6.00×10^{-3} s	
t_{2u}	1.50×10^{-2} s	
downdip depth	**12.8 m**	
updip depth	**31.9 m**	

I interpret V_1 as representing the till layer below the water table and V_2 as representing the bedrock.

Refraction seismic lines 86 (reverse) and 87 (forward) were shot at 3 m spacing along the fairway of hole #11, parallel to lines 82 and 83 above (see Figure 27a). Each geophone was spaced 3 m apart, however, the shot point was 4 m away from the first geophone for line 86. The following travel times were recorded:

Seismic Line 86 reverse, 3m spacing 4m gap between SP and GP1		**Seismic Line 87** forward, 3m spacing	
Distance (m)	86 Time (ms)	Distance (m)	87 Time (ms)
0	0.000	0	0.000
3	-	3	6.000
6	19.968	6	5.568
9	19.680	9	7.440
12	17.952	12	9.312
15	16.080	15	10.032
18	15.168	18	12.672
21	13.440	21	13.968
24	12.192	24	15.744
27	11.328	27	17.616
30	9.792	30	20.352
33	7.968	33	21.024
36	6.720	36	23.952

Refraction lines 86 and 87 were interpreted in a similar manner and produced the slopes set out below and the results shown in Table 6.

Line	**Slope**	**Avg. Slope**
V_1	2.000 (Line 86)	2.000
V_{2d}	0.5988	
V_{2u}	0.4547	

V_{2d} corresponds line to 87 and V_{2u} corresponds to line 86.

Table 6 – Refraction seismic lines 86 and 87 interpretation and results

Seismic Lines 86 and 87		
V_1	500 m/s	
V_{2d}	1670 m/s	Line 87
V_{2u}	2200 m/s	Line 86
α	2.1°	
Θ_c	15.3°	
V_2	**1897 m/s**	
t_{2d}	1.80×10^{-3} s	
t_{2u}	5.00×10^{-3} s	
downdip depth	**0.47 m**	
updip depth	**1.30 m**	

I interpret V_1 as representing the layer of dry till and V_2 as representing the till layer below the water table. There was no return from the bedrock at this location.

3.1.4.2 Reflection

The second seismic study at the Clyburn Brook was conducted in September 2001. This time, I attended Dr. Patrick Ryall and Charlie Walls of Dalhousie University to the site. First, a decision had to be made whether the second study should involve refraction or reflection techniques. According to Pullan and Hunter (1990), the advantages of reflection as compared to refraction techniques are as follows:

(1) reflection is not subject to the assumption that velocity increases with depth;

(2) reflection requires smaller sources and shorter spread lengths to map a given interface than refraction, i.e. reflections may be as much as an order

of magnitude greater in amplitude than the refracted wave from the same horizon; and

(3) reflection techniques have the potential of resolving depositional features within the overburden materials, whereas detailed structures on the target horizon may be difficult to map with refraction techniques.

There are limitations to the use of reflection. First, reflection requires high frequencies to resolve a shallow target. However, these high frequencies are strongly attenuated during transmission through the Earth. As a result, high-pass analog filters are necessary to compensate for the low-pass frequencies of the Earth. Second, it is impractical to record data and to then engage in digital filtering (Pullan and Hunter, 1990). Such filters must be applied at the same time that the data is recorded. Pullan and Hunter (1990) conclude that shallow reflection surveys require geophones with frequencies of 50 to 100 Hz, with the 'buffalo gun' approach being the recommended seismic energy source.

It was, therefore, decided that the second seismic study would be run in reflection mode using 100 Hz geophones and analog filters. In addition, the optimum offset technique was undertaken to facilitate the interpretation of the shallow reflection data that was expected, and to create a lateral profile of the canyon bottom. This technique is, in general, best suited to mapping the overburden-bedrock interface, produces a large amplitude reflection and gives the best results in areas where the Earth materials are fine-grained and water saturated (Pullan and Hunter, 1990). Therefore, seismic lines were shot in the bed of the Clyburn Brook in an area in which the brook crossed the floor of the canyon (Figure 33).

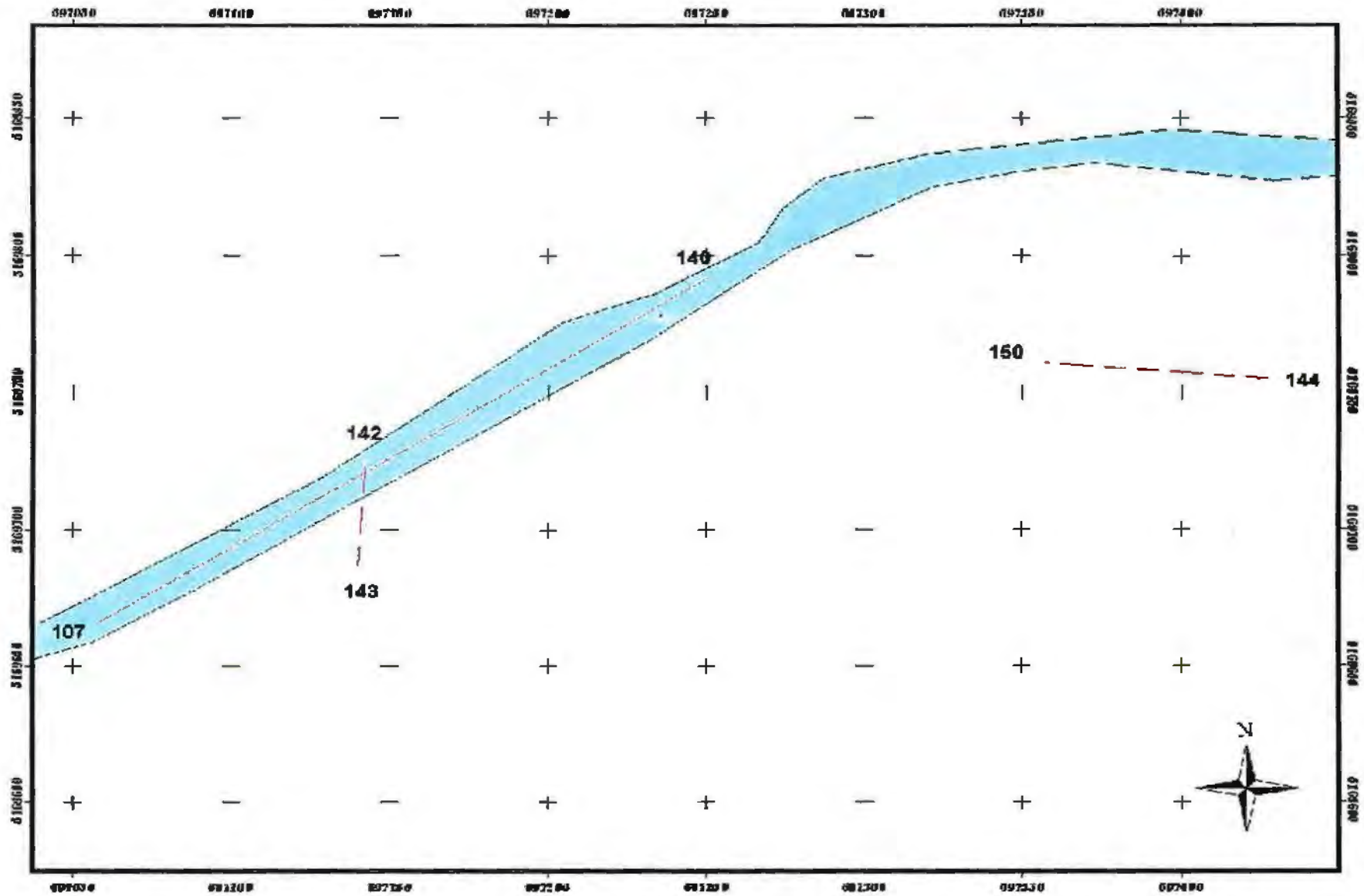

Figure 33. Reflection seismic study location map (with location of the Clyburn Brook shown).

The methods of processing the reflection seismic data are outlined in Section 3.1.2 above. The equations used are referred to by number. Once again, only the most representative seismic lines are outlined in this study.

The reflection study was also conducted to ascertain the depth to bedrock in a particular section of the Clyburn Brook canyon, but attempted to reach greater depths of penetration than the refraction study. First, seismic lines 107 to 140 inclusive were shot along the edge of the brook, starting under the golf cart bridge (seismic line 107 location) and continued down the brook for about 200 m, to obtain a lateral profile of the canyon. This section of the brook was chosen since it crossed the floor of the canyon. Most of the shots were made in the standing water of the brook, however, a few shots were made in dryer areas which were in close proximity to the brook. Second, a separate line was shot perpendicular to the brook (seismic lines 142 and 143). Finally, seismic lines 144 to 150 inclusive were shot in close proximity to the brook in an area referred to as the 'trough'. These lines were used to generate a 'trough-like' profile. Calculated apparent velocities were 1500 to 3000 m/s, a range typical of till below the WT. Depths of penetration ranged from 15 to 47 m, with an average depth being 30 m.

As anticipated, most of the reflection data produced a hyperbola-shaped reflector. The reflection data was analyzed using one or all of three different methods. Firstly, each individual reflection seismic line, which showed a well-defined reflector, was analyzed using eqns. 16 and 14, respectively. A typical well-defined reflector is shown in Figure 34. The geophone number is located above each line and the vertical time scale is 0 to 100 ms.

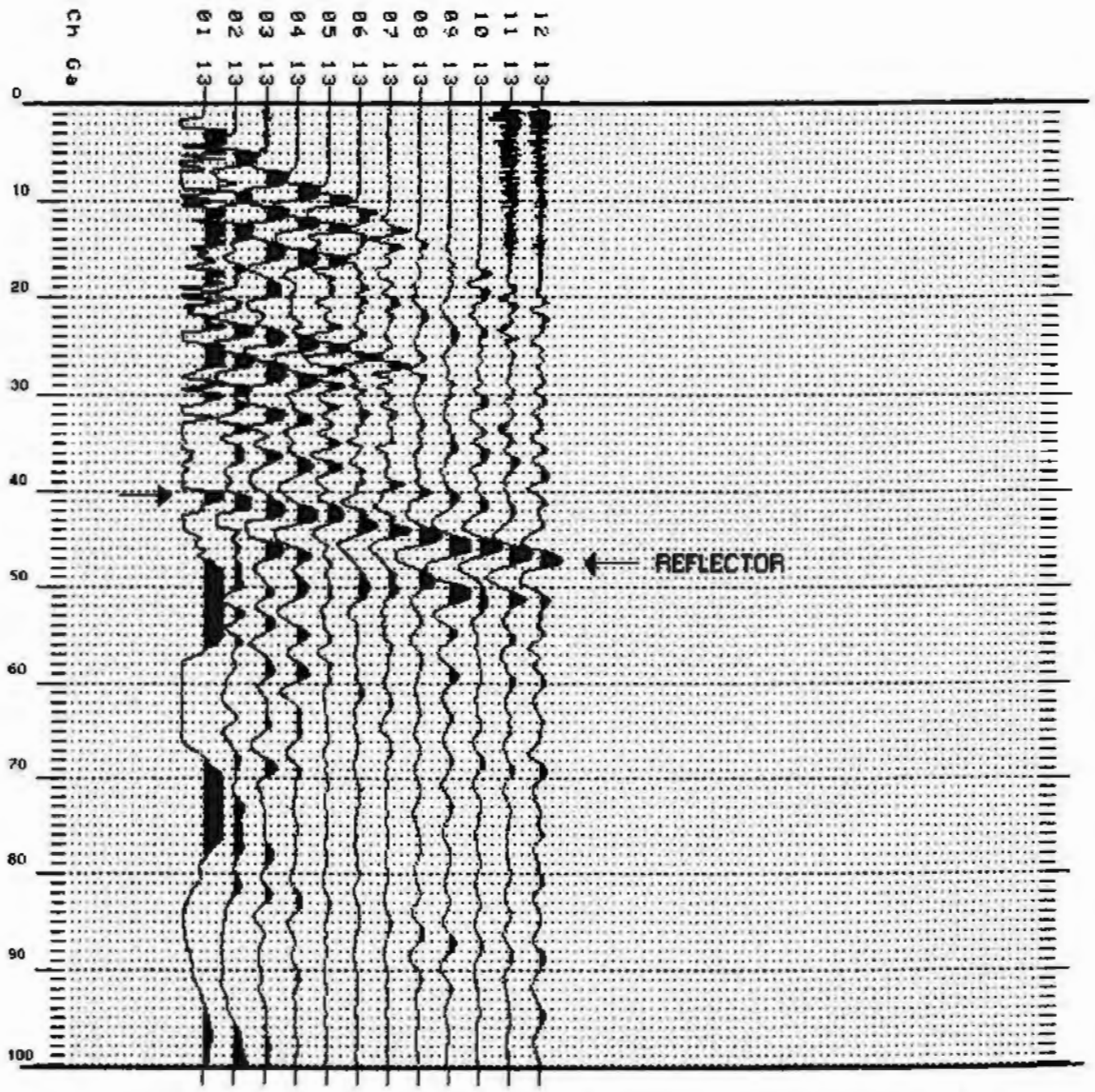

Figure 34. Raw seismic reflection data with the typical hyperbola-shaped reflector arriving between 40 and 50 ms (10^{-3} s).

Seismic lines 125, 131, 133, 136, 137, and 139, located between lines 107 and 140 on Figure 33, were analyzed individually using the $T^2 - X^2$ method (eqns. 15 and 14) and produced the results shown in Table 7.

Table 7 - Reflection seismic lines 125, 131, 133, 136, 137, and 139 interpretation and results

Seismic Line	Geophone	Distance (m)	Time (ms)	V_I (m/s)	t_o (s)	h depth (m)
125	2	9	44.2	1825.7	0.044	39.8
	12	39	48.5			
131	6	18	42.0	1825.7	0.041	37.6
	12	36	45.0			
133	4	12	41.0	2236.1	0.040	44.7
	10	30	43.0			
136	8	24	38.7	1825.7	0.036	32.9
	12	36	41.5			
137	5	15	37.0	2236.1	0.036	40.3
	12	36	39.9			
139	9	27	29.2	2236.1	0.026	29.6
	12	36	31.0			

All of the records, which ran through the brook (records 107 to 140 inclusive) and displayed a well-defined reflector, were interpreted in a similar manner. Calculated depths ranged from 22.4 to 47.4 m and apparent velocities ranged from 1581 to 3162 m/s, with an average velocity of 1860 m/s. I interpret this apparent velocity range as representing wet till lying below the water table.

Secondly, the seismic data was interpreted using the common mid-point method. This interpretation used eqns. 16 and 14, respectively. The t_o value was found by plotting T^2 versus X^2 and finding the y-intercept value. The information was gathered using three seismic lines, which traversed over a common midpoint. The first set of seismic lines interpreted were lines 116, 118, and 119 and produced the results shown in Table 8.

Table 8 - Reflection seismic lines 116, 118, and 119 interpretation and results

Seismic line	Geophone	x distance (m)	Time (ms)	to (s)	*d* t (s)	*d* x (m)	Velocity (m/s)	h depth (m)
116	9	27	42	0.040	0.002	24	1897.37	37.9
118	5	15	41					
119	1	3	39.8					

[Note: seismic line 116 is similar to 117]

In a similar manner, seismic lines 126, 127, and 128 were analyzed and produced the results shown in Table 9.

Table 9 - Reflection seismic lines 126, 127, and 128 interpretation and results

Seismic line	Geophone	x distance (m)	Time (ms)	to (s)	*d* t (s)	*d* x (m)	Velocity (m/s)	h depth (m)
126	9	30	45	0.042	0.003	24	1511.86	31.7
127	5	18	44					
128	1	6	42					

This method of interpretation was applied to all of the data obtained from the seismic lines in the brook. Calculated depths of penetration ranged from 15.8 to 47.4 m and apparent velocities ranged from about 1581 to 2236 m/s. I interpret this velocity range as representing a layer of wet till lying below the water table.

The final interpretation of the reflection seismic data was through interpretation of a strong reflector arriving at one particular geophone using the optimum offset technique (Pullan and Hunter, 1990) set out in Section 3.1.2. Upon examination of the reflection data, it was determined that geophone 8 consistently provided a good quality reflected arrival across seismic lines 112 to 140 inclusive. At 3 m spacing, geophone 8 is 24 m from shot point 1. Since a reflected raypath is v-shaped, the

optimum offset is half of that distance, i.e. 12 m. This value was used in eqn. 17. A profile of the raw seismic data is set out in Figure 35. The numbers at the top represent the geophone number, with geophone 8 being the main object of interest, and the vertical scale is 100 ms.

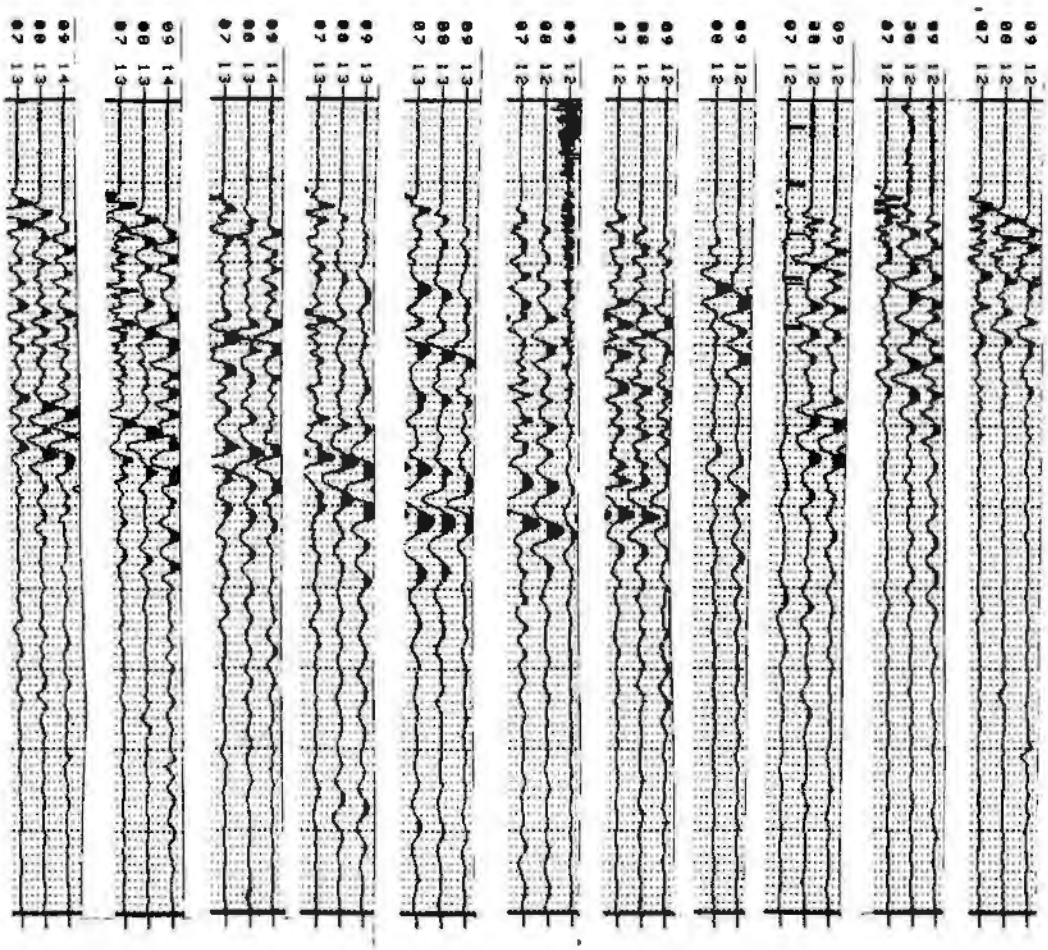

Figure 35. Raw seismic reflection data – optimum offset method (lines shown from left to right: 113, 115, 117, 119, 121, 124, 126, 132, 136, 138, and 140).

Using this method, data was extracted from all of the lines to generate a lateral profile. For the analysis, a 2000 m/s velocity was chosen to represent the wet till layer overlying the bedrock, as determined in the first two methods of reflection

analysis and the refraction study. This data was analyzed using eqn. 17 and produced the results shown in Table 10.

Table 10 - Reflection seismic lines 112 to 140 interpretation and results (exclusive of lines 122, 129, and 130)

Seismic line	Geophone	x distance from SP1 (m)	Time (ms)	Velocity (m/s)	h depth (m)
112	8	42	36.5	2000	34.5
113	8	48	37.0	2000	35.0
114	8	54	38.0	2000	36.1
115	8	60	40.0	2000	38.2
116	8	66	42.0	2000	40.2
117	8	72	42.5	2000	40.8
118	8	72	43.2	2000	41.5
119	8	78	43.4	2000	41.7
120	8	84	44.0	2000	42.3
121	8	90	45.0	2000	43.4
123	8	99	46.0	2000	44.4
124	8	102	46.8	2000	45.2
125	8	105	46.0	2000	44.4
126	8	108	44.5	2000	42.9
127	8	111	45.0	2000	43.4
128	8	114	43.5	2000	41.8
131	8	123	43.0	2000	41.3
132	8	129	42.5	2000	40.8
133	8	135	41.5	2000	39.7
134	8	141	39.0	2000	37.1
135	8	147	38.9	2000	37.0
136	8	159	38.7	2000	36.8
137	8	171	38.0	2000	36.1
138	8	183	35.0	2000	32.9
139	8	195	28.0	2000	25.3
140	8	207	21.0	2000	17.2

Calculated depths of penetration ranged from 17 to 45 m. This method produced greater depths of penetration than the other methods of reflection study or the previous refraction study (see Section 4.1.3). A lateral profile of the depth to bedrock

was generated in Excel (Figure 36). The elevation of the ground surface is based on the Canadian Geodetic Datum (CGD) with the depth to bedrock shown below.

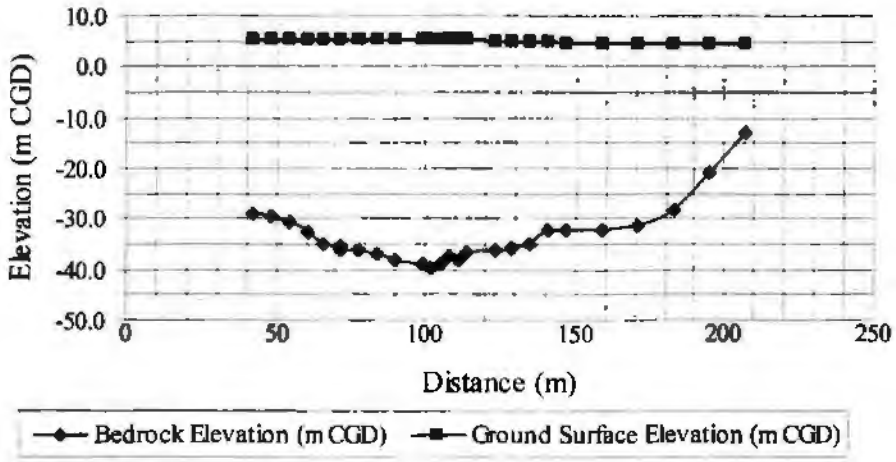

Figure 36. Lateral profile of depth to bedrock in the Clyburn Brook ascertained from reflection data.

A separate reflection seismic line was shot perpendicular to the brook (see Figure 33). Seismic line 142 represents the forward shot and seismic line 143 the reverse shot. These lines were located about 100 m east of the golf cart bridge. The data was interpreted on an individual basis using eqns. 15 and 14. Analysis of the data produced the results shown in Table 11.

Table 11 - Reflection seismic lines 142 and 143 interpretation and results

Seismic Line	Geophone	Distance (m)	Time (ms)	V1 (m/s)	to (s)	h depth (m)
142	8	24	46	1825.7	0.045	40.8
	12	36	48			
143	8	24	45	1581.1	0.042	33.5
	12	36	48			

Since velocities of over 1500 m/s were obtained, I would interpret this as representing a layer of wet till.

Finally, the reflection seismic lines shot in the 'trough', in close proximity to the brook, were analyzed using the optimum offset technique (see Figure 33). Seismic lines 144 to 150 inclusive displayed a consistent, strong reflector at geophone 9 and, therefore, the optimum offset was set at 13.5 m (GP 9 is 27 m away from SP1; Op = 27/2). Using this data in eqn. 17 produced the results shown in Table 12.

Table 12 - Reflection seismic lines 144 to 150 interpretation and results (exclusive of lines 145 and 147)

Seismic line	Geophone	x distance from SP1 (m)	Time (ms)	Velocity (m/s)	h depth (m)
146	9	9	43.5	2000	41.4
144	9	27	46.0	2000	44.0
148	9	39	42.5	2000	40.3
149	9	51	42.0	2000	39.8
150	9	63	41.9	2000	39.7

Calculated depths of penetration ranged from 39 to 44 m. These depths were consistent with the depths calculated for the lateral profile of the brook. A profile of the 'trough-like' area is shown in Figure 37.

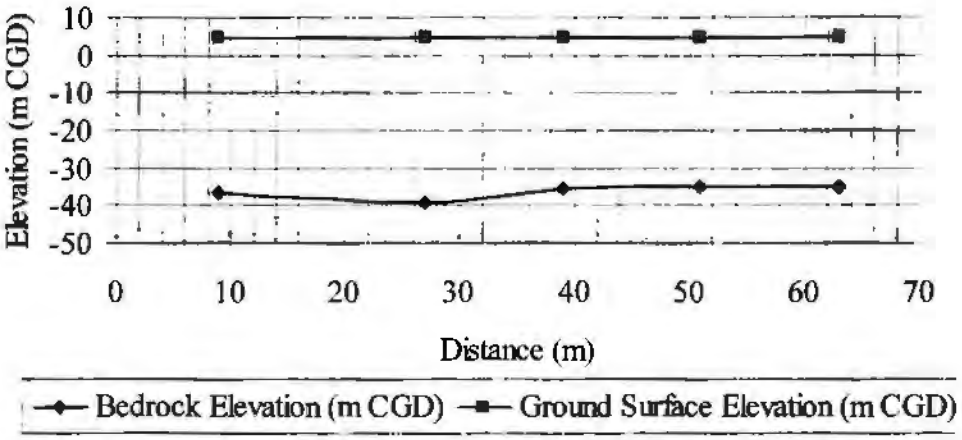

Figure 37. Trough profile of depth to bedrock near the Clyburn Brook based on reflection data.

In summary, the first study, using refraction, encompassed a velocity range of 350 to 5700 m/s and detected refractors at depths ranging from 6.6 to 12.8 m. The second study, using reflection, contained an average velocity range of 1500 to 3000 m/s and detected reflectors at depths ranging from 15 to 47 m (average 30 m). Although the velocities of the first study were higher, the depth of penetration achieved was greater during the reflection seismic study. This greater depth of penetration was anticipated and was the reasoning behind performing the second seismic study in reflection mode. This premise was confirmed when greater depths of penetration were achieved during the second seismic study.

The raw geophysical data and the calculations made for the refraction and reflections seismic studies are contained in Appendix B (CD-ROM).

3.2 Numerical Modelling

3.2.1 Hydraulic and Finite Difference Theory

The movement of groundwater is induced by differences in pressure and elevation, i.e. hydraulic potential. Hydraulic head (also known as the piezometric head and potentiometric head) is defined as the sum of the elevation head and the pressure head (Freeze and Cherry, 1979). It is defined as:

$$h = z + \frac{P}{\rho g} \qquad [18]$$

where h = hydraulic head (L)
z = elevation about a datum (L)
P = pressure (F/L^2)
ρ = fluid density (M/L^3)
g = gravity (L/T^2)

Groundwater flows from higher to lower hydraulic potential. In an unconfined aquifer, the water table (WT) is the upper boundary of the region of flow. The hydraulic gradient represents the change in hydraulic head with distance along the curvilinear path of flow. It is defined as:

$$i = \frac{\Delta h}{L} \qquad [19]$$

where i = hydraulic gradient (L/L)
Δ h = difference in hydraulic head (L)
L = length of flow path (L)

In unconfined flow, the hydraulic gradient usually increases in the direction of flow, whereas, the hydraulic head decreases (Fetter, 1994). The hydraulic gradient increases because the height of the WT table and the cross-sectional area decrease in the direction of flow. The flow of groundwater through homogeneous isotropic

porous media under steady state conditions is governed by a second order partial differential equation known as the Laplace equation (Wang and Anderson, 1982). This equation can be expressed in 2-D Cartesian coordinates as:

$$\frac{\partial^2 h}{\partial x^2} + \frac{\partial^2 h}{\partial y^2} = 0 \qquad [20]$$

where h = scalar potential (hydraulic head in this case) (L)
x = horizontal distance (L)
y = vertical distance (L)

One way to solve eqn. 20 is through the finite difference method, in which continuous hydraulic gradients are approximated by finite differences in head over finite lengths. The finite difference solution to eqn. 20 is (Wang and Anderson, 1982):

$$h_c = \frac{1}{4}(h_1 + h_2 + h_3 + h_4) \qquad [21]$$

where h = hydraulic head (L)
h_i = hydraulic head at neighbouring node i (see Figure 39)
h_c = center node

The derivation of eqn. 21 is contained in Appendix C. Equation 21 applies if the aquifer is homogeneous and isotropic (see Section 3.2.1.1).

According to Wang and Anderson (1982), a model is a tool designed to represent a simplified version of reality, with mathematical modelling of groundwater flow having been performed since the late 1800's. The finite difference (FD) method may be set up in a spreadsheet (Olsthoorn, 1985). Each cell in the spreadsheet represents a FD node and is given specific dimensions (see Figure 38). These dimensions are set for a given FD model according to the desired resolution. For example, if the geographical area of study is large, such as a province, Δx and Δy in Figure 32 might be in kilometres, whereas if the geographical area of study is modest, such as a

watershed, the dimensions represented by one node might be in metres. The porous media must be discretized into many nodes if high-resolution results are needed (Boonstra and de Ridder, 1981). The resolution of the model has implications for the amount of output that is generated and the accuracy that this output represents. The nodal dimensions are, therefore, assigned on a case-by-case basis (Boonstra and de Ridder, 1981).

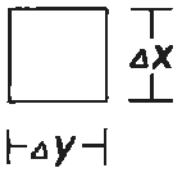

Figure 38. Definition of a finite difference node.

The arrangement of heads implied by eqn. 21 and Figure 39 is sometimes referred to as a FD star (Freeze and Cherry, 1979). The FD star reflects the fact that eqn. 21 computes the head at any point in the porous medium as the average of the heads in the nodes found above, below, and on each side of the central node (as in Figure 39).

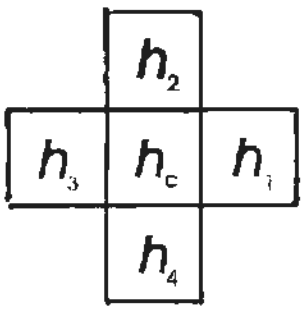

Figure 39. Standard finite difference star, with neighboring cell designations shown (Olsthoorn, 1985).

The FD solution represented by eqn. 21 and Figure 39 must be modified in locations next to impermeable boundaries. Such boundary conditions 'constrain' the problem. This makes the solution of the equation unique to each situation (Wang and Anderson, 1982). Two representations of impermeable boundaries are possible (if Figure 33 represents the default FD star). The first is a flat impermeable boundary beside node h_c (Figure 40):

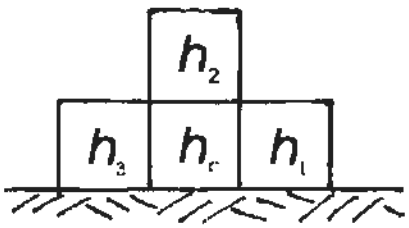

Figure 40. Finite difference star beside an impermeable boundary (Wang and Anderson, 1982).

To calculate h_c for the impermeable boundary shown in Figure 40, the following equation is used:

$$h_c = \frac{1}{4}(h_1 + 2h_2 + h_3) \qquad [22]$$

The second type occurs when two impermeable boundaries exist beside node h_c, also known as a corner boundary, as shown in Figure 41 (Wang and Anderson, 1982).

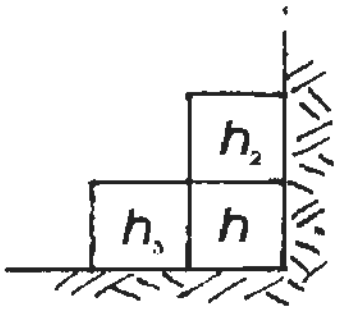

Figure 41. Finite difference star beside two impermeable boundaries.

In this case, h_c is determined using the following equation:

$$h_c = \frac{1}{4}(2h_2 + 2h_3) \qquad [23]$$

The FD star results in a 'circular referencing error' in spreadsheet solutions. This is easily overcome by specifying 'iterative calculation mode'. Another special case occurs when a FD star 'intercepts' a sloping boundary and becomes foreshortened, as in Figure 42 (Kleiner, 1985). This is necessary in FD models that do not have a sufficiently fine resolution. However, this can be overcome if the nodal size is sufficiently small (Boonstra and de Ridder, 1981).

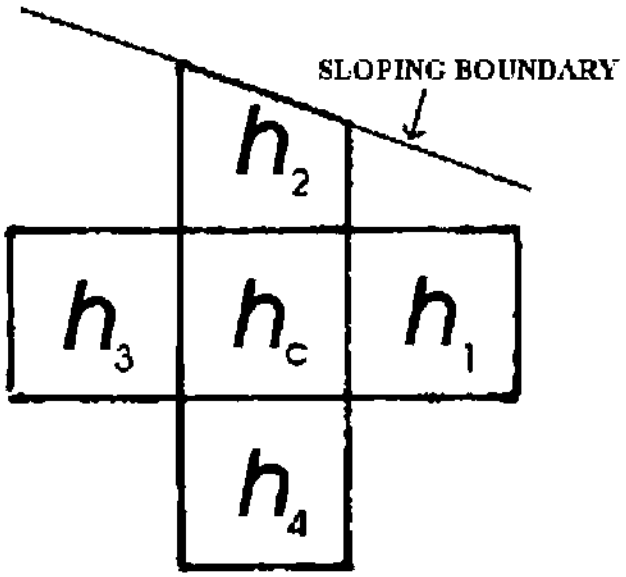

Figure 42. Foreshortened finite difference star intercepted by a sloping boundary.

In this case, the head at the central node in Figure 42 is calculated using eqn. 24:

$$\left(3+\frac{1}{x}\right)h_c = h_1 + \frac{1}{x}h_2 + h_3 + h_4 \qquad \textbf{[24]}$$

where x = vertical length of foreshortened finite difference node, center of h_c to sloping boundary (see Figure 38)

The final values of the interior nodes determined through iteration ultimately depend on the imposed boundary conditions. Full 'relaxation' of the model occurs when the nodal values stop changing by a predetermined tolerance. This tolerance is set, for example, as the head in the third or fourth place behind the decimal. The manner in which a nodal value changes leading up to complete relaxation is known as convergence.

The rate of movement of water through porous media can be calculated using Darcy's Law:

$$Q = -KiA \quad [25]$$

where Q = discharge (L^3/T)
K = hydraulic conductivity (L/T)
i = hydraulic gradient (see eqn. 19)
A = area (L^2)

The negative sign indicates that flow is in the direction of decreasing hydraulic head (Fetter, 1994) and is often dropped.

3.2.1.1 Dupuit Assumptions

The examination of groundwater flow in an unconfined aquifer is complicated by the fact that the hydraulic gradient actually varies two-dimensionally. This can sometimes be overcome using the Dupuit assumptions. These assumptions are as follows (Fetter, 1994):

(1) the hydraulic gradient is equal to the slope of the WT,

(2) the streamlines are horizontal, and

(3) the equipotential lines are vertical.

These assumptions are equivalent to the assumption that the flow is one-dimensional and the pressure is hydrostatic through a given vertical. If the slope of the WT is greater than about 0.1, the Dupuit assumptions become invalid because the flow is too strongly two-dimensional.

3.2.2 Finite Difference Method

For this geographic area of study, the flow of water through the unconfined aquifer was modelled in a spreadsheet using the FD method. All modelling efforts were based upon the survey data obtained by D. Hansen (see Section 2.3) and a topographic map of the area. FD models were prepared to represent the Upstream Reach of the brook in plan view and a thin 'bottleneck' area (XS 1) in a cross-sectional view.

For the plan-view modelling effort described herein, the FD grid was oriented horizontally (Figure 43). This effort invoked, and was therefore constrained by, the Dupuit assumptions. This meant that at each node or cell, the hydraulic head and other aquifer properties were assumed to be constant throughout each vertical (i.e. depth) down to the bedrock.

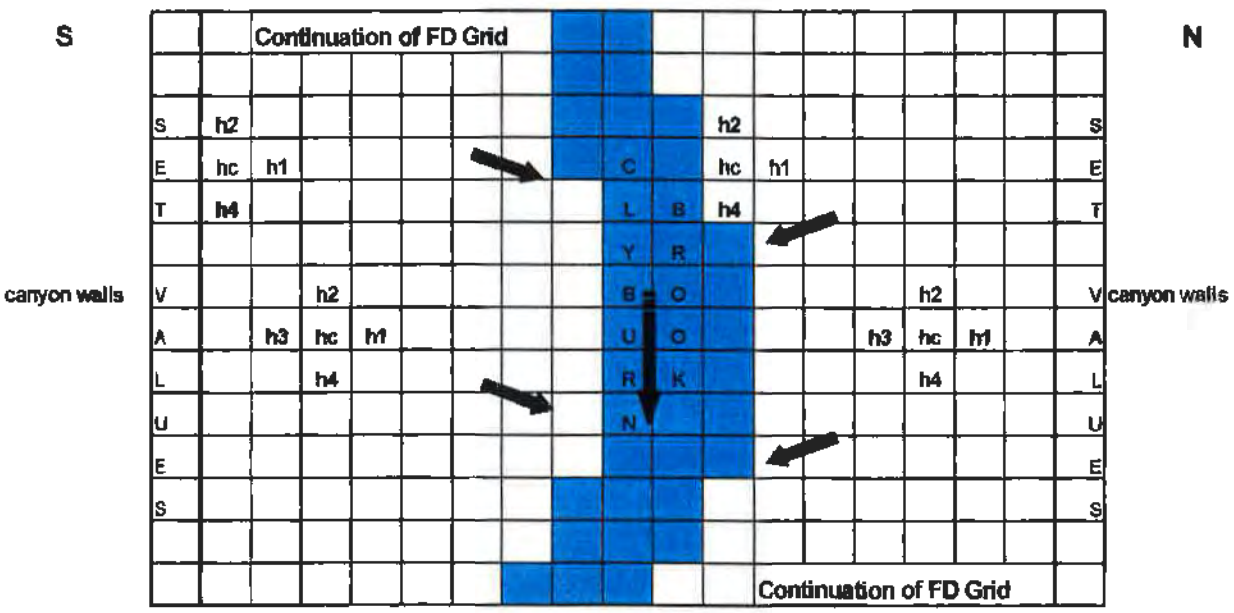

Figure 43. Schematic of part of plan-view finite difference grid (not to scale) (arrows approximate the direction of surface water flow and groundwater flow into the brook).

The plan-view model resembled the portion of the brook from the golf cart bridge (XS 8) to the 'bottleneck' (XS 1), known as the 'Upstream Reach' (see Figure 14). The cross-sections from XS 8 to XS 1 formed the western and eastern boundaries, respectively. The northern and southern boundaries of the model were determined by the 10-metre elevation contour on the topographical map. This curved elevation contour line was taken as the intersection of the WT with the canyon wall.

The FD method was utilized to examine theoretical hydraulic head values in a variety of steady-state conditions (six scenarios). In each scenario, different parameters were used for the boundary conditions to simulate a WT elevation difference between the canyon walls and the brook. The nodes in the model were 5 m x 5 m. This relatively fine resolution was necessary to achieve sufficient accuracy and detail in the output. Within the model, nodes with known values (e.g. hydraulic head), such as in the brook or along the canyon boundary, were linked to spreadsheet tables containing WT elevation data. In this way, boundary conditions could be conveniently specified and these nodal values were kept separate from the actual model. In particular, the surveyed portions of the brook contained measured values and the values for the remainder of the brook were interpolated, also using the FD method. These brook calculations were performed in isolation from the rest of the model. The canyon wall heads were calculated as the adjacent brook value plus a WT super-elevation representative of the particular scenario under examination.

The plan-view model of the Upstream Reach was formatted for each of the six scenarios by editing the data tables. For instance, a high WT could be represented by a difference in WT elevation of 3 m between the brook and the canyon walls. In this

case, the canyon-wall head values would be set to equal the adjacent stream head plus an additional 3 m of head. The values of all other nodes were ascertained through iteration, in which all FD stars interacted with each other and with the known nodal values (the boundary conditions).

Iterations to 'relax' the grid (Southwell, 1946) were continued until all nodes became fully relaxed. The convergence of a relatively central node in one of the models was tracked and plotted to verify that full grid relaxation had indeed occurred (Figure 44).

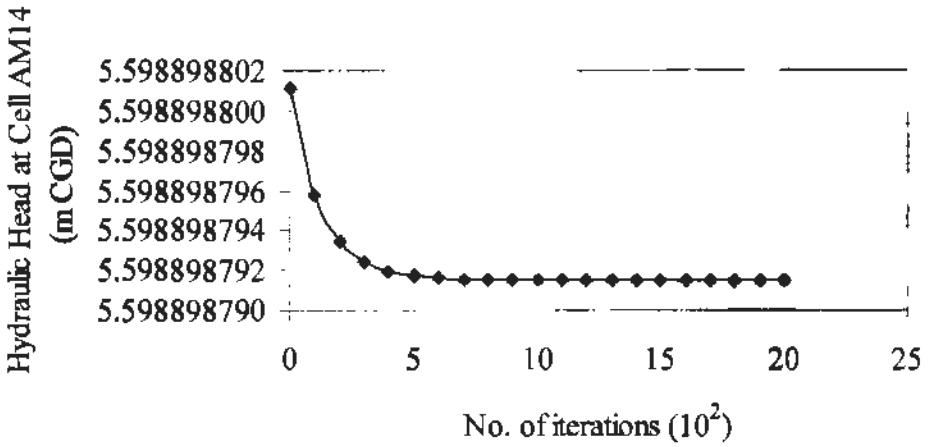

Figure 44. Tracked convergence of one node in the FD model.

In this instance, the head was tracked until the ninth decimal place stopped changing. It was found that about 2000 iterations were sufficient. This minimum number of iterations was then used in all other modelling efforts.

Using the hydraulic head values obtained for the Upstream Reach of the Clyburn Brook and Darcy's Law (eqn. 25), a discharge rate at the 'bottleneck' area (XS 1) was obtained for each of the six scenarios (WT elevation differences of 0.0, 0.05, 0.5, 1.0, 2.5, and 3.0 m between the brook and the canyon walls). As mentioned in Section

2.3, the hydraulic conductivity was determined by CBCL (1995) to be 213.3 m/d. The cross-sectional area calculation was made using the depths to bedrock ascertained from the seismic study (Section 3.1.4). In areas where the depth to bedrock was unknown, a value was obtained through interpolation between known values. The hydraulic gradient was calculated using adjacent nodal or cell values that bordered the stream, that is, the value of head in the cell on the south (or north side) of the stream minus the value of head in the stream. In this manner, discharge rates were calculated for the south and north sides of the stream. These were added cumulatively to determine a total discharge for the Upstream Reach of the Clyburn Brook at the 'bottleneck'.

In order to determine a total discharge rate at the 'bottleneck', an approximation of the rate of discharge into the upstream limit of the Upstream Reach was required (Figure 45). The discharge into the 'top' of the model was intended to represent the flow received from farther upstream. To this end, the length of stream above the golf cart bridge (i.e. beyond the modelled portion of the brook), comparable in topography to the modelled portion, was approximated. The discharge rate was assumed to have a linear relationship to stream length, that is:

$$\frac{Q_1}{L_1} = \frac{Q_2}{L_2} \qquad [26]$$

where Q units = m^3/s
L units = m

The length of stream above the golf cart bridge was assumed to have a similar quantity of glaciofluvial material based on surficial geology and topography (see

Section 3.2.3). In this manner a total rate of discharge at the 'bottleneck' was estimated.

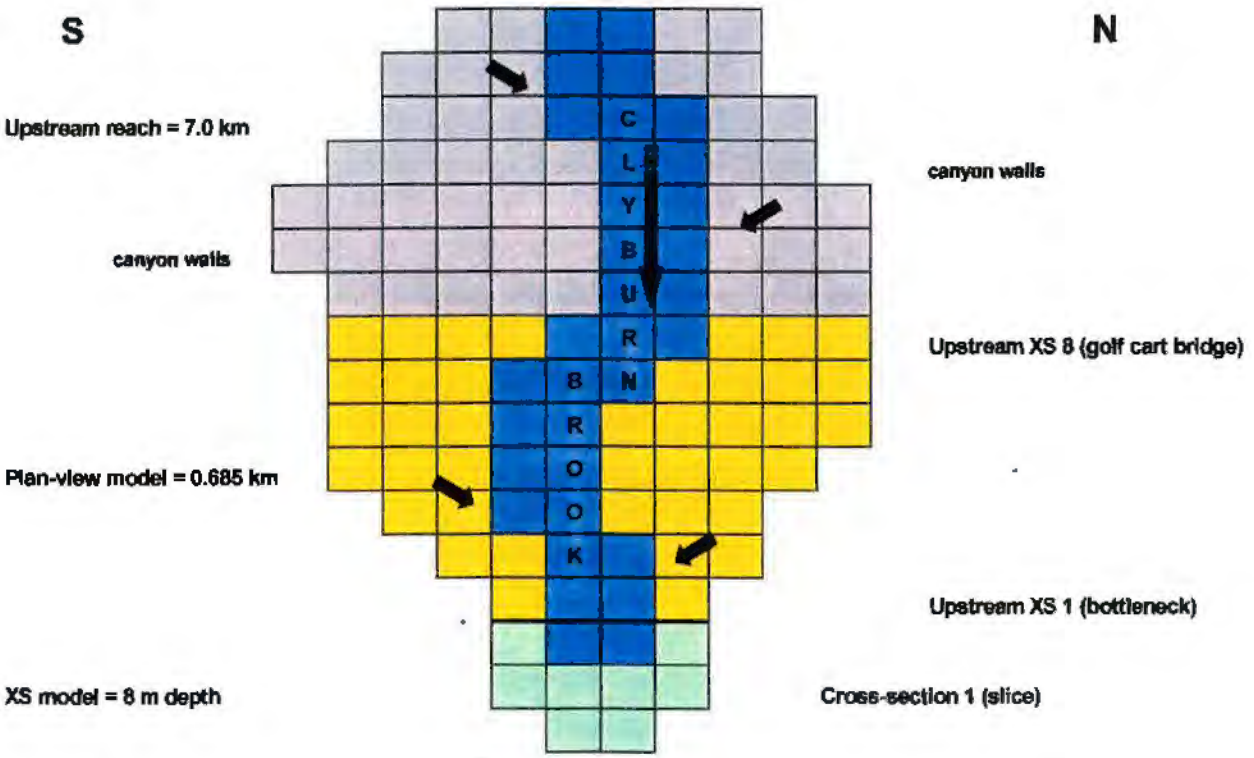

Figure 45. Diagrammatic sketch of Clyburn Brook canyon (not to scale) (arrows approximate the direction of surface water flow and groundwater flow into the brook).

3.2.3 Data

The survey data from the year 2000 and topographic data, upon which the models were based, is summarized in Table 13. The width of the canyon was determined using the 10 m contour on the topographic map as the boundary of the canyon.

Table 13 - Basic data for plan-view FD modelling

Cross-section	Water level in brook (m CGD)	Hydraulic head (m CGD)	Width of surface water in brook (m)	Width of canyon (m)
8.0	5.456	5.456	24.6	165.0
7.0	5.199	5.199	22.9	175.0
6.0	3.877	3.877	29.0	185.0
5.0	4.124	4.124	21.3	170.0
4.0	4.126	4.126	23.3	150.0
3.0	3.890	3.890	21.1	165.0
2.0	3.667	3.667	14.7	130.0
1.0	3.543	3.543	26.2	102.0

A finite difference model was created to represent the Upstream Reach of the Clyburn Brook, as outlined in Section 3.2.2. The model represented an area of roughly 685 m (east-west) by 220 m (north-south). One node in the FD grid represented 5 m x 5 m. [Due to their size, the plan-view models are contained in digital form as Appendix D (CD-ROM).]

This model was fine-tuned to simulate each of six scenarios, which reflected a WT elevation difference of 0.0, 0.05, 0.5, 1.0, 2.5, and 3.0 m between the brook and the canyon wall. The hydraulic head values obtained for each scenario were examined in relation to discharge rate into the brook, using Darcy's Law (eqn. 25). The results obtained are shown in Table 14.

Table 14 – Plan-view model discharge calculations

Scenario #	Difference in WT elevation* (m)	Q (m^3/s)
1	0.0	-0.042
2	0.05	0.054
3	0.5	0.923
4	1.0	1.889
5	2.5	4.785
6	3.0	5.750

[Note: The negative flow value obtained for Scenario #1 is a numerical artifact caused by the need of the model to discretize the system. It has no real (physical) significance and can be taken as being equal to zero.]

* Difference in WT elevation means the difference between a canyon wall nodal value and the adjacent stream value.

Discharge into the 'top' of the model (the west side) was calculated using an approximate length of 7.0 km (beyond the Upstream Reach) and eqn. 26. This upstream length was calculated, using the 3-D elevation model, from the location of survey XS 8 to DEM Cross Profile 5 (on Figure 2). This area is shown on the surficial geology map as containing glaciofluvial deposits. The calculation of the discharge contribution into the 'top' of the model and the resultant total discharge at the 'bottleneck' produced the results shown in Table 15.

Table 15 – Plan-view model discharge into 'top' of model and total discharge calculations

Scenario #	Q from upstream (m^3/s)	Total Q at bottleneck* (m^3/s)
1	0.433	0.475
2	0.554	0.608
3	9.433	10.356
4	19.299	21.187
5	48.896	53.681
6	58.762	64.512

*including contribution from upstream of Upstream Reach

A further examination of the plan-view model outcomes were undertaken in relation to baseflow contribution (see Section 3.3.3).

3.3 Baseflow Contribution Study

3.3.1 Theory

The amount of groundwater seeping into a stream *via* its bed and banks, and forming part of the total discharge of the stream, is known as baseflow (Fetter, 1994). A plot of stream discharge versus time is known as a hydrograph. During the summer or periods without precipitation (recharge), a stream drains water from the surrounding aquifers and the WT falls. As the WT lowers, the baseflow contribution declines. A stream hydrograph plotted on a semi-logarithmic scale is often used to analyze the baseflow recession portion of a hydrograph. Such recession plots tend to be straight lines (e.g. lines AB and CD in Figure 46).

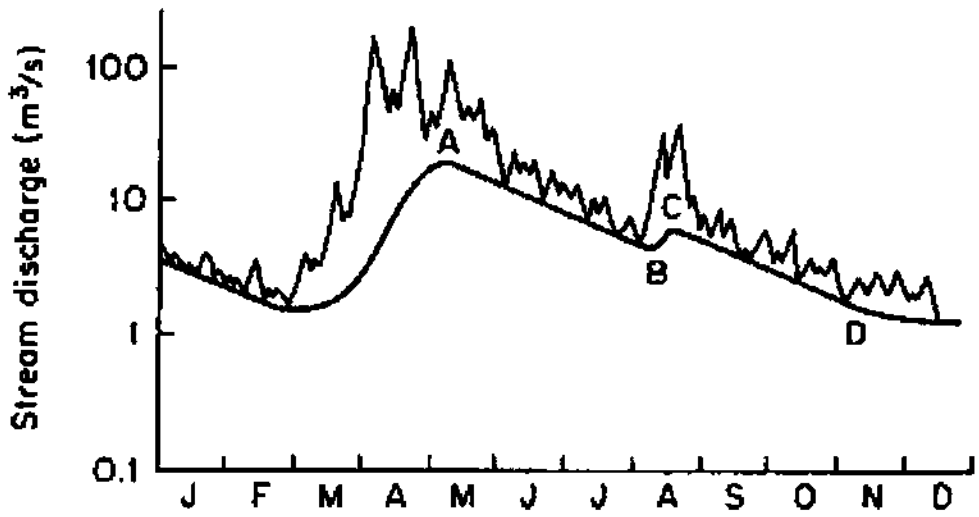

Figure 46. Sample baseflow recession hydrograph (Freeze and Cherry, 1979).

One equation that is used to describe these recessions is (Freeze and Cherry, 1979):

$$Q = Q_o \exp\left[-\frac{t}{t_s}\right] \quad [27]$$

where Q = flow at some time t after recession started (L^3/T)
Q_o = initial flow, at the beginning of the recession (L^3/T)
t = time associated with a decline from Q_o to Q (T)
t_s = time of storage (T)

Another such equation is:

$$Q = Q_o K_{rec}^{t} \quad [28]$$

where K_{rec} = recession constant (dimensionless), typically between 0.85 and 1.0

It is merely a matter of 'taste' as to whether one uses eqn. 27 or 28. Both t_s and K_{rec} are watershed dependent, and one uniquely defines the other. If the aquifer generating the baseflow in a given watershed was found entirely in a loose unconsolidated material, t_s would be relatively short (perhaps only a few days) and K_{rec} would be relatively small. Once a recession constant (either t_s or K_{rec}) for a stream has been determined, the baseflow after a given period of recession can be ascertained.

The volume of water lost from the aquifer can be analytically determined using the following equation (Fetter, 1994):

$$S = (Q_o - Q)t_s \quad [29]$$

where S = volume of water lost (L^3)
Q_o, Q = discharge (L^3/T), where T is in the same units as t_s (usually days).

3.3.1.1 Dupuit Assumptions

It was considered that it would also be interesting to analyze baseflow influx to the Clyburn Brook using two-dimensions rather than one. In such case, the streamlines are not generally horizontal, but curved. Further, the equipotential lines are not vertical. As stated previously, if the slope of the WT is greater than about 0.1, the Dupuit assumptions become invalid because the flow will become too strongly two-dimensional. The degree of this 'two-dimensionality' in the flow field was of interest.

3.3.2 Method

Using the survey, topographical, and seismic data, a 2-D (or cross-sectional) FD model of the 'bottleneck' area (XS 1) of the Clyburn Brook was developed. This was a thin-section only 5 m in longitudinal (downstream) length. The 'bottleneck' area was chosen to examine the effects of a changing WT on baseflow because the depth to bedrock was ascertained with some certainty in the seismic study and, at this location, the Clyburn Brook is more constricted than anywhere else along its length.

Known hydraulic head values from the survey data were set for the brook. The canyon wall values were assigned the values used to simulate each of the six scenarios. These settings reflected WT elevation differences of 0.0, 0.05, 0.5, 1.0, 2.5, and 3.0 m between the brook and the canyon wall. Each node in the model represented 0.5 m x 0.5 m, by 5 m of downstream length. The FD star in Figure 39 was used and appropriate boundary conditions were imposed. The remaining nodal values were determined through iteration until the nodes became relaxed, as before.

For the modelling effort described herein, the FD grid was oriented vertically, giving a cross-sectional view of a 'slice' of the brook (Figure 47). This approach was, therefore, not constrained or affected by the Dupuit assumptions (see Section 3.3.1.1).

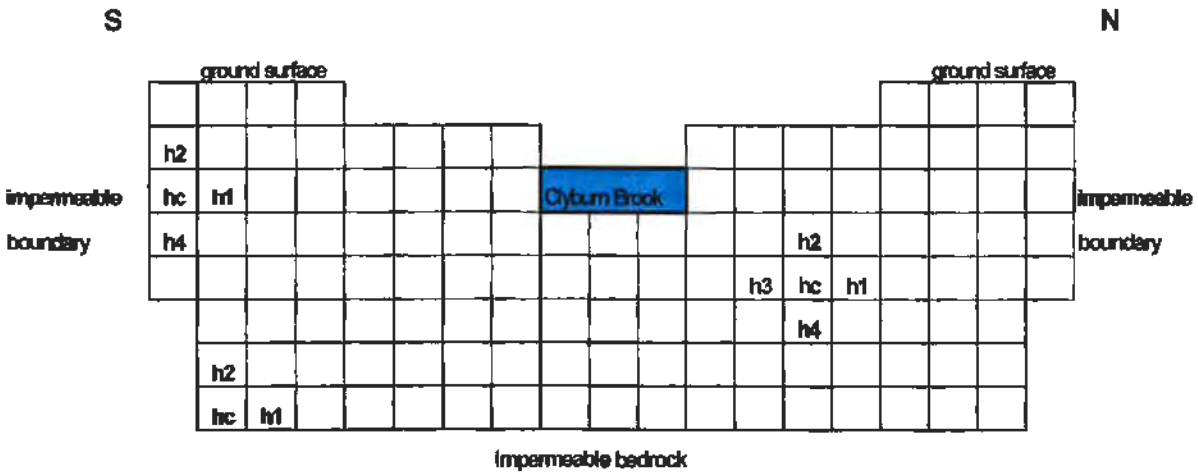

Figure 47. Schematic of cross-sectional view of finite difference grid (not to scale).

As stated in Section 2.3, the hydraulic conductivity was determined to be 213.3 m/d by CBCL (1995). By applying Darcy's Law to the fully-relaxed FD grid of hydraulic heads, a discharge rate into the brook was obtained for the cross-sectional model for each of the six scenarios. This discharge rate is per 5 m of downstream length. The discharge rate for this 'slice' of the Clyburn Brook was then compared to the discharge rate obtained from the 'bottleneck area only' in the plan-view model.

The time of storage (t_s) of the Clyburn Brook was estimated by Hansen *et al.* (unpublished) to be 8.35 days. Using this information in eqn. 27, the time increment

(t) that would elapse between an initial discharge rate and a final discharge rate was calculated. To this end, the plan-view model (Upstream Reach of the Clyburn Brook) and the cross-sectional model were analyzed for each of the six scenarios.

Volume calculations were made for both the plan-view and the cross-sectional models in relation to the obtained discharge rates. The volume (S) of water lost from storage was ascertained for each of the six scenarios using eqn. 29 (i.e. the relation giving the volume under a baseflow recession curve). This calculation is graphically shown in Figure 48, with the initial flow condition shown as Q_a and the final flow condition as Q_b. This calculation provides a hydrograph recession-based volume ($\forall_{hyd}$) under the baseflow curve. These volume calculations were made using the discharge rate obtained for the modelled area only and did not incorporate a discharge rate into the 'top' of the model.

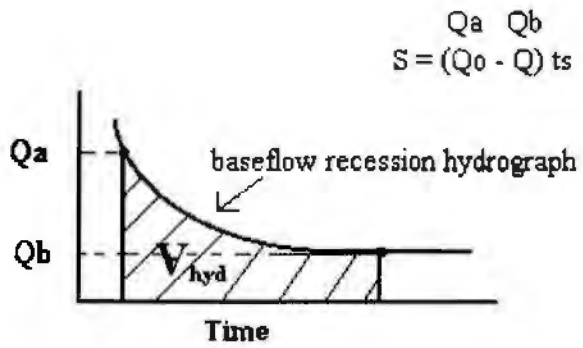

Figure 48. Hydrograph recession-based volume ($\forall_{hyd}$) calculation made from baseflow recession data (Q in m^3/s).

For one scenario (difference in WT elevation of 2.5 m) modelled in plan view, a second volume calculation was performed. This involved finding the difference in head for each node in the model (when compared to the adjacent stream value) and

multiplying it by the area of a node (5 x 5 m) to obtain a volume. The volumes of all the nodes in the model were then added to obtain a total volume change represented by the model (Figure 49). This calculation provided an estimate of the geometric volume ($\forall_{geo}$).

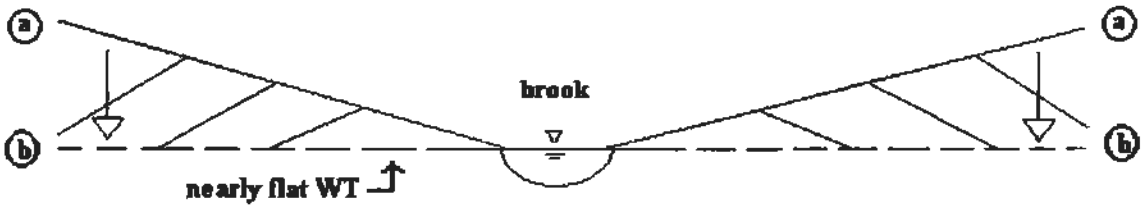

Condition (a) *baseflow$_{(a)}$ from plan view FD modelling**

Condition (b) *baseflow$_{(b)}$ from plan view FD modelling**

* must assume a K in Darcy's Law in order to get a flow
** done using fixed (temporally-invariant) boundary conditions

Figure 49. Geometric volume ($\forall_{geo}$) calculation made on the basis of FD model data.

The $\forall_{geo}$ was then used to make a direct comparison to the $\forall_{hyd}$ calculation for scenario #5 (difference in WT elevation of 2.5 m) and to make an approximation of the hydraulic conductivity (K). The $\forall_{geo}$ must take the porosity of the sediments into consideration. Fetter (1994) states the porosity range for glacial till as 10-20% and mixed sand and gravel as 20-35%. The porosity of the glaciofluvial sediments in the plan-view modelled area was, therefore, estimated to be 20-25%, since it is glacial till that has most likely been reworked by the brook over time. The $\forall_{hyd}$ depends on the value of K assumed. Initially, a value of 213.3 m/d (CBCL, 1995) was used in the

discharge calculations. This time, the value of K was adjusted until a volume comparable to the $\forall_{geo}$ was attained.

Finally, the discharge rates obtained through analysis of the FD modelling study using Darcy's Law were examined in relation to fish habitat quality. This examination took into consideration information gathered by Hansen *et al.* (unpublished) on fish habitat preferences presented in Figure 20. In particular, the depth versus flow at two cross-sections is presented and fish habitat preferences are indicated thereon. This figure was re-analyzed, using baseflow recession eqn. 27, to produce a graph of depth versus time. The discharge rates on the x-axis were converted into time increments in relation to the known baseflow recession parameters of the Clyburn Brook. For instance, the time of storage was known to be 8.35 days. The resulting graph, presented in Section 3.3.3, was used as the basis for a comparative analysis presented in Section 4.3.2.

3.3.3 Data

The survey, seismic, and topographical data used to build the cross-sectional model is summarized in Table 16.

Table 16 - Basic data for FD modelling of Cross-section 1

Feature	Elevation or Dimension
Water level in brook (m CGD)	3.543
Hydraulic head (m CGD)	3.543
South bank elevation (m CGD)	4.986
North bank elevation (m CGD)	5.385
Depth to bedrock (m)	8.0
Width of surface water in brook (m)	26.2
Width of canyon (m)	102.0

Again, the canyon walls were set at the 10 m elevation contour on the topographic map. The model represented an area of roughly 14.5 m (vertical) by 102 m (horizontal). One node in the FD grid represented 0.5 m x 0.5 m by 5 m of upstream length. [Due to their size, the cross-sectional models are contained in digital form as Appendix D (CD-ROM).]

This model was also fine-tuned to simulate each of six scenarios: WT elevation differences of 0.0, 0.05, 0.5, 1.0, 2.5, and 3.0 m between the brook and the canyon wall. A range of hydraulic head values was obtained in the FD grid after relaxation, which reflect the variance of hydraulic potential underground. These were used to determine the discharge rate into the brook using Darcy's Law (eqn. 25). This data

was then used to analyze baseflow recession components of the brook, to determine the volume of water lost from storage, and an appropriate hydraulic conductivity value.

For the cross-sectional model, an examination of hydraulic head to obtain discharge rate was conducted in a manner similar to that outlined in Section 3.2.2. Using Darcy's Law (eqn. 26), the results shown in Table 17 were produced.

Table 17 – Cross-sectional model discharge calculations

Scenario #	Difference* in WT elevation (m)	Q per 5 m (L/s)**
1	0.0	0.242
2	0.05	0.309
3	0.5	1.75
4	1.0	3.15
5	2.5	8.20
6	3.0	10.6

[Note: The flow value obtained for Scenario #1 is a numerical artifact caused by the need of the model to discretize the system. It has no real (physical) significance and can be taken as being equal to zero.]

* Difference in WT elevation means the difference between a canyon wall nodal value and the adjacent stream value in the FD model.
** 1 L/s = 1×10^{-3} m^3/s

The cross-sectional discharge rates were used to make a direct comparison to the plan-view model discharge rates (see Tables 18-22 below), and hydraulic head values obtained in the cross-sectional model were analyzed with respect to the degree of 'two-dimensionality' in the flow field. This analysis involved drawing equipotential lines and flowlines on a printed copy of the model. Equipotential lines describe lines

of equal hydraulic potential and flowlines occur at right angles to equipotential lines. These results are discussed in Section 4.3.1.

The cross-sectional discharge rates were compared to the discharge rate at the 'bottleneck area only' in the plan-view model. This produced the results shown in Table 18.

Table 18 – Comparison of Plan-view model and Cross-sectional model discharge calculations

Scenario #	Difference in WT elevation (m)	Plan-view Model: Q at 'bottleneck' only per 5 m (L/s)	Cross-sectional Model: Q of 'slice' per 5 m (L/s)
1	0.0	0.675	0.242
2	0.05	0.932	0.309
3	0.5	3.25	1.75
4	1.0	5.82	3.15
5	2.5	13.5	8.20
6	3.0	16.1	10.6

For both the plan-view and the cross-sectional models, baseflow recession analyses were performed, using eqn. 29, based on the discharge rate obtained for each scenario. This analysis produced the results shown in Tables 19 and 20.

Table 19 – Plan-view model baseflow recession calculations

Initial WT – Final WT elevation (m)	Initial Q – Final Q per 5 m (m^3/s)	elapsed time, t (10^6 s)	elapsed time, t (days)
0.05 – 0.0	0.608 – (-0.475)	0.178	2.1
0.5 – 0.05	10.356 – 0.608	2.05	23.7
1.0 – 0.05	21.187 – 0.608	2.56	29.7
2.5 – 0.05	53.681 – 0.608	3.23	37.4
3.0 – 0.05	64.512 – 0.608	3.36	39.0

Table 20 – Cross-sectional model baseflow recession calculations

Initial WT – Final WT elevation (m)	Initial Q – Final Q per 5 m (10^{-3} m^3/s)	elapsed time, t (10^6 s)	elapsed time, t (days)
0.05 – 0.0	0.309 – 0.242	0.175	2.02
0.5 – 0.0	1.75 – 0.242	1.42	16.5
1.0 – 0.0	3.15 – 0.242	1.85	21.4
2.5 – 0.0	8.20 – 0.242	2.54	29.4
3.0 – 0.0	10.6 – 0.242	2.73	31.6

[Note: The final flow value obtained is a numerical artifact caused by the need of the model to discretize the system. It has no real (physical) significance and can be taken as being equal to zero.]

For both the plan-view and cross-sectional models, the volume (S) lost from storage (or hydrograph recession-based volume, $\forall_{hyd}$) was calculated using eqn. 29 and the discharge rates obtained using Darcy's Law, eqn. 25. The volume calculations involved the modelled portion only and produced the results shown in Tables 21 and 22.

Table 21 – Plan-view model volume lost from storage calculations

Initial WT – Final WT elevation (m)	Initial Q – Final Q per 5 m (10^3 m^3/d)*	Volume, S (10^6 m^3)
0.05 – 0.0	4.68 – 3.66	0.0085
0.5 – 0.05	79.8 – 4.68	0.627
1.0 – 0.05	163 – 4.68	1.32
2.5 – 0.05	413 – 4.68	3.41
3.0 – 0.05	497 – 4.68	4.11

* 4.68 means 4.68×10^3 m^3/d

Table 22 – Cross-sectional model volume lost from storage calculations

Initial WT – Final WT elevation (m)	Initial Q – Final Q per 5 m (m^3/d)	Volume, S per 5 m (10^3 m^3)
0.05 – 0.0	26.7 – 20.95	0.0479
0.5 – 0.0	151 – 20.95	1.08
1.0 – 0.0	272 – 20.95	2.10
2.5 – 0.0	709 – 20.95	5.74
3.0 – 0.0	916 – 20.95	7.48

For the plan-view model, a geometric volume ($\forall_{geo}$) calculation for scenario #5 (difference in WT elevation of 2.5 m) was undertaken following the method described in Section 3.3.2. This method of calculation produced a volume of 4.89×10^4 m^3. However, the volume of water represented by this $\forall_{geo}$ is 9.79×10^3 m^3 with 20% porosity and 12.2×10^3 m^3 with 25% porosity. The porosity-based $\forall_{geo}$ were then used to make a direct comparison to the $\forall_{hyd}$ calculation for scenario #5 (difference in WT elevation of 2.5 m) and to make an approximation of the hydraulic

conductivity (K). The examination of K in relation to S (or $\forall_{hyd}$), outlined in Section 3.3.2, produced the results shown in Table 23.

Table 23 – Hydraulic conductivity as inferred from baseflow and modelling efforts

K value (m/d)	WT elevation = 2.5 m Q_o (m^3/s)	WT elevation = 0.05 m Q (m^3/s)	S (m^3)
100.0	2.243	0.025	1600153.9
50.0	1.122	0.013	800077.0
25.0	0.561	0.006	400399.2
20.0	0.449	0.005	320319.4
10.0	0.224	0.003	159438.2
8.0	0.179	0.002	127694.9
5.0	0.112	0.0013	79863.4
1.0	0.022	0.0003	15655.2
0.765	**0.0172**	**0.0002**	**12271.7**
0.76	0.0170	0.00019	12127.4
0.7	0.0157	0.00018	11196.7
0.65	0.0146	0.00017	10410.4
0.62	0.0139	0.00016	9912.6
0.615	0.0138	0.00016	9840.4
0.61	**0.0137**	**0.00016**	**9768.3**
0.60	0.0135	0.00015	9631.2
0.5	0.0112	0.00013	7986.3

Note: Volume (S) is inferred from eqn. 29

A hydraulic conductivity (K) value of 0.61 m/d was required to obtain the 20% porosity volume (9790 m^3) and a value of 0.765 m/d to obtain the 25% porosity volume (12 237 m^3). This suggests much lower hydraulic conductivity values than that reported by CBCL (1995) of 213.3 m/d. The lower K values were chosen because they produced volumes ($\forall_{hyd}$) for the model, which gave the most comparable value to the porosity-based $\forall_{geo}$ calculation. That is, the desired volumes

to match were 9.79×10^3 m^3 and 12.2×10^3 m^3 for 20% and 25% porosity, respectively.

The examination of discharge rate in relation to fish habitat quality was undertaken using baseflow recession analysis (eqn. 27) of the model discharge rates. The information contained in Figure 20 (shown below) summarized by Hansen *et al.* (unpublished), depth versus flow for two riffle sections, was used to prepare an associated figure of depth versus time. The corresponding time data was gathered using the known baseflow recession components of the brook. This examination produced the results shown in Figure 50. An initial flow rate of 10 m^3/s and a final flow of 0.0001 m^3/s were used in eqn. 27 to generate Figure 50.

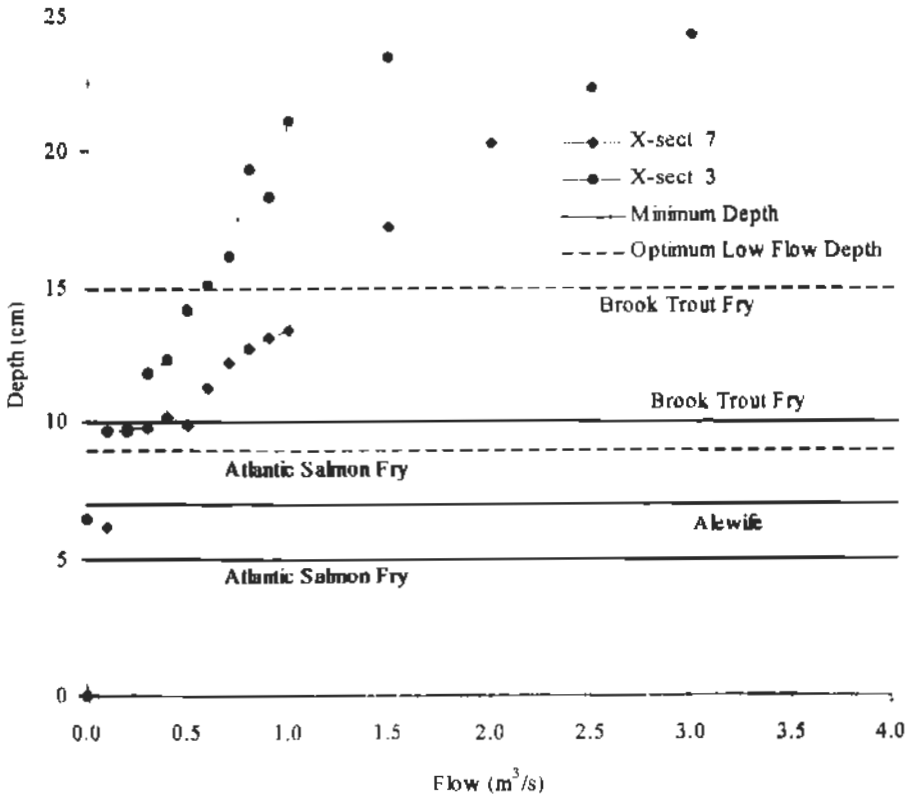

[**Figure 20.** Depth versus flow for two riffle sections and some fish habitat preferences. Cross-sections 3 and 7 were located in the Upstream Reach of the Clyburn Brook (Hansen *et al.*, unpublished).]

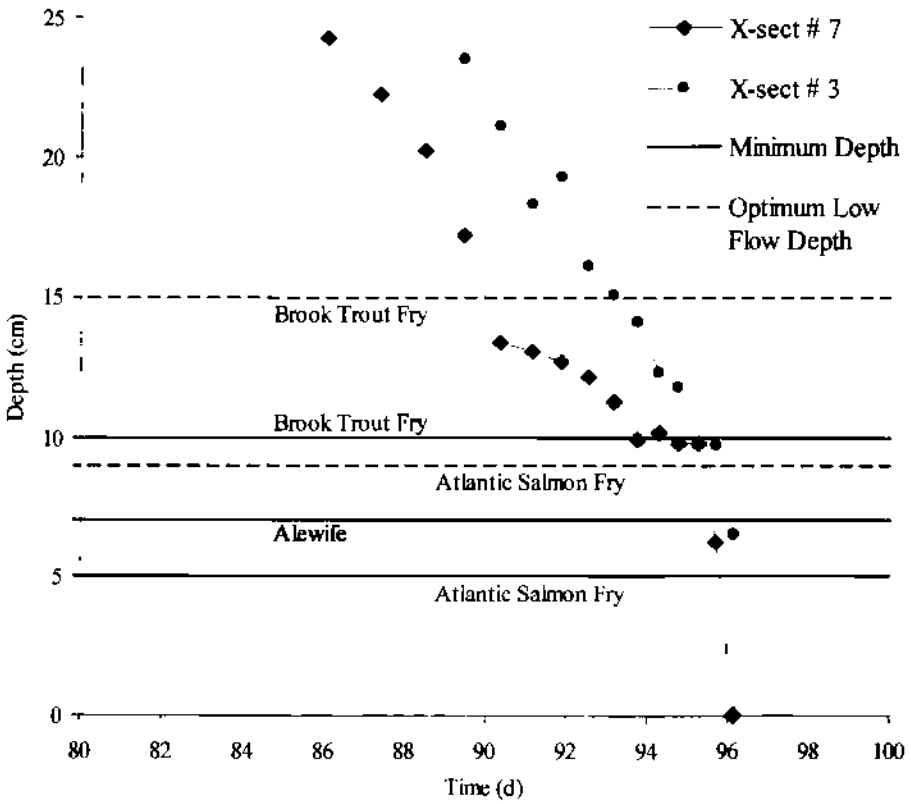

Figure 50. Depth versus time for two riffle sections and some fish habitat preferences (using an initial flow rate of 10 m^3/s and a final flow of 0.0001 m^3/s). Cross-sections 3 and 7 were located in the Upstream Reach of the Clyburn Brook.

In preparing the graph, information was obtained in relation to baseflow recession, see Table 24, such as, it takes 88.5 days to recess from a flow of 4.0 to 0.0001 m^3/s.

Table 24 - Baseflow recession information relating to fish habitat quality

Recession time (days)	Initial Q (m^3/s)	Final Q (m^3/s)
88.5	4.0	0.0001
82.7	2.0	0.0001
76.9	1.0	0.0001
71.1	0.5	0.0001

Figure 50 will be used in the comparative analysis presented in Section 4.3.2.

4 DISCUSSION OF RESULTS

4.1 Seismic Study

4.1.1 Refraction Results

The refraction seismic study produced apparent velocities ranging from 350 to 6500 m/s and a calculated V_2 ranging from 2000 to 5700 m/s. In Section 3.1.4.1, the lower velocity range (350 to 500 m/s) was interpreted as dry till lying above the WT, the median velocity range (1500 to <3000 m/s) as a layer of wet till below the WT, and the higher velocity range (>3000 m/s) as bedrock (Figure 51). Depths to bedrock ranged from 6.6 to 31.9 m, while the average depth of penetration was 8 m (Figure 52). The top of the WT was measured at 1.30 and 0.47 m on lines 86 and 87.

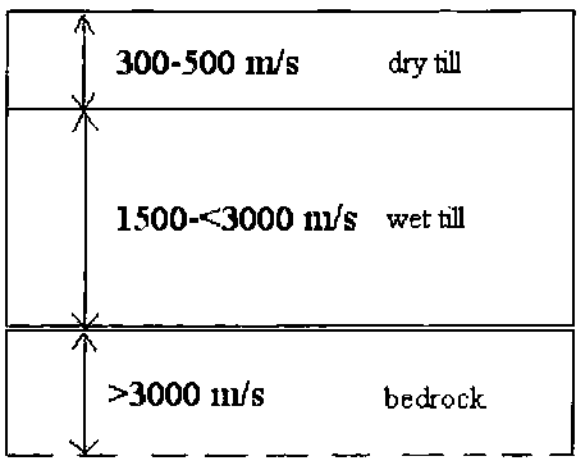

Figure 51. Stratigraphic profile determined by refraction seismic study.

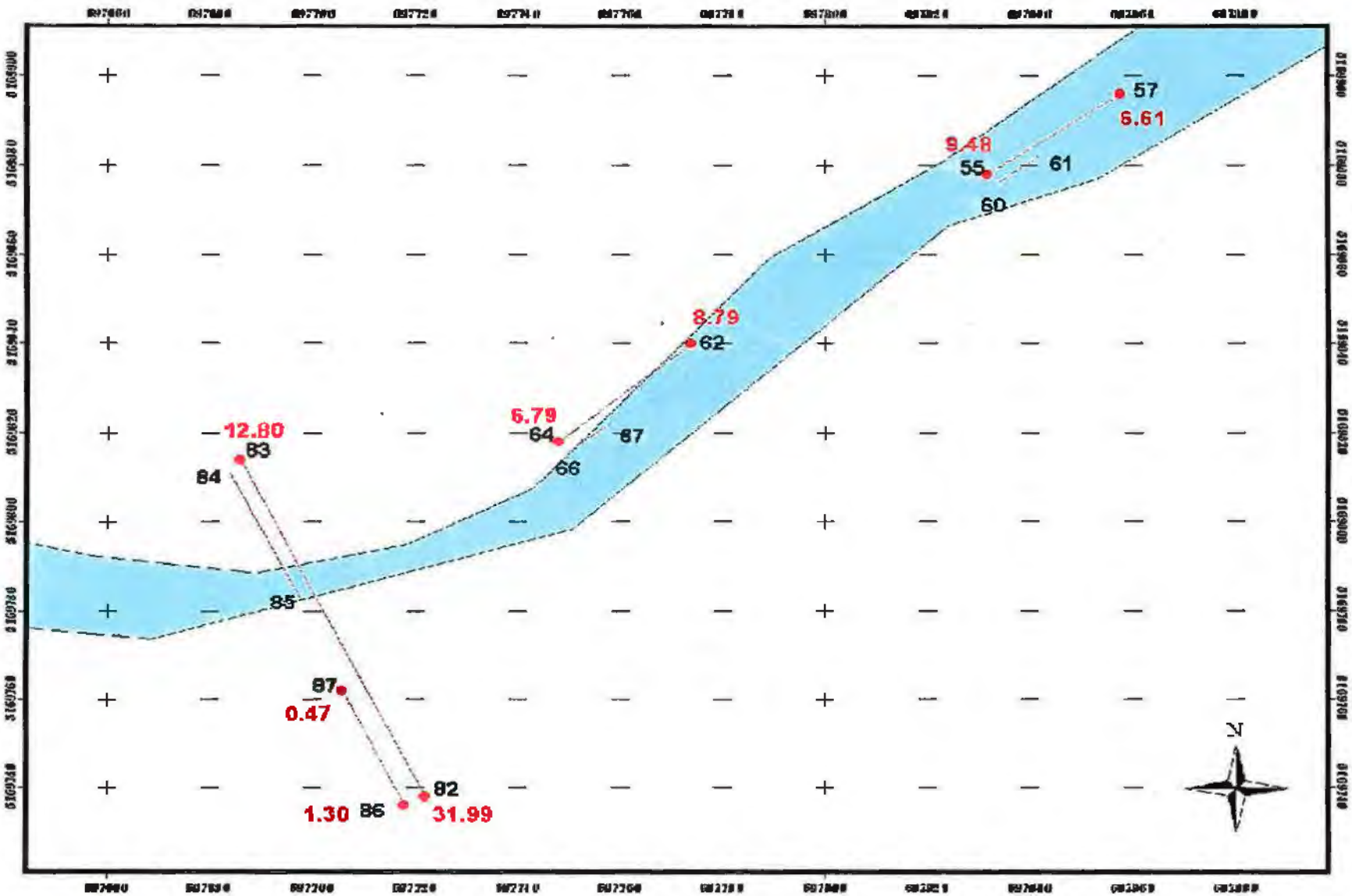

Figure 52. Depths to refractor obtained in refraction seismic study - useful results in eastern end only (Note: Lines 86 and 87 only reached the top of the WT).

The refraction seismic study conclusively identified bedrock in the area of the 'bottleneck', where the depth to bedrock was shallow. The results are summarized in Table 25.

Table 25 - Refraction seismic depths and interpretation

Seismic Line	Depth to refractor (m)	Interpretation
55 57	6.6 downdip 9.5 updip	layer of wet till above dipping bedrock
62 64	6.8 downdip 8.8 updip	layer of wet till above dipping bedrock
82 83	12.8 downdip 31.9 updip	layer of wet till above dipping bedrock
86 87	0.5 downdip 1.3 updip	layer of dry till above a dipping surface of wet till

There was no return from the bedrock along lines 86 and 87. Through interpretation of the last arrival time from line 87, the slope of a hypothetical bedrock line from this starting point was extrapolated back to the y-axis to get an intercept time. The intercept time was analyzed to produce a depth to bedrock. This exercise showed that the bedrock must be deeper than 11.5 m (if $V_{bedrock}$ = 4000 m/s) to 14.6 m (if $V_{bedrock}$ = 6000 m/s) through this section.

The successful refraction seismic lines were located in areas in close proximity to the 'bottleneck' where the depth to bedrock was shallow. With increasing distance from the 'bottleneck' area, the bedrock was found to be located at a greater depth, and after a certain point the bedrock could no longer be reached with the geophone spread that was available.

4.1.2 Reflection Results

The reflection seismic study produced velocities ranging, on average, from 1500 to 3000 m/s. In Section 3.1.4.2, this velocity range was interpreted as being wet till below the WT. Calculated depths of penetration ranged from 15 to 47 m. The reflection seismic study was conducted mainly in the bed of the Clyburn Brook.

Reflection occurred from the top of layer 2 (see Figure 23) and, therefore, velocities for layer 2 were not obtained in the reflection seismic study. However, since the reflection study produced a high quality reflector (see Figure 34), it is believed that bedrock was encountered at these depths.

The reflection seismic study reached greater depths of penetration than the refraction study. The results are summarized in Table 26.

Table 26 – Reflection seismic results
[all depths represent thickness of wet till layer]

Method of Interpretation	Seismic Line	Depth to reflector (m)
Individual basis ($T^2 - X^2$ method)	125 131 133 136 137 139	39.8 37.6 44.7 32.9 40.3 29.6
	142 143	40.8 33.5
Common mid-point	116 118 119	37.9
	126 127 128	31.7
Optimum offset	112 to 140	17.2 to 45.2
	144 to 150	39.7 to 44.0

The interpretation of the lateral profile of the Clyburn Brook canyon and the trough-like profile utilized an average velocity of 2000 m/s, representing the wet till layer. The lateral profile, shown again below, produced depths of penetration ranging from 17 to 45 m. This profile was generated using seismic lines 112 to 140, which are located on the 107 to 140 line in Figure 33.

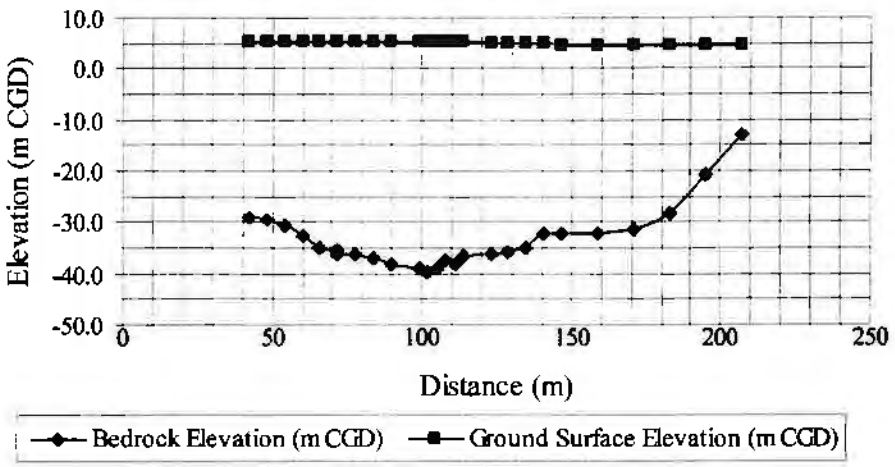

[**Figure 36.** Lateral profile of depth to bedrock in the Clyburn Brook ascertained from reflection data.]

The trough-like profile, shown again below, produced depths of penetration ranging from 39 to 44 m. This profile was generated using seismic lines 144 to 150, locations shown in Figure 33.

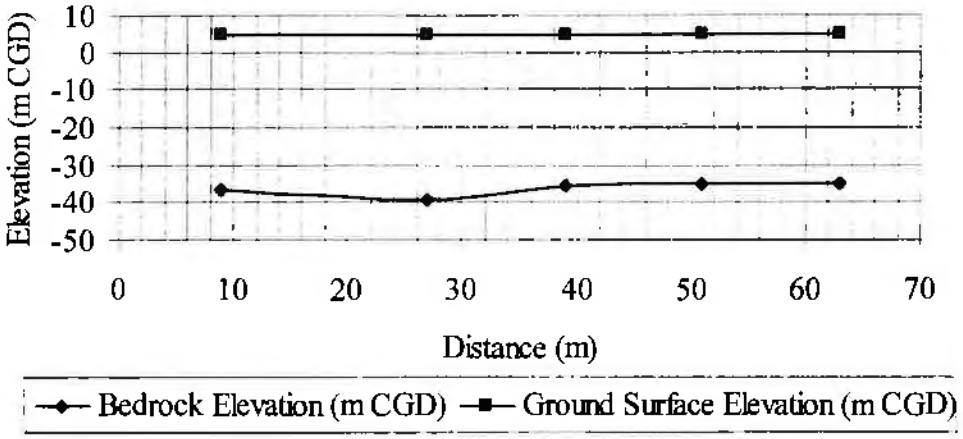

[**Figure 37.** Trough profile of depth to bedrock near the Clyburn Brook based on reflection data.]

4.1.3 Discussion

During the refraction seismic study, 33 lines were shot, however, only 8 lines produced useful results. Most of the shots, especially in the western end, did not reach bedrock and only produced returns from shallow depths (0.25 to 3.5 m). These depths were interpreted as being the top of the WT.

A refraction signal has a relatively low frequency. Therefore, 30 Hz geophones were employed in the study. A greater depth of penetration in the refraction seismic study may have been possible if a longer spread of geophones had been available. In addition, it was not known for certain if the source used was strong enough for the larger distances implied. In order to determine depth to bedrock at greater depths, the use of reflection was considered (see Section 3.1.4.2).

The reflection seismic study used 100 Hz geophones, rather than 30 Hz, and these were placed in areas where the ground was known to be water-saturated. During the reflection-based seismic study, 50 seismic lines were shot, with 38 seismic lines

producing useful results. The reflection study yielded an excellent hyperbola-shaped reflector and the greater depths of penetration that had been hoped for. The results of the optimum offset technique were plotted and a lateral profile of the canyon bottom and a 'trough-like' profile were generated. The depths of penetration obtained for the 'trough-like' profile corresponded well with the depths obtained for the lateral profile. The lateral profile of depth to bedrock was generally U-shaped, typical of a glaciated valley.

Errors can occur in depth determinations during the interpretation of raw seismic data. Since raw seismic data provides time and distance values, these are the only two factors in which error can occur. Errors in distance are usually quite small and are considered insignificant. However, errors in choosing the appropriate arrival times from the raw seismic data can be the main source of error. For instance, when looking at the raw seismic data for refraction line 55, an arrival time of 10.8 ms was chosen for geophone 7 when in fact this arrival time could have been 10.7 or 10.9 ms. The travel time uncertainty is, therefore, ± 0.1 ms. Since the travel times are plotted and analyzed using a best-fit line, from which the slope and velocity are ascertained, the best-fit line provides the largest source of error with refraction data. This could lead to a velocity uncertainty of ± 100 m/s (100/2000 = 5%) and a depth uncertainty of ± 1.0 m (4/5 = 8%). This means that a refraction depth could be 5 m ± 1 m. For reflection seismic line 125, an arrival time of 44.2 ms was recorded for geophone 2 when in fact this arrival time could have been 44.3 ms. The travel time uncertainty with reflection data is ± 0.1 ms, which would lead to a velocity and depth uncertainty

of ± 0.12 m (or 12%). This means that a reflection depth of 40 m could be 40 m ± 5 m.

The depths to bedrock ascertained in both the refraction and reflection seismic studies were utilized in generating the boundary conditions for the FD models for baseflow contribution analysis, as discussed in Section 3.3.

4.2 Numerical Modelling

4.2.1 Results

The hydraulic heads obtained through finite difference modelling for the plan-view model were used to examine rates of discharge for the Upstream Reach of the Clyburn Brook for each of the six scenarios. The examination of the rate of discharge at XS 1, outlined in Section 3.2.3, produced the results in Table 14. These results are discussed in Section 4.2.2 in relation to the baseflow recession hydrographs in Section 2.3.3.1.

In Section 3.2.3, the rate of total discharge at the bottleneck was also examined for each of the six scenarios. The total discharge included an estimated discharge rate into the 'top' of the model, that is, from further upstream. This produced the results in Table 15. These results are used in the baseflow recession calculations made in Section 3.3.3 (Table 19) and are discussed in Section 4.3.2.

4.2.2 Discussion

The Upstream Reach section of the Clyburn Brook was modelled to examine the relationship between the elevation of the top of the unconfined aquifer (i.e. the WT) and the resulting discharge rate into the brook.

It was of interest to compare these various baseflow scenarios in relation to the Clyburn Brook hydrographs generated by Hansen *et al.* (unpublished), shown in Figures 17, 18, and 19. In particular, Figure 18 displays several peak flow rates, with a maximum being about 4.6 m^3/s. The peaks appear to recess down to a flow rate of about 0.5 m^3/s at several points on the graph. If this lower flow rate is taken as a

'baseflow only' discharge rate, a comparison can be made to the discharge rates obtained in the finite difference modelling study.

Scenario #1 (no difference in WT elevation) produced a discharge rate of –0.042 m^3/s for the unconfined aquifer. The negative flow rate occurred because the model was attempting to discretize the system. The model was only a simplification of reality and it would take an infinite amount of time for the discharge to recess down to 0 m^3/s. As stated below Table 14, this value has no real (physical) significance and can be considered to equal zero. In any event, a flow of this magnitude (42 L/s) would only appear as a trickle at XS 1.

Scenario #2 (difference in WT elevation of 0.05 m) produced a discharge rate of 0.054 m^3/s for the unconfined aquifer. This discharge rate represented a slightly elevated WT and the result is more in line with the 'baseflow only' discharge rate observed in Figure 18.

Scenario #3 (difference in WT elevation of 0.5 m) produced a discharge rate of 0.923 m^3/s for the unconfined aquifer. This discharge rate was slightly above the average discharge rate in Figure 18. It, therefore, indicated a WT elevation that was slightly above average.

Scenario #4 (difference in WT elevation of 1.0 m) produced a discharge rate of 1.889 m^3/s for the unconfined aquifer. This discharge rate is between the average discharge and the flooding discharge rates shown in Figure 18.

Scenario #5 (difference in WT elevation of 2.5 m) produced a discharge rate of 4.785 m^3/s for the unconfined aquifer. This discharge rate was more typical of the flooding events noted on the hydrographs. Scenario #6 (difference in WT elevation

of 3.0 m) produced a discharge rate of 5.750 m^3/s for the unconfined aquifer. This discharge rate was also more typical of the flooding events noted on the hydrographs.

Based on the above examination of discharge rates, it is surmised that a WT difference of 3 m was likely to represent the upper limit of WT elevation that could occur. Also, the WT at the canyon wall can only rise so much higher than the brook before it would intersect the ground surface somewhere between the canyon wall and the brook. With the survey data of the Clyburn Brook in mind, in particular, the south and north bank elevations and the water level (W/L) elevations noted in Section 2.3.3.1, it would be logical to conclude that the difference between the water level and the bank elevations would be close to the maximum difference in WT elevation. This value ranged from 0.56 to 1.8 m.

Using the discharge rates obtained for the six scenarios, an examination of baseflow recession components of the Clyburn Brook was also undertaken. Baseflow recession, such as, the time increment to go from a high WT to a lower WT elevation and the volume of water lost from storage as a result, forms part of the discussion presented in Section 4.3.2. The discharge rates are also examined in relation to fish habitat quality in Section 4.3.2.

4.3 Baseflow Contribution Study

4.3.1 Results

The hydraulic heads obtained through finite difference modelling for the cross-sectional model were used to examine rates of discharge of the 'slice' for each of the six scenarios. The examination of the rate of discharge at XS 1, outlined in Section 3.2.3, produced the results in Table 17. The comparison of discharge rates obtained in the cross-sectional model to that obtained in the 'bottleneck area only' of the plan-view model produced the results in Table 18.

Analysis of the degree of 'two-dimensionality' in the flow field produced equipotential lines that were generally vertical but curved slightly towards the brook and streamlines that were also curved towards the brook, with some entering the base of the brook, as expected.

Baseflow recession analysis of the plan-view model utilized the total discharge value obtained (Upstream Reach plus flow into 'top' of model from further upstream) and produced the results in Table 19. Baseflow recession analysis of the cross-sectional model used the discharge rates obtained for the modelled area per 5 m of stream length and produced the results in Table 20.

An examination of the volume of water lost from storage (S or $\forall_{hyd}$) for the modelled portion only produced the results in Tables 21 and 22. The geometric volume calculation for scenario #5 (difference in WT elevation of 2.5 m) for the plan-view model produced a calculated $\forall_{geo}$ of 4.89×10^4 m^3, which represents volumes of 9.79×10^3 m^3 and 12.2×10^3 m^3 with 20% and 25% porosity, respectively.

The examination of a hydraulic conductivity value, used in calculating Q and $\forall_{hyd}$, sufficient to obtain a volume comparable to the porosity-based $\forall_{geo}$ calculation for scenario #5 (difference in WT elevation of 2.5 m) produced the results shown in Table 23.

An examination of fish habitat data summarized by Hansen *et al.* (unpublished) and shown in Figure 20, depth versus flow for riffle sections 3 and 7, was used to prepare an associated figure of depth versus time. The flow information shown in Figure 20 was used in combination with known baseflow components of the brook, such as, the time of storage (8.35 days) and an initial flow rate of 10 m^3/s and a final flow rate of 0.0001 m^3/s in eqn. 27, to compute the corresponding times associated with the decline in flow. This analysis produced the following results:

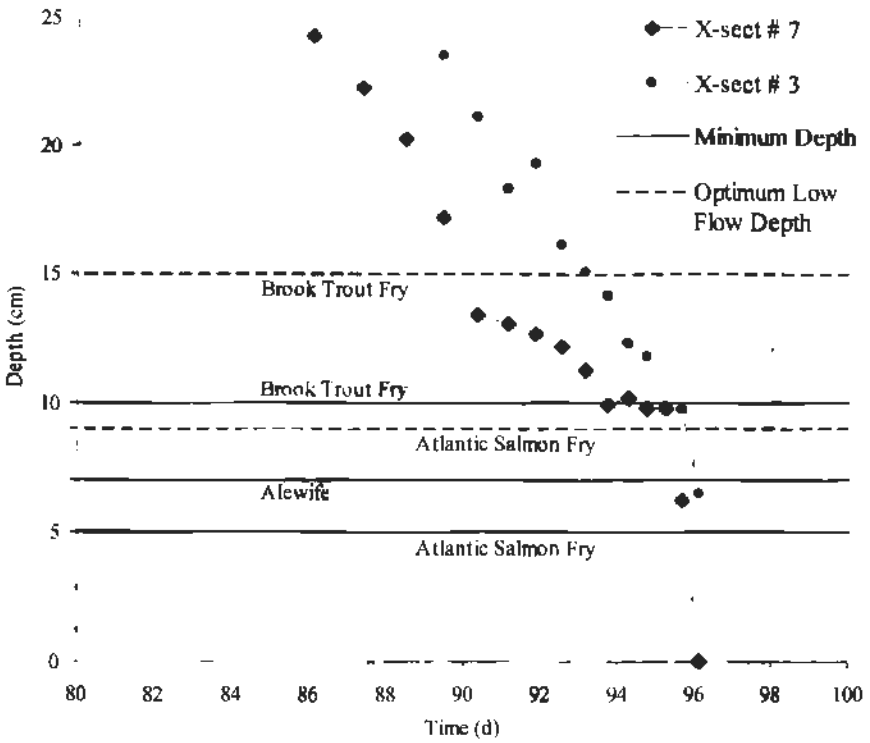

[Figure 50. Depth versus time for two riffle sections and some fish habitat preferences (using an initial flow rate of 10 m^3/s and a final flow of 0.0001 m^3/s). Cross-sections 3 and 7 were located in the Upstream Reach of the Clyburn Brook.]

4.3.2 Discussion

A comparison of the discharge rates obtained for the cross-sectional model to the hydrographs (Figures 17, 18 and 19) indicated that the magnitudes of the discharge for all scenarios were reasonable. That is, all discharge rates obtained through FD modelling were below the 'baseflow only' discharge rate of about 0.5 m^3/s shown on Figure 18, the July 2000 hydrograph. It was also found that the flow in the cross-sectional model was indeed two-dimensional.

For given values of hydraulic conductivity and hydraulic gradient, the discharge increases with the cross-sectional area through which flow is taking place. A comparison was made between the discharge results for the cross-sectional model and the discharge results of the 'bottleneck area only' in the plan-view mode (see Table 18). Even though these were both calculated to equal a discharge rate per 5 m of downstream length, the results of the plan-view model were slightly higher than the cross-sectional model study. The 'bottleneck area' of the plan-view model may have been influenced by the higher heads of its nodal neighbors (upstream) and the larger model size.

The baseflow recession analysis undertaken gave an indication of the time interval that would pass while the unconfined aquifer recessed from one WT elevation setting to a lower one. For the plan-view model, time intervals ranged from 23.7 to 39.0 days to recess from an initial WT elevation of 0.5 m and 3.0 m down to 0.05 m, respectively. For the cross-sectional model, time intervals ranged from 2.0 to 31.6 days to recess from an initial WT elevation of 0.05 m and 3.0 m down to about 0.0 m, respectively. This would indicate that, for a small increase in WT elevation (at

the canyon walls), precipitation would impact the unconfined aquifer in a relatively short period of time. However, for a large increase in WT elevation (e.g. 3.0 m), precipitation would probably cause a minor flooding event on the unconfined aquifer and its effects were more likely to last longer (e.g. up to 40 days).

A variety of hydrograph recession-based volume estimates (values of $\forall_{hyd}$) were obtained for the modelled area of the Clyburn Brook, using baseflow recession equations. For the plan-view model, these volumes ranged from 6.96×10^4 m^3 to 6.90×10^6 m^3 for WT elevations of 0.05 to 3 m, respectively. For the cross-sectional model, volumes ranged from 28.9 to 5693.5 m^3 for WT elevations of 0.05 to 3 m, respectively. It should be noted that the cross-sectional model volumes represent a WT recessing down to about a 0.0 m elevation point, whereas the plan-view model volumes represent a WT recessing down to a 0.05 m elevation point.

To give an indication of the accuracy of the volume estimation, a geometric volume ($\forall_{geo}$) calculation was made for the plan-view model scenario #5 (difference in WT elevation of 2.5 m). The $\forall_{geo}$ obtained was 4.89×10^4 m^3, whereas, the hydrograph recession-based volume ($\forall_{hyd}$) obtained, using Darcy's Law with K= 213.3 m/d and baseflow recession analysis, was 3.41×10^6 m^3. The $\forall_{hyd}$ estimate was made through baseflow recession analysis of a WT recessing from 2.5 to 0.05 m elevation and was, therefore, representative of a nearly flat WT. Since the $\forall_{geo}$ must take the porosity of the sediments into consideration, the porosity-based $\forall_{geo}$ for 20% and 25% porosity were 9.79×10^3 m^3 and 12.2×10^3 m^3, respectively.

An examination of hydraulic conductivity for plan-view model scenario #5 (difference in WT elevation of 2.5 m) indicated that a value of 0.61 m/d (7.1×10^{-4}

cm/s) was required to produce a $\forall_{hyd}$ similar to 20% of the $\forall_{geo}$ and a value of 0.765 m/d (8.9×10^{-4} cm/s) was required to produce a $\forall_{hyd}$ similar to 25% of the $\forall_{geo}$. These values differed greatly from the 213.3 m/d (2.5×10^{-1} cm/s) value determined by the CBCL (1995) pump test. The inferred K values are three orders of magnitude lower than the CBCL (1995) value. One reason for the discrepancy could be that the CBCL (1995) K value was based on the localized area affected by the pump test, whereas the inferred K values were determined through FD modelling of a much larger area.

According to Fetter (1994), a hydraulic conductivity value for glacial outwash can range from 10^{-3} to 10^{-1} cm/s. The CBCL (1995) value is slightly above the range and the inferred K values appear to be below the range indicated by Fetter (1994). According to Freeze and Cherry (1979), a hydraulic conductivity value for glacial till is in the range of 10^{-10} to 10^{-4} cm/s. This range of hydraulic conductivity values could be interpreted as representing poorly-sorted glacial material. In comparison to this range, the CBCL (1995) value is well above the range, however, the inferred K values fit well within this range. Based on the inferred K values, the sediments should be classified as glacial till. Nevertheless, some of the sediments in the Clyburn Brook canyon, which has been infilled as a result of glaciation, have been reworked by the brook over time and, therefore, the hydraulic conductivity value probably varies considerably throughout the canyon bottom.

The flow rates obtained as a result of the FD modelling and baseflow contribution studies were analyzed in relation to fish habitat preferences (Figure 50). In general, it was ascertained that fish habitat is negatively impacted after 90 to 96 days of

recession when rates of flow range from 1.0 m^3/s to 0.1 m^3/s, respectively. In particular, the impact on fish habitat at XS 7, ascertained from the graph, was that after 90 days of recession, the Brook Trout Fry would have a less suitable habitat and the water depth would fall below the minimum acceptable depth for this species after 94 or 95 days. After about 95.5 days of recession, the water depth would no longer be suitable for the Alewife. After 95.8 days of recession, the water depth would fall below the minimum acceptable depth for the Atlantic Salmon Fry and, therefore, would no longer be a suitable habitat.

The impact on fish habitat at XS 3, ascertained from the graph, was that after 93 days of recession, the Brook Trout Fry would have a less than suitable habitat and the water depth would fall below its minimum acceptable depth after about 95 days. After 95.5 days of recession, the Atlantic Salmon Fry would be affected, but the water depth would not fall below the minimum acceptable depth. After 96 days of recession, conditions would no longer be suitable for Alewife.

During periods of high flow rates, a larger quantity of water would be present in the aquifer and there would be more baseflow contribution to the stream. This would occur because an elevated WT is associated with a steeper hydraulic gradient. During periods of low flow, a smaller quantity of water would be present in the aquifer to contribute baseflow to the stream.

4.3.2.1 Water Quantity Implications

The implications on water quantity may seem obvious. If the WT became very low, the stream could become a losing stream rather than a gaining stream. Losing streams contribute a portion of their discharge to the aquifer, and tend to dry up. In

these situations, care should be taken to closely monitor the volume of groundwater being pumped from the wells near the Clyburn Brook. Overpumping when the brook is at a critical level could cause detrimental effects on the quantity of water in the brook.

4.3.2.2 Water Quality Implications

During periods of low flow, shallow areas in the brook may form an algae layer and the bacterial content of the water may increase due to stagnation (low turbulence), warm temperatures, and the presence of organic material. Organic material requires oxygen in order to be broken down. Algal material and microorganisms require oxygen to grow and may use the organic material as an energy source (Fetter, 1994). All of these processes lead to depletion of the dissolved oxygen levels in the brook and, therefore, a net removal of oxygen from the water could occur. Since a certain level of oxygenation is required to promote a healthy environment for fish development and growth, low rates of flow for extended periods of time often have a very negative impact on water quality and the quality of fish habitat.

5 CONCLUSIONS

5.1 Conclusions

The seismic study confirmed depths to bedrock in the area of the bottleneck and along the Upstream Reach portion of the Clyburn Brook, from the golf cart bridge to XS 6. Depths to bedrock ranged from 6.6 to 47 m, demonstrating the variability in thickness and location of glaciofluvial material in the canyon bottom. The canyon bottom appeared to be generally U-shaped, typical of glaciated valleys.

The FD modelling effort produced a variety of flow rates. These were examined in relation to baseflow contribution, volume estimations, and fish habitat quality. It was determined that the unconfined aquifer may have a hydraulic conductivity value as low as 0.61 m/d and that, during periods of low flow (as indicated by depth), fish habitat quality and water quality could be negatively impacted. These two phenomenon tend to occur simultaneously.

6 RECOMMENDATIONS FOR FURTHER WORK

6.1 Recommendations

With respect to mathematical modelling of the Clyburn Brook, the Upstream Reach of the brook could be modelled in such a manner so that time can be incorporated. This would involve the solution of the Boussinesq equation (Fetter, 1994):

$$\frac{\partial}{\partial x}\left(h\frac{\partial h}{\partial x}\right)+\frac{\partial}{\partial y}\left(h\frac{\partial h}{\partial y}\right)=\frac{S_y}{K}\left(\frac{\partial h}{\partial t}\right) \qquad \textbf{[30]}$$

where h = saturated thickness of aquifer (L)
S_y = specific yield (dimensionless)
K = hydraulic conductivity (L/T)

A software package, such as MODFLOW, can handle the problem and could be used to aid in visualizing changes in WT elevations with respect to time.

Simultaneous WT and low flow measurements could be taken to provide additional information with respect to WT fluctuations in the lower reaches of the Clyburn Brook canyon. This field information could then be applied in further finite difference modelling efforts.

Further seismic studies could be conducted along the length of the Clyburn Brook in reflection mode and interpreted to generate additional profile data. Using several lateral profiles, a 3-D surface of the bedrock could be generated for the Upstream Reach.

REFERENCES

ADI-Nolan Davis (NS) Limited. 1993. Clyburn River, Study of Coastal and Fluvial Processes. Project No. S92291.

Allen, D. 1999. Clyburn River Watershed and Sub-watershed Metrics. Canadian Heritage Parks Canada.

Barr, S.M., Jamieson, R.A. and Raeside, R.P. 1992. Geology, Northern Cape Breton Island, Nova Scotia; Geological Survey of Canada, Map 1752A, scale 1:100 000.

Boonstra, N.A. and de Ridder, N.A. 1981. Numerical modelling of groundwater basins. ILRI publication 29. International Institute for Land Reclamation and Improvement: The Netherlands.

CBCL Limited. 1995. Aquifer Yield Assessment, Clyburn Brook Infiltration Gallery Site.

Fetter, C.W. 1994. Applied Hydrogeology, 3rd edition. Prentice-Hall, Inc.: New Jersey.

Freeze, R.A. and Cherry, J.A. 1979. Groundwater. Prentice-Hall, Inc.: New Jersey.

Grant, D.R. 1988. Surficial geology, Cape Breton Island, Nova Scotia. Geological Survey of Canada, Map 1631A, scale 1:125 000.

Grant, D.R. 1994. Quaternary Geology, Cape Breton Island, Nova Scotia. Geological Survey of Canada, Bulletin 482, 159 p.

Hansen, D. 2001. Course Notes: CIVL4410 Engineering Hydrogeology. Department of Civil Engineering. Dalhousie University (Sexton Campus).

Hansen, D., Cavers, B. and Bridgeland, J. (unpublished) Hydraulic Assessment of the Salmonid habitat quality of the Clyburn Brook, Cape Breton Island.

Herschy, R.W. 1998. Encyclopedia of hydrology and water resources. 1st ed. Dordrecht: Boston.

Kleiner, D.E. 1985. Engineering with spreadsheets. ASCE Civil Engineering Magazine, October, pp. 55-57.

Lillie, Robert J. 1999. Whole Earth Geophysics: An Introductory Textbook for Geologists & Geophysicists. Prentice-Hall, Inc.: New Jersey.

Lin, S. 1995. Structural evolution and tectonic significance of the Eastern Highlands shear zone in Cape Breton Island, the Canadian Appalachians. Canadian Journal of Earth Sciences. 32: 545-554.

Olsthoorn, T.N. 1985. Computer notes – the power of the electronic worksheet: modelling without special programs. Groundwater, May-June, pp. 381-390.

Prest, V.K., and Grant, D.R. 1969. Retreat of the last ice sheet from the Maritime Provinces-Gulf of St. Lawrence region. Geological Survey of Canada, Paper 69-33, 15 p.

Pullan, S.E., and Hunter, J.A. 1990. Delineation of buried bedrock valleys using the optimum offset shallow seismic reflection technique. Geotechnical and Environmental Geophysics, Volume III. Society of Exploratory Geophysicists. Ward, S.H. (edit). pp. 75-87.

Raeside, R.P. and Barr, S.M. 1992. Geology of the Northern and Eastern Cape Breton Highlands, Nova Scotia. Geological Survey of Canada, Paper 89-14, 39 p.

Raeside, R.P., Barr, S.M., and Jong, W. 1984. Geology of the Ingonish River-Wreck Cove Area, Cape Breton Island, Nova Scotia. Nova Scotia Department of Mines and Energy Report 84-1, pp. 249-258.

Southwell, R.V. 1946. Relaxation methods in theoretical physics. Oxford University Press.

Telford, W.M., Geldart, L.P., Sheriff, R.E., and Keys, D.A. 1976. Applied Geophysics. Cambridge University Press: London, New York, Melbourne.

Tennant D.L. 1976. Instream flow requirements for fish, wildlife, recreation and related environmental resources. Proceedings of the symposium and specialty conference on instream flow needs. American Fisheries Society, Western Division and American Society of Civil Engineers, Power Division, Boise, ID, May 3-6, 1976, vol. 2, pp.359-363.

Wang, H.F. and Anderson, M.P. 1982. Introduction to Groundwater Modelling: Finite Difference and Finite Element Methods. W.H. Freeman & Company.

Topographical map:

Ingonish Centre, Victoria County, Nova Scotia Topographic Series, 1:10 000 (Sheet 10 46 6500 60 400), Department of Housing and Municipal Affairs, Land Information Services.

APPENDICES

APPENDIX A

Aquifer – Rock or sediment in a formation, group of formations, or part of a formation that is saturated and sufficiently permeable to transmit economic quantities of water to wells and springs.

Aquifer, confined – An aquifer that is overlain by a confining bed. The confining bed has a significantly lower hydraulic conductivity than the aquifer.

Aquifer, unconfined – An aquifer in which there are no confining beds between the zone of saturation and the surface. There will be a water table in an unconfined aquifer (also referred to as a water-table aquifer).

Baseflow – That part of the stream discharge from groundwater seeping into the stream.

Baseflow recession – The declining rate of discharge of a stream fed only by baseflow for an extended period. Typically, a baseflow recession will be an exponential decay.

Baseflow recession hydrograph – A hydrograph that shows a baseflow-recession curve.

Cold-based conditions – The conditions present when the basal ice of a cold, dry glacier is frozen to the ground and most of the movements take place above the base through plastic deformation (Grant, 1994).

Crag-and-tail – Rock hill with drift lodged on down-glacier side (Grant, 1988).

Discharge – The volume of water flowing in a stream or through an aquifer past a specific point in a given period of time.

Discharge area – An area in which there are upward components of hydraulic head in the aquifer. Ground water is flowing toward the surface in a discharge area and may escape as a spring, seep, or baseflow or by evaporation and transpiration.

Downdip – In a seismic survey of a dipping reflector, it is the direction of raypath travel when shooting down-gradient toward the receivers. Shooting downdip results in an apparent velocity that is lower than the true velocity (Lillie, 1999).

Dupuit assumptions – Assumptions for flow in an unconfined aquifer that (1) the hydraulic gradient is equal to the slope of the water table, (2) the streamlines are horizontal, and (3) the equipotential lines are vertical [see Section 3.3.1.1].

Equipotential line – A line in a two-dimensional ground-water flow field such that the hydraulic head is the same for all points along the line.

Finite-difference model – A method for solving partial differential equations that is based on the discretization of space and/or time. The method determines the effects of the boundary conditions on the particular section of space/time of interest by iterative calculation.

Flow line – An imaginary line that traces the path that a particle of groundwater would follow as it flows through an aquifer.

Groundwater – The water contained in interconnected pores located below the water table in an unconfined aquifer or located in a confined aquifer.

Hydraulic conductivity – A coefficient of proportionality in Darcy's Law describing the ease with which water can move through a permeable medium. The density and kinematic viscosity of the fluid must be considered in determining hydraulic conductivity.

Hydraulic head – The sum of the elevation head and pressure head at a given point in an aquifer.

Hydraulic gradient – The difference in hydraulic head with a change in distance in a given direction. The direction is that which yields a maximum rate of decrease in head.

Saturation zone – The zone in which the voids in the rock or soil are filled with water at a pressure greater than atmospheric. The water table is the top of the saturation zone in an unconfined aquifer.

Solifluction – 1. The creep of soil saturated with water on top of a frozen layer of soil. The thawed layer of soil becomes so saturated with water that it can carry rocks and debris with it downslope. This movement only occurs in cold regions as a result of alternative freezing and thawing. 2. The slow, downhill movement of soil or other material in areas typically underlain by frozen ground.

Updip – In a seismic survey of a dipping reflector, it is the direction of raypath travel when shooting up-gradient toward the receivers. Shooting updip results in an apparent velocity that is higher than the true velocity (Lillie, 1999).

Water table – The surface in an unconfined aquifer or confining bed at which the pore water pressure is atmospheric. It can be measured by installing shallow wells extending one metre (a few feet) into the zone of saturation and then measuring the water level in those wells.

APPENDIX C

Relevant Derivation

It can be shown that two-dimensional steady flow through a homogeneous and isotropic porous media is governed by the following second-order linear elliptic partial differential equation:

$$\frac{\partial^2 h}{\partial x^2} + \frac{\partial^2 h}{\partial y^2} = 0 \qquad [A1]$$

where the derivatives represent the second-order change in hydraulic head h in the x and y directions, respectively. The first-order rate of change in the first term in eqn [A1] can be approximated at node 1 in Figure 1 by:

$$\frac{\partial h_1}{\partial x} \approx \frac{\Delta h}{\Delta x} = \frac{(h_1 - h_c)}{\Delta x} \qquad [A2]$$

We need a second-order rate of change in head. We therefore need the first-order rate of change for the first term in eqn [A1] at another location:

$$\frac{\partial h_c}{\partial x} \approx \frac{\Delta h}{\Delta x} = \frac{(h_c - h_3)}{\Delta x} \qquad [A3]$$

By substitution of [A2] & [A3] into [A1]:

$$\frac{\partial^2 h_c}{\partial x^2} \approx \frac{\dfrac{\partial h_1}{\partial x} - \dfrac{\partial h_c}{\partial x}}{\partial x} = \frac{\dfrac{(h_1 - h_c)}{\Delta x} - \dfrac{(h_c - h_3)}{\Delta x}}{\Delta x} = \frac{(h_1 - 2h_c + h_3)}{\Delta x^2} \qquad [A4]$$

Using the same procedure in the y-direction we may readily obtain:

$$\frac{\partial^2 h_c}{\partial y^2} \approx \frac{\dfrac{(h_2 - h_c)}{\Delta y} - \dfrac{(h_c - h_4)}{\Delta y}}{\Delta y} = \frac{(h_2 - 2h_c + h_4)}{\Delta y^2} \qquad [A5]$$

Substituting [A4] and [A5] into [A1] gives:

$$\frac{(h_1 - 2h_c + h_3)}{\Delta x^2} + \frac{(h_2 - 2h_c + h_4)}{\Delta y^2} = 0 \qquad [A6]$$

In our case $\Delta x = \Delta y$ so:

$$h_c = \frac{1}{4}(h_1 + h_2 + h_3 + h_4) \qquad [A7]$$

For simple impermeable boundaries, eqn [A7] is modified by simply doubling the nodal head on the 'mirror image' side of the impermeable boundary, leading to equation [2]:

$$h_c = \frac{1}{4}(h_1 + 2h_2 + h_3)$$

[Hansen (2001), course notes]